

https://dspace.org/

Mapping and monitoring shoreline changes along South Africa's southwestern coastline from 1937 to 2020 using multisource remote sensing data and techniques

Murray, Jennifer Joan

2021
https://hdl.handle.net/10539/33090

Downloaded from a DSpace repository. https://dspace.org/



UNIVERSITY OF THE
WITWATERSRAND,
JOHANNESBURG

GEOG 7000A: Environmental Studies Research Report

MAPPING AND MONITORING SHORELINE CHANGES ALONG SOUTH AFRICA'S SOUTHWESTERN COASTLINE FROM 1937 TO 2020 USING MULTISOURCE REMOTE SENSING DATA AND TECHNIQUES.

Name: Jennifer Joan Murray

Student Number: 1406538

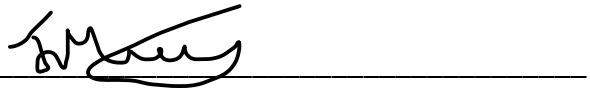
Supervisors: Dr Mary Evans and Prof Elhadi Adam

A research report submitted in partial fulfilment of the requirements for the degree of Master of Science in Geographic Information Systems and Remote Sensing in the School of Geography, Archaeology and Environmental Studies.

Johannesburg, 2021

DECLARATION

I declare that this research report is my own unaided work. It is being submitted for the partial fulfilment for the Degree of Master of Science (Coursework and Research Report) in Geographic Information Systems and Remote Sensing at the University of the Witwatersrand, Johannesburg. It has not been submitted before for any degree or examination at any other University.



(Signature of candidate)

__13__ day of _September_____ 2021 at Johannesburg.

ABSTRACT

Coastal erosion is a risk presented to sandy beaches around the world. In June 2017, a large storm surge eroded a section of Sixteen-Mile Beach along South Africa's southwestern shoreline. To understand events like these, and how to manage coastal erosion, one has to analyse how beaches have changed over the long-term. This can be effectively achieved through remote sensing. This study aims to assess the spatio-temporal changes to South Africa's southwestern shoreline between 1937 and 2020 and projects future shoreline changes. This is achieved by integrating different remote sensing data sources and techniques. Firstly, historical aerial photographs from 1937, 1960 and 1977 were georeferenced, and their shoreline positions were manually digitised. Secondly, shoreline positions were automatically delineated from Landsat 5, 7 and 8 and Sentinel-2 imagery between 1985 and 2020 using the *CoastSat* toolkit and Google Earth Engine. These two datasets were then combined to quantify the rate and magnitude of shoreline erosion and accretion that has taken place over these eight decades using the Digital Shoreline Analysis System (DSAS). Additionally, the short-term shoreline variability, seasonality and storm surge impact were investigated by creating cross-shore change profiles delineated from Sentinel-2 data. Finally, DSAS was used to model future shoreline positions for 2030 and 2040 based on the long-term changes. The results revealed that the shoreline has undergone dynamic changes between 1937 and 2020, culminating in an average net erosion of 39 m, predominantly due to the June 2017 storm surge. Yet, the shoreline forecasts indicate a slight shoreline retreat for the upcoming two decades. It must be noted that these remote sensing data are limited by their underlying uncertainties. Therefore, recommendations for future studies include integrating additional remote sensing and field data to present a more holistic understanding of the coastal environment.

Keywords: *Digital Shoreline Analysis System (DSAS), CoastSat, Coastal Erosion, Yzerfontein, Sixteen-Mile Beach.*

ACKNOWLEDGEMENTS

I wish to thank the many individuals who have made this degree possible and who have guided me along the way. Firstly, I would like to acknowledge my supervisors, Dr Mary Evans and Prof Elhadi Adam, for their guidance and support throughout this research report. Many thanks to Dr Stephan Woodborne and Dr Duncan Miller for their valuable insights and expertise, and for introducing me to the magnificent Yzerfontein area. Additionally, thank you to Stephen Davey for providing me with extra drone footage and helpful advice.

I wish to acknowledge SANParks for granting access to conduct research within the West Coast National Park (Ref: MILD/AGR/006--2018/2018-2019/V1). Thank you to National Geo-spatial Information (NGI) for providing invaluable data for this research, especially Mr Mzuyanda Nkukwana for his assistance. This project was funded by the Postgraduate Merit Award Scholarship Programme from the University of the Witwatersrand.

I am extremely grateful to Dr Rose Grant for all your encouragement and support in standing by my side and giving me the strength to write-up and finalise this report. Finally, thank you to my family for your endless care and devotion throughout these past two years. Chris and Dolly, thank you for being my sunshine during these 'unprecedented' times.

TABLE OF CONTENTS

DECLARATION ..... **i**

ABSTRACT ..... **ii**

ACKNOWLEDGEMENTS ..... **iii**

TABLE OF CONTENTS ..... **iv**

LIST OF ACRONYMS ..... **vi**

LIST OF FIGURES ..... **vii**

LIST OF TABLES ..... **ix**

Chapter 1: **1**

INTRODUCTION **1**

1.1 Background 1

1.2 Problem Statement and Rationale 2

1.3 Aim 4

1.4 Objectives 4

1.5 Outline of the research report 5

Chapter 2: **6**

STUDY SITE **6**

2.1 General setting 6

2.2 Description of the three shoreline beaches 7

2.3 Climate, ocean and landscape of the study site 11

2.4 Summary 17

Chapter 3: **18**

LITERATURE REVIEW **18**

3.1 Introduction 18

3.2 Coastal systems and processes 18

3.3 History and background of shoreline change analysis 21

3.4 Debates within shoreline change analysis 25

3.5 Remote sensing for mapping and monitoring shorelines changes 27

3.6 The Digital Shoreline Analysis System 32

3.7 Summary 35
Chapter 4: 36
METHODOLOGY 36
4.1 Introduction 36
4.2 Shoreline extraction from historical aerial photography 36
4.3 *CoastSat* shoreline extraction 40
4.4 Long-term analysis 48
4.5 Short-term analysis 50
4.6 Future shoreline forecasting 54
4.7 Summary 54
Chapter 5: 57
RESULTS 57
5.1 Introduction 57
5.2 Long-term shoreline change 57
5.3 Short-term shoreline change 70
5.4 Future shoreline changes 73
5.5 Summary 75
Chapter 6: 77
DISCUSSION 77
6.1 Introduction 77
6.2 Analysis and critique of results 77
6.3 Limitations 83
6.4 Recommendations for further research 85
6.5 Summary 87
Chapter 7: 88
CONCLUSION 88
7.1 Overview of research 88
7.2 Limitations and recommendations of research 90
REFERENCES 91
APPENDICES 97

LIST OF ACRONYMS

AMBUR	Analyzing Moving Boundaries Using R
CSIR	Council for Scientific and Industrial Research
CSV	Comma-separated values
DSAS	Digital Shoreline Analysis System
EPR	End Point Rate
ESA	European Space Agency
ESRI	Environmental Systems Research Institute
GEE	Google Earth Engine
GENESIS	GENEralized model for Simulating Shoreline Change
GIS	Geographic Information Systems
GPS	Global Positioning System
HWL	High-Water Line
IPCC	Intergovernmental Panel on Climate Change
kyr	Thousand years
LiDAR	Light Detection and Ranging
LRR	Linear Regression Rate
MNDWI	Modified Normalized Difference Water Index
MPA	Marine Protected Area
NGI	National Geo-spatial Information
NOAA	National Oceanic and Atmospheric Administration
NOS	National Ocean Service
NSM	Net Shoreline Movement
OGAS	Orthogonal Grid Address System
QGIS	Quantum Geographic Information System
RMSE	Root Mean Square Error
SAR	Synthetic Aperture Radar
SCA	Shoreline Change Analysis
SCE	Shoreline Change Envelope
SLC	Scan Line Correction
SWIR	Short-Wave Infrared
USGS	United States Geological Survey
WCNP	West Coast National Park
WLR	Weighted Linear Regression

LIST OF FIGURES

Figure 1.1: Comparison of before and after the June 2017 storm, which damaged the dune cordon and infrastructure along the southern section of Sixteen-Mile Beach…….. 2

Figure 2.1: a) Satellite image of the study site and the three sections of shoreline under investigation: Sixteen-Mile Beach, Yzerfontein Main Beach and Pearl Bay. b) Study site's location within the Western Cape Province and c) within South Africa…….. 6

Figure 2.2: a) Map of Yzerfontein indicating the names of the beaches and rock outcrops. b) Oblique drone photograph of Gabbro Point looking south towards Yzerfontein Main Beach and the town centre. c) View from Die Skeiding along Pearl Bay looking southwards…….. 8

Figure 2.3: a) Map of Sixteen-Mile Beach with the main features labelled. b) Oblique drone photograph of the southern end of Sixteen-Mile Beach facing north-west. c) The view from Tsaarbank at the northern end of Sixteen-Mile Beach 10

Figure 2.4: Average monthly rainfall and temperature graph for Yzerfontein…….. 12

Figure 2.5: Wind-rose plots of the wind direction and speed showing the annual averages, and the Summer and Winter differences, recorded between 1960 to 2014 for the Robben Island to Dassen Island area…… 12

Figure 2.6: Average wave swell height and direction recorded between 1960 and 2014 for the Robben Island to Dassen Island area…… 13

Figure 2.7: a) Topography and bathymetry of the study site overlaid with the main geological formations. b) Geology of the region showing the longshore drift patterns and swell barriers next to Dassen Island and Robben Island…….. 14

Figure 3.1: Cross-section diagram of the different proxy and datum shoreline indicators…….. 21

Figure 4.1: Screenshot of the georeferencing process within ArcMap (v10.6) showing the historical aerial photograph overlayed onto an ESRI high-resolution imagery basemap, the eight ground control points, and root mean square error table…… 37

Figure 4.2: Example of CoastSat shoreline detection process, indicating the shoreline in black on a Sentinel-2 true colour image (left), the classified image of sand, white-water, water and other (centre), and the MNDWI values showing low values in blue and high values in red (right)…… 42

Figure 4.3: Flowchart of processes conducted within the CoastSat toolkit…….. 47

Figure 4.4: a) Map of a perpendicular transect through the shoreline positions from the different time periods and their respective uncertainty values as buffers. b) Plot of the linear regression and weighted linear regression for distance from the baseline versus time…… 50

Figure 4.5: Location of six case-study sites selected for the short-term analysis…… 52

Figure 4.6: Transect intersecting with the short-term shorelines at Yzerfontein Main Beach…….. 53
Figure 4.7: Summary flowchart of the entire research report methodologies…….. 56
Figure 5.1: A) Map of net shoreline movement (NSM) along the study site with warm colours representing erosion and cool colours representing accretion. B) Graph of NSM vs. the 100 m-transects along the coast…….. 58
Figure 5.2: A) Map of the Weighted Linear Regression rates along the study site with warm colours representing erosion and cool colours representing accretion. B) Graph of WLR at every 100m transect along the coast and the 95% confidence interval…… 65
Figure 5.3: Summary of DSAS results showing a) the Net Shoreline Movement (NSM), b) Shoreline Change Envelope (SCE), c) End Point Rate (EPR), d) Linear Regression Rate (LRR), and e) the Weighted Linear Regression (WLR)…….. 67
Figure 5.4: Timeseries heat-matrix representing the amount of change to the shoreline with regards to the 1937 shoreline position over the eleven time periods…….. 69
Figure 5.5: Cross-shore change between August 2015 and December 2020, derived from Sentinel-2 data, for six locations along the study site…….. 71
Figure 5.6: Shoreline position forecasts for the next 10 and 20 years with their horizontal uncertainty for four locations along the study site: a) Yzerfontein Main Beach and the southern end of Sixteen-Mile, b) the northern end of Pearl Bay, c) the erosion hotspot located 6 km north of Gabbro Point, and d) the northern end of Sixteen-Mile Beach at Tsaarbank. …….. 74
Figure 6.1: A comparison between the historical aerial photograph from 1937 and the panchromatic Landsat 8 image from 2020 showing the change in shoreline position and coastal dune distribution…… 79
Figure 6.2: Screenshot of the results obtained from the global study on long-term shoreline change conducted by Luijendijk *et al*. (2018) for Yzerfontein and Sixteen-Mile Beach…… 81
Figure 6.3: Signposts around Yzerfontein promoting dune protection and rehabilitation…….. 87

LIST OF TABLES

Table 4.1: Summary of the historical aerial photographs data…….. 36
Table 4.2: Estimated total shoreline uncertainty for each of the historical aerial photographs……. 39
Table 4.3: Summary of satellite imagery used by CoastSat…….. 42
Table 4.4: Landsat image selection dates for the long-term analysis…….. 45
Table 4.5: Estimated total shoreline uncertainty for each of the Landsat images…….. 47
Table 5.1: Summary of Net Shoreline Movement (NSM) to the study site shoreline and its three beaches with landward movement as negative and seaward movement as positive…… 59
Table 5.2: Summary of Shoreline Change Envelope (SCE) along the study site shoreline and its three beaches irrespective of the direction of movement. 60
Table 5.3: Summary of End Point Rates of change (EPR) to the study site shoreline and its three beaches with erosional rates as negative and accretional rates as positive…… 61
Table 5.4: Summary of Linear Regression Rates of change (LRR) to the study site shoreline and its three beaches with erosional rates as negative and accretional rates as positive…… 62
Table 5.5: Summary of Weighted Regression Rates of change (WLR) to the study site shoreline and its three beaches with erosional rates as negative and accretional rates as positive…….. 64

Chapter 1:

INTRODUCTION

1.1 Background

The world's coastlines are ever-changing dynamic environments, which vary over space and time; from bi-daily tidal cycles, to rapid storm surges and tsunamis, to being submerged and exposed during glacial cycles over millennia (Boak & Turner, 2005; Masselink *et al*., 2011; Jackson & Short, 2020). Moreover, the Intergovernmental Panel on Climate Change (IPCC) has identified Earth's coastlines as being one of the worst affected zones because of anthropogenic climate change resulting in increased mean sea-level, storm surges and coastal erosion (Oppenheimer *et al*., 2019). In particular, sandy coastlines are at high risk to erosion and sediment loss, leading to the destruction of human settlements and ecosystems in these affected regions (Hinkel *et al*., 2013; Luijendijk *et al*., 2018; Mentaschi *et al*., 2018; Vousdoukas *et al*., 2020). It is reported by Hinkel *et al*. (2013: pp.150) that "about 6000 to 17000 km^2 of land is expected to be lost during the 21^{st} century due to enhanced coastal erosion associated with sea level rise, in combination with other drivers"; whereas Vousdoukas *et al*. (2020: pp.260) project a more drastic outlook of a "near extinction of almost half of the world's sandy beaches by the end of the century". These findings emphasise the need to understand trends of coastal erosion which present a global risk to coastal communities.

Africa has the largest proportion of sandy coastlines in the world, consisting of 66% of the continent's perimeter (Luijendijk *et al*., 2018). Moreover, 80% of South Africa's coastlines are composed of sandy beaches, signifying that a large proportion of this country's coastal

settlements and environments could be at an increased risk of destruction from coastal erosion (Theron and Rossouw, 2008; Wigley, 2011). In June 2017, a strong low pressure system, locally named 'Cape Storm', moved over the country's Western Cape Province. It brought extreme wind, rain, significant swell waves and storm surges that caused extensive damage to infrastructure and eroded stretches the region's coastline, including Sixteen-Mile Beach (Renwick, 2018; Rautenbach *et al*., 2020; Barnes *et al*., 2021; Troch *et al*., 2021).

1.2 Problem Statement and Rationale

Sixteen-Mile Beach, located in southwestern South Africa, near the small town of Yzerfontein, is said to be one of the country's longest continuous sandy beaches, stretching approximately 26 km through the West Coast National Park and Marine Protected Area (WCNP & MPA) (Yzerfontein.net, 2021). This nature and tourism destination is known for its wild beauty, however, the 'Cape Storm' of 2017 resulted in significant damage to a section of dune cordon, and the destruction of properties and businesses along the eroded dune (Renwick, 2018) (Figure 1.1).



Figure 1.1: Comparison of before and after the June 2017 storm, which damaged the dune cordon and infrastructure along the southern section of Sixteen-Mile Beach. (Sources: left photograph from Dance Floor Hire (www.dancefloorhire.co.za/project/strandkombuis-wedding/strandkombuis-wedding-2/), right photograph by Duncan Miller, used with permission).

Increased coastal erosion and storm surges may affect the community of Yzerfontein and the unique coastal fynbos ecosystems within the West Coast National Park (WCNP). Therefore, it is important to investigate and understand how this coastal environment has changed in the past and to determine if the rates of change are increasing. Understanding long-term changes and short-term variability can aid in determining future changes to the shoreline, thereby helping to assess which areas are most at risk to coastal geohazards (Luijendijk *et al*., 2018; Oppenheimer *et al*., 2019).

In South Africa, there are various national legislations which address the country's coastlines, such as the Integrated Coastal Management Act (Act 24 of 2008), as well as provincial policies which delineate 'coastal set-back lines' for new developments (Umvoto Africa, 2011; Stewart *et al*., 2013; Van Weele *et al*., 2014; Colenbrander and Sowman, 2015). Shoreline monitoring has been conducted along Saldanha Bay (located north-east of Sixteen-Mile Beach), where a 3.5 km artificial barrier beach was built within the Bay to protect the Saldanha iron ore jetty from strong swell waves (Zwemmer and van't Hoff, 1982; Schoonees *et al.,* 1990; Flemming, 2020). Several studies have been conducted to monitor historical shoreline changes on some of South Africa's beaches, especially around Cape Town (Callaghan, 2014; Callaghan *et al*., 2015; Fourie *et al*., 2015). Additionally, sediment samples have been dated and characterised by Franceschini (2003), Compton and Franceschini (2005), and Franceschini and Compton (2006). However, to date, no literature has been found to monitor the long-term shoreline changes on the West Coast, specifically, Yzerfontein and Sixteen-Mile Beach. This research report will contribute valuable insight into how this stretch of sandy coastline has changed over the last eight decades, and how it may change in the near future.

Remote sensing has commonly been the most popular, efficient and cost-effective method to track the horizontal changes to shoreline environments over time (Gens, 2010; Burningham and Fernandez-Nunez, 2020) and has been used as far back as the late 1940s and 1950s through aerial photography analyses (Shalowitz, 1940; McCurdy, 1947; McBeth, 1956). Yet, as earth observation techniques and computational abilities have improved over time, so have remote sensing methodologies, allowing for shoreline change studies to take place at various spatial and temporal scales (Gens, 2010; Teodoro, 2016; Luijendijk and de Vries, 2020). This research report utilises these remote sensing advancements by combining different methodologies to extract and analyse horizontal shoreline changes, namely *CoastSat* and the *Digital Shoreline Analysis System* (DSAS). DSAS is an ArcGIS extension, which calculates the amounts and rates of change to shoreline data, and *CoastSat* is a novel Python toolkit that automatically extracts shoreline positions from public satellite imagery (Himmelstoss *et al*., 2018; Vos *et al*., 2019b).

1.3 Aim

The aim of this research report is to investigate the spatiotemporal changes to the shoreline around Yzerfontein and Sixteen-Mile Beach between 1937 and 2020 and to project future shoreline changes, using integrated remote sensing data, the *CoastSat* automatic shoreline extraction software, and the Digital Shoreline Analysis System (DSAS).

1.4 Objectives

1. To extract shoreline positions from historical aerial photographs dated 1937, 1960 and 1977, by digitising the high-water line.

2. To automatically extract shoreline positions from Landsat 5, 7 and 8 and Sentinel-2 imagery between 1985 and 2020 using the *CoastSat* toolkit and Google Earth Engine.
3. To quantify and analyse rates of shoreline change from aerial and satellite datasets using the Digital Shoreline Analysis System (DSAS) to present long-term and short-term representation of the coastline's dynamics.
4. To model future (10 and 20 year) shoreline positions using the DSAS shoreline forecasting tool.

1.5 Outline of the research report

Following on from this introductory chapter, which provides the background, rationale, aims and objectives to the study, the following six chapters of this research report are divided into standard reporting themes. Chapter 2: Study Site, describes the background of the area and its climate, landscape, and geology. Chapter 3 presents a literature review covering the themes of shoreline change, the use of remote sensing, as well as the advancements and debates in the field. Chapter 4 describes the various data sources and methodologies used to delineate the shoreline positions and calculate the changes, which are subsequently presented and explained in the Results of Chapter 5. The Discussion (Chapter 6) explores how the findings of this report relate to other studies and the implications that can be extrapolated from the results, as well as its limitations and suggestions for potential future research. Finally, Chapter 7 provides the overall conclusion of the study.

Chapter 2:

STUDY SITE

2.1 General setting

The research report study site covers a 30 km stretch of South Africa's southwestern coastline situated around the West Coast National Park and the small town of Yzerfontein (33°20'50"S; 18°08'60"E) which is approximately 80 km north of Cape Town in the Western Cape Province (Figure 2.1). This coastline comprises of three different sandy beaches which are the main areas under investigation; namely Sixteen-Mile Beach, Yzerfontein Main Beach to the north of the town, and Pearl Bay to the south of the town.

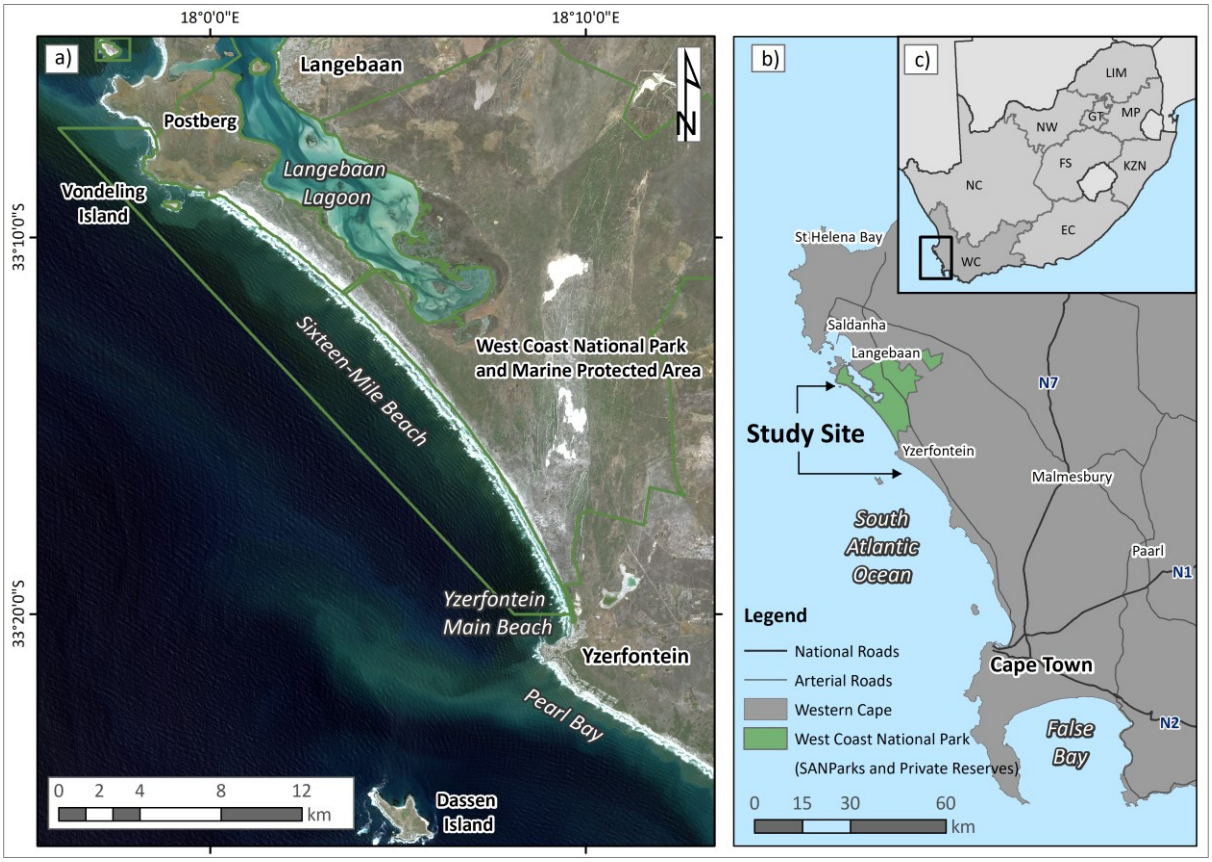


Figure 2.1: a) Satellite image of the study site and the three sections of shoreline under investigation: Sixteen-Mile Beach, Yzerfontein Main Beach and Pearl Bay. b) Study site's location within the Western Cape Province and c) within South Africa (See Appendix A1 for map data sources).

Sixteen-Mile Beach is known to be one of the longest uninterrupted sandy beaches in South Africa and most of it falls within the West Coast National Park and Marine Protected Area (WCNP). The Park was officially proclaimed in 1985 to protect and conserve the unique and ecologically sensitive Langebaan Lagoon and surrounding coastal fynbos ecosystems (Hanekom *et al*., 2009; WCNP, 2013). At the southern end of Sixteen-Mile Beach is the small town of Yzerfontein. The town's name translates from Afrikaans and Dutch to "iron fountain", named after a small natural spring producing dark ferrous water. Yzerfontein was founded as a town in 1937 when portions of farmland along the coast were marked out for development (Yzerfontein Tourism, 2021). Over the decades, it has gradually grown into a small town of more than 1500 people, with the main draw of the town being tourism and the development of second homes (Lemmen, 2011).

2.2 Description of the three shoreline beaches

2.2.1 Yzerfontein Main Beach

Yzerfontein Main Beach is the prominent tourist beach for the town. It spans 800 m from the harbour and rocky headland, on which most of the town is built, to the small rock outcrop of Gabbro Point (also known as *Rooipan se Klippe*) (see Figure 2.2a and b). It is a gently-sloping, fine-grain beach, approximately 60 m wide. Half the beach is backed by the public access car park while a small, protected dune cordon backs the other half, opposite to the town's caravan park. Out to sea, there is another rock outcrop called *Meeurots*, which, in conjunction with the harbour seawall, dissipates some of the wave energy before it reaches the beach (Figure 2.2a).

2.2.2 Pearl Bay

Pearl Bay is the name given to the southern and newer side of Yzerfontein which has seen the continuous growth of luxury holiday-home properties since the early 2000s (Lemmen, 2011). The Pearl Bay coastline measures 3.5 km from Skaap Island to the southern edge of the town (Figure 2.2a). Pearl Bay consists of four smaller embayments around various rock outcrops, namely *Skaap Island, De Goede se Baai, Bakoond* and *Die Skeiding* (Figure 2.2a). However, this report groups these smaller beaches together as 'Pearl Bay'. These smaller beaches have slightly steeper profiles with partially vegetated dunes backing them, followed by houses (Figure 2.2 c).



Figure 2.2: a) Map of Yzerfontein indicating the names of the beaches and rock outcrops. b) Oblique drone photograph of Gabbro Point looking south towards Yzerfontein Main Beach and the town centre (Photograph by Stephen Davey 2019, used with permission). c) View from *Die Skeiding* along Pearl Bay looking southwards (Author's photograph, November 2020).

2.2.3 Sixteen-Mile Beach

This stretch of coast is known as one of the longest uninterrupted sandy beaches in South Africa, arching 26 km in a log-spiral shape from Gabbro Point in the south, to Tsaarbank in the north (Figure 2.3). From south to north, the steepness of the beach and the coarseness of the sand increases slightly as less terrestrial sediment travels northwards via longshore drift (Franceschini *et al*., 2003; Franceschini and Compton, 2006). Franceschini and Compton, (2006) describe the site as forming part of a larger dune complex, comprising of the beach, the active foredunes and partially-vegetated to vegetated parallel dune cordons stretching 24 km inland to the Geelbek Dunes (Figure 2.3a). Approximately 3 km south from Tsaarbank is another small igneous outcrop known as Black Rock, which is only visible during low tide and does not interrupt the sandy beach. It is also at this location that the *Pantelis A. Lemos* cargo ship was shipwrecked in 1978 (South African History Online, 2020).

The northern half of Sixteen-Mile Beach forms a peninsular that separates Langebaan Lagoon and Saldanha Bay from the South Atlantic Ocean, while the southern half forms part of the mainland. Inland, at the central portion of Sixteen-Mile Beach, is a place referred to as Abrahamskraal. This portion was land was once controlled by the Department of Forestry who aimed to stabilise and vegetate the large plumes of drift sand in the 1970s, before it was amalgamated into the West Coast National Park (Boucher, 1981; Franceschini, 2003; Franceschini and Compton, 2006). The beach is classified by the WCNP as a ‘remote zone’ as it maintains its “intrinsically wild appearance and character” (WCNP, 2013: pp.19) and there is little direct access to it, apart from three footpaths (at Yzerfontein, Tsaarbank and Abrhamskraal).

Most Sixteen-Mile Beach falls within the WCNP, except for the southern end near Gabbro Point where there are a row of holiday accommodations and a restaurant behind the dune, as well as a new housing complex that is being developed. This southern end of Sixteen-Mile Beach is where a large amount of the foredune was eroded during the June 2017 storm and where the dunes continue to experience erosion (see Figure 1.1). Behind these dunes is also a coastal salt pan called Rooipan (Figure 2.2a).

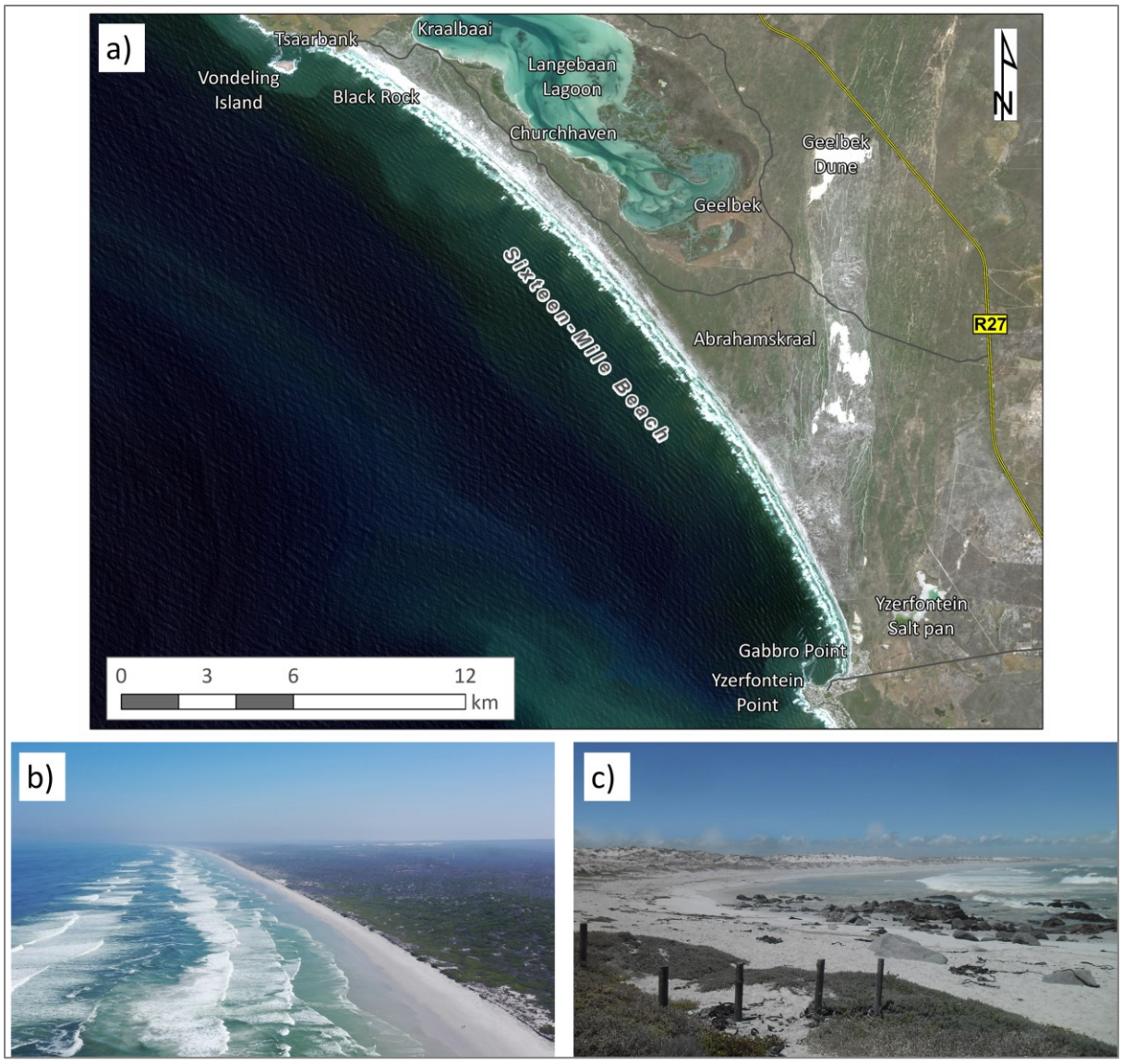


Figure 2.3: a) Map of Sixteen-Mile Beach with the main features labelled. b) Oblique drone photograph of the southern end of Sixteen-Mile Beach facing north-west (Photograph by Stephen Davey 2019, used with permission). c) The view from Tsaarbank at the northern end of Sixteen-Mile Beach (Author's photograph, November 2020).

2.3 Climate, ocean and landscape of the study site

This southwestern region of South Africa has a semi-arid Mediterranean climate, with dry, warm summers and cool, wet winters. Summer temperatures range between 12°C and 28°C and average at 19°C, while winter temperatures average at 13°C (Mauger and Compton, 2011; Climate-Data.org, 2021) (Figure 2.4). The majority of rainfall occurs in the winter months over a concentrated period of 49 days per annum (Flemming, 2015) and totals to 355 mm per annum (Climate-Data.org, 2021). The seasonal differences occur as a result of global circulation patterns, whereby the South Atlantic Anticyclone brings dry and stable conditions in the summer, which then shifts northward in the winter and is replaced by mid-latitude cyclones (Franceschini *et al*., 2003; Roberts *et al*., 2009; Browning and Roberts, 2015). These mid-latitude cyclones usually present as cold-front systems, which move from west to east across the southern Western Cape Province, bringing rainfall.

The pressure systems also drive the prevailing wind patterns (Figure 2.5). In summer, the South Atlantic Anticyclone drives strong southerly to south-westerly winds onshore, while the winter cold-fronts bring north-westerly winds (Franceschini *et al*., 2003; CSIR, 2014; Flemming, 2015). However, the southern summer winds dominate the annual wind patterns (Figure 2.5). Additionally, average annual offshore winds around the study site range between 5 and 6 m/s (CSIR, 2014).

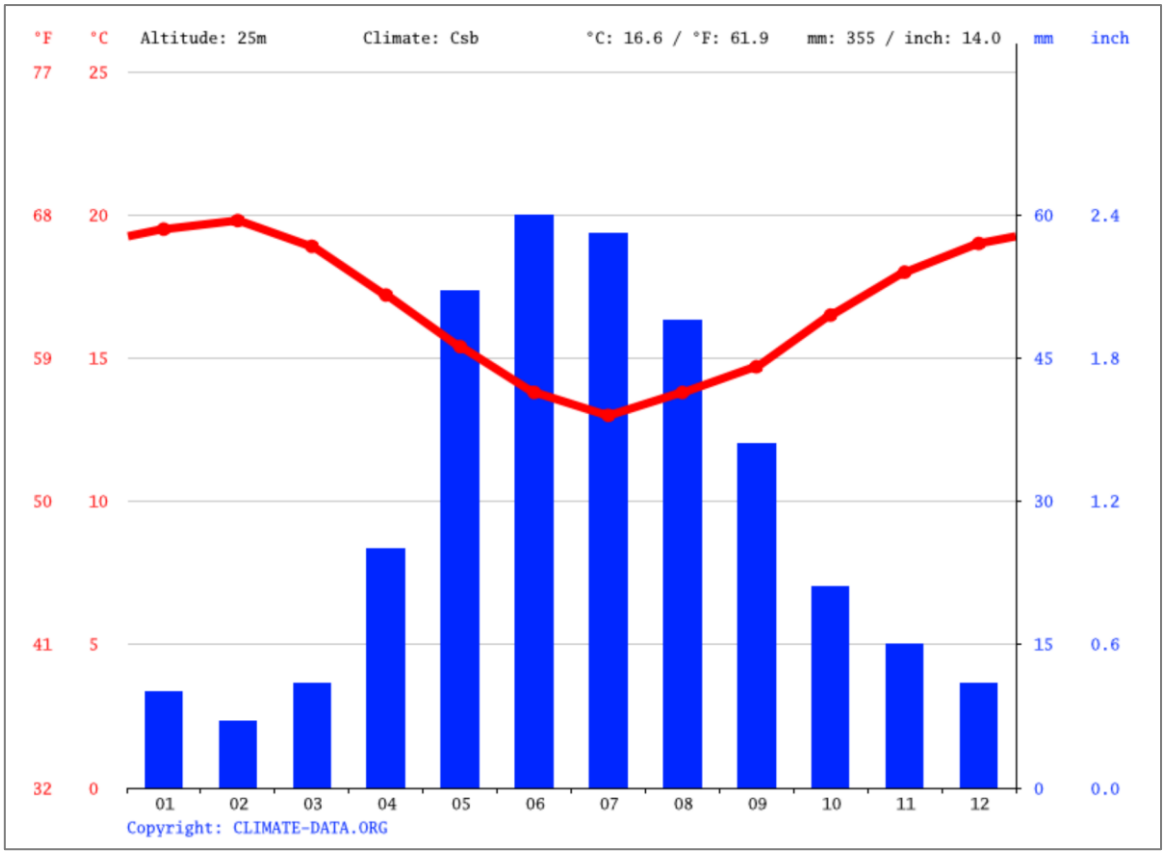


Figure 2.4: Average monthly rainfall and temperature graph for Yzerfontein (Source: Climate-Data.org, 2021).

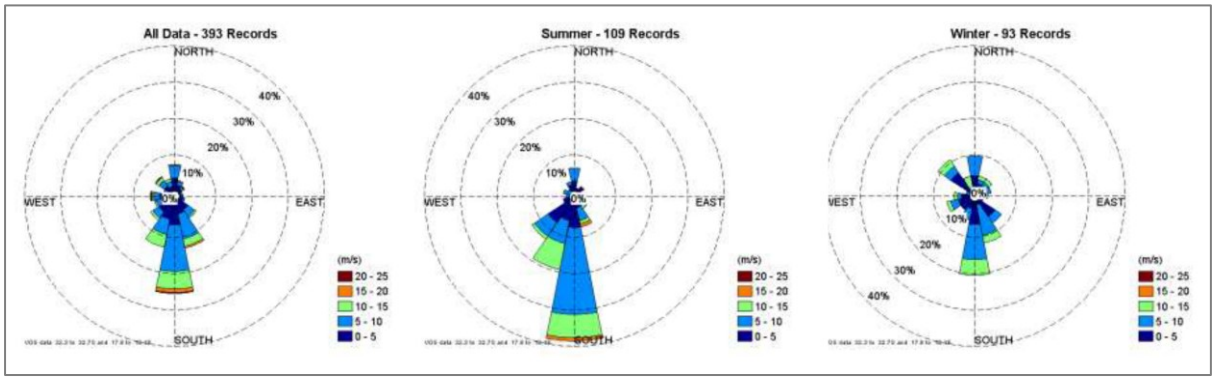


Figure 2.5: Wind-rose plots of the wind direction and speed showing the annual averages, and the Summer and Winter differences, recorded between 1960 to 2014 for the Robben Island to Dassen Island area (Source: CSIR, 2014 pp.72).

According to global coastal system classifications, this region is microtidal, with a tidal range of less than 2 m, and is dominated by a west coast swell (Masselink *et al*., 2011; Musekiwa *et*

al., 2015). This means that the coast receives most of its energy from waves instead of the tides. The beach profile has a gentle gradient; consisting of a wide beach width and surf-zone with multiple lines of breaker waves. Hence, the morphodynamics of the site are dissipative instead of reflective (Harris *et al*., 2011). The region experiences an average swell height of 3 m from a southerly to south-westerly direction (Figure 2.6) and is controlled by the dominant cold Benguela current, which travels north from the Antarctic Circle and against southern Africa's western coast. As a result of both the prevailing southerly winds, the south to south-westerly swell and Benguela current, the coastline experiences a net longshore drift of sediment in a northerly direction (Figure 2.6 and Figure 2.7b).

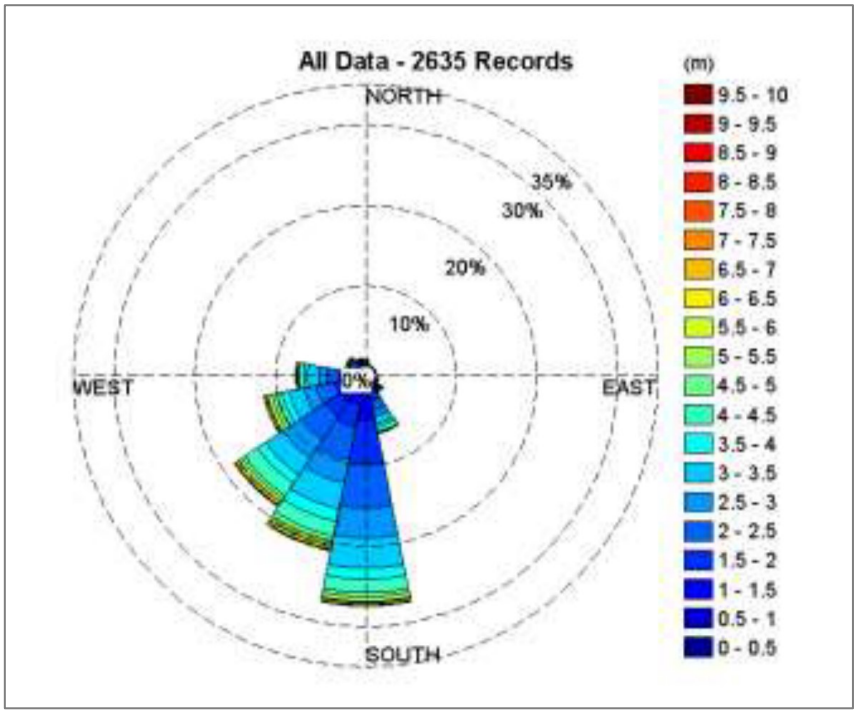


Figure 2.6: Average wave swell height and direction recorded between 1960 and 2014 for the Robben Island to Dassen Island area (Source: CSIR, 2014 pp.76).

The terrestrial sediments that are transported by longshore drift originate from rivers that drain around Cape Town into False Bay and Table Bay, such as the Eerste and Diep River

(Figure 2.7b). These perennial rivers are fed from larger water catchment areas that receive higher annual rainfall compared to further up the coast where the annual rainfall decreases and no perennial rivers drain into the ocean (Compton, 2016). Franceschini *et al*. (2003) found that the varying sediment supply from rivers and the longshore drift patterns resulted in changes of beach sand composition in the region. Specifically, more fine-grain terrigenous-rich sand is found closer to Cape Town, while the sand becomes coarser and more carbonate-rich towards Saldanha Bay (Franceschini, 2003; Franceschini *et al*., 2003).

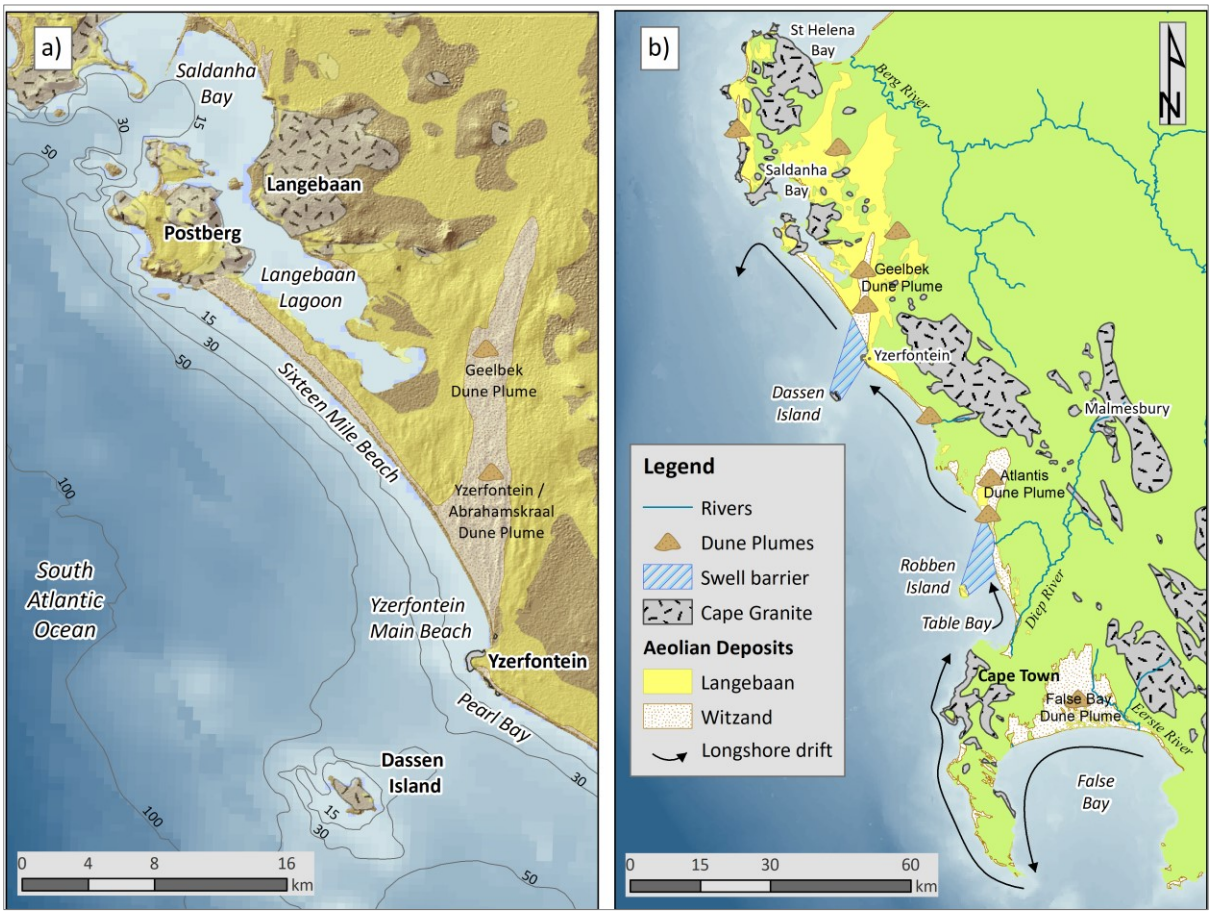


Figure 2.7: a) Topography and bathymetry of the study site overlaid with the main geological formations. b) Geology of the region showing the longshore drift patterns and swell barriers next to Dassen Island and Robben Island (adapted from Compton, 2016: 75).

According to Compton (2016), Robben Island and Dassen Island intercept the southwestly ocean swell creating a 'swell barrier'. These barriers then allow for ocean sediment to accumulate and be transported inland by the southerly winds, forming the extensive dune plumes seen at Atlantis (between Yzerfontein and Cape Town), and Geelbek (inland from Sixteen-Mile Beach) (Figure 2.7).

These dune plume systems have been extensively studied by Franceschini (2003) Compton and Franceschini (2005), Franceschini and Compton (2006), Roberts *et al*. (2009), Roberts *et al*. (2014), and Browning and Roberts (2015). The dunes plumes extend along the West Coast from False Bay to St Helena Bay and are composed of fine white sand deposited in a north-south orientation to the coastline (Boucher, 1981). They form part of the Witzand Formation, which are the youngest geological deposits in the region, and are thought to have been formed during the Holocene (~ last 10,000 years) (Franceschini, 2003; Compton and Franceschini, 2005; Franceschini and Compton, 2006; Browning and Roberts, 2015).

Several studies by Franceschini (2003), Franceschini and Compton (2006), Kandel and Conard (2013) and Henrico *et al*., (2020) have identified that the Geelbek-Yzerfontein dune system is dynamic and has seen a significant movement and reduction in size over the decades. This further highlights the need to conduct a shoreline change analysis study along this Witzand coast since it forms part of a larger dynamic geological system.

Other researchers such as Flemming (1977), Compton (2001), Mauger and Compton (2011), Roberts *et al*. (2011) and Flemming (2015), have all theorised how the landscape and shoreline would have looked like thousands of years ago with respect to varying sea-levels.

For example, Compton (2001) has investigated fluctuations in sea-level over the last 6,800 years (6.8kyr) by radiocarbon dating samples of salt marshes at the southern end of Langebaan Lagoon; finding that in the last 4.9 kyr, the sea-level has remained within ±1 m of present-day levels. Flemming (2015) also illustrates how Langebaan Lagoon formed and has been reshaped over thousands of years, with the northern part of Sixteen-Mile Beach once being a barrier island during the Last Interglacial (120 kyr) and again during the Holocene at 6.3 kyr. Over the millennia, these Holocene dunes have prograded, forming the peninsula between the South Atlantic Ocean and Langebaan Lagoon (Figure 2.7).

In addition, at the southern end of Sixteen-Mile Beach are Yzerfontein Pan and Rooipan (see Figure 2.2a). Mauger and Compton (2011) highlight how these were once connected to the ocean as a lagoon during the Last Interglacial, when the sea levels were higher. The coastline then started to prograde and dune cordons started to develop. This cut off the Yzerfontein Pan, leaving only Rooipan to be inundated by sea water until the Holocene dune cordons further developed (Mauger and Compton, 2011). The evaporated seawater left behind a layer of salt, all of which was mined by early Dutch settlers and shipped to Cape Town. Presently, Yzerfontein Pan is mined for gypsum.

The region is also home to various significant archaeological findings (Orton *et al*., 2020). For example, a rock shelter next to Yzerfontein's harbour was found to contain Middle Stone Age artefacts and evidence of human occupation dating between 110 kyr and 71 kyr (Avery *et al*., 2008; Wurz, 2012). Geelbek Dune was also found to contain vast amounts of archaeological and paleontological discoveries, ranging from the Middle and Late Stone Age (Kandel and Conard, 2013). In addition, fossilised human footprints from 117 kyr were discovered along

the northwestern bank of Langebaan Lagoon, near Kraalbaai (Roberts and Berger, 1997) (see Figure 2.3a). Compton and Franceschini (2005) also note of more modern (<1 kyr) shell middens along Sixteen-Mile Beach's active foredunes. All these archaeological sites show how humans have utilised this region's coastal resources for thousands of years. This gives society a greater understanding into southern Africa's extensive human history. Coastal erosion and storm surge events pose a risk to some of these archaeological sites, and could possibly damage or destroy sites which have yet to be discovered along this pristine coastline.

2.4 Summary

This chapter presents the study site of the research report by summarising the general characteristics of the Yzerfontein and Sixteen-Mile Beach coastline. The study site is also contextualised within its wider region by showing how the climate, ocean and landscape are all interconnected. This chapter also highlights the importance of the site in terms of its social and economic value as a tourism destination, its environmental value as a national conservation area and its heritage value from the unique archaeological sites found at the harbour and within the dune systems. Hence, it is important to map and monitor how the shoreline has changed in the past decades and model how it might change in the future.

Chapter 3:

LITERATURE REVIEW

3.1 Introduction

The purpose of this literature review is to provide a theoretical foundation for the evaluation of the field of Shoreline Change Analysis (SCA). The chapter begins with an overview of the coastal processes and morphodynamics that result in shoreline changes. It then summarizes how the field of SCA has developed over time by providing a chronological review of its background, key authors and the significant improvements in data and techniques. Additionally, the review addresses key issues and debates associated with SCA. There is also a specific focus on how remote sensing and the Digital Shoreline Analysis System (DSAS) have advanced the field of SCA.

3.2 Coastal systems and processes

The land-sea interface is considered one of the most dynamic zones on Earth, where multiple forces join together to continuously shape and change this zone at varying spatial and temporal scales (Masselink *et al*., 2011; Jackson and Short, 2020). These forces and sources of energy acting on coastlines include the global atmospheric patterns of wind and precipitation, and marine forces of waves, tides and currents. Coastal environments are complex open systems with energy and matter entering and exiting the system wherein there are the internal components of landforms and geology, which self-organise to maintain system equilibrium (Masselink *et al*., 2011).

In particular, sandy beaches are the most dynamic type of coastal landforms as the loose sediment is more easily moved and reworked (Hinkel *et al*., 2013; Vousdoukas *et al*.,

2020). This is dependent on the sediment budget, where a net loss in sediment results in erosion, and a net gain in accretion. There are different drivers for erosion and accretion, which include the amount of sediment supply from rivers and runoff, wave and tide energy, as well as longshore drift (Jackson and Short, 2020). Anthropogenic drivers of erosion occur when river courses are controlled and dammed, leading to less terrestrial sediment entering the oceans, or when beach sand is directly mined (Defeo *et al*., 2009; Mentaschi *et al*., 2018). Alternatively, accretion can be caused when beaches are artificially built up (also known as beach nourishment) or beach barriers are put in place (Defeo *et al*., 2009; Mentaschi *et al*., 2018; Flemming, 2020).

Changes in sea-level are considered to be a dominant and global force for coastal erosion, as stated in Bruun's Rule of Erosion (Bruun, 1988). The rule states that the shoreface profile always aims to maintain an equilibrium, such that "when sea levels rise, the shoreface profile adjusts by rising and moving landward by coastal erosion" which results in a horizontal shoreline retreat (Masselink *et al*., 2011: 216). Many researchers have opposed Bruun's Rule and claim that it is out of date and has not been sufficiently supported by actual field measurements as it over-simplifies the complexities of coastal systems (Cooper and Pilkey, 2004; Masselink *et al*., 2011; Cooper *et al*., 2020). However, Bruun himself has always warned of the limitation of the 'rule' as it is a theoretical two-dimensional model which may not fully translate to the 'real' three-dimensional coastal setting, and has also observed how it tends to be misused by coastal researchers (Bruun, 1988).

A key component of understanding coastal systems and their dynamics is how we define coastal zones, coastlines, and shorelines. Coastal zones are considered to be the wider area

between the +200 m and -200 m elevation contours (Gens, 2010) or from the coastal plain to the continental shelf (Masselink *et al*., 2011), whereas the shoreline is defined more specifically as "the intersection of water and land surfaces" (Boak and Turner, 2005: 688). Boak and Turner (2005) provide the most substantial review of various shoreline definitions as there are many ways to delineate the land and sea interface. These can be grouped into three main categories: visual proxies, datum proxies and remote sensing proxies. Figure 3.1 illustrates examples of these different markers with the visual proxies in black and datum proxies in blue. Visual proxies include features that are easily identified on the ground or from aerial imagery such as the cliff edge, dune edge, seaward vegetation line, instantaneous water line, or high water line. In contrast, datum lines use tidal data which are calibrated to a geodetic system and elevation model over a span of time (usually 19 years) which measures the mean sea level and mean high and low water levels (Ruggiero and List, 2009; Moore *et al*., 2006). Shorelines can also be delineated from remote sensing data such as multispectral satellite imagery. These shoreline markers are further analysed and critiqued later in the literature review (see Section 3.4 and 3.5).

Applying these fundamental concepts of how coastal systems operate, as well as the different ways of defining the shoreline, can help us to study how shorelines change and ways in which changes and be quantified. The following sections aim to provide a historical overview of the SCA literature and methodologies that have been specifically developed to address how coastal researchers map, measure and model shoreline dynamics.

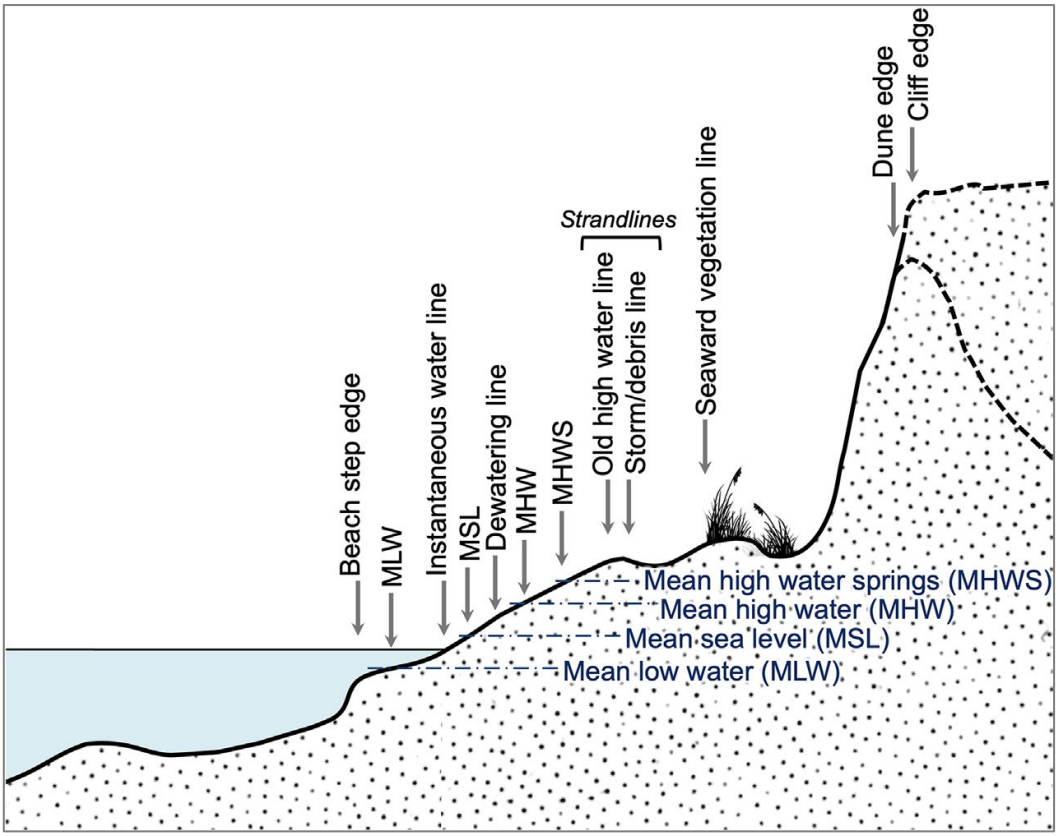


Figure 3.1: Cross-section diagram of the different proxy and datum shoreline indicators (Source: Burningham and Fernandez-Nunez, 2020: 442, in Jackson and Short, 2020).

3.3 History and background of shoreline change analysis

The field of shoreline change analysis (SCA) was formally established in the 1970s when the technologies and methodologies became sufficiently advanced to measure and evaluate shoreline dynamics, but its origins can be traced back to previous shoreline studies from earlier decades including research conducted by Shalowitz (1940), McCurdy (1947), and McBeth (1956). Shalowitz (1940), who mapped the impact of hurricanes and large storms along Long Island in the United States and promoted the importance of surveying and resurveying coastal areas to better understand and manage coastlines, published one of the earliest academic publications into mapping coastal changes. Moreover, McCurdy (1947) established a photogrammetry manual on interpreting shorelines and coastal features from aerial photographs as this field rapidly developed after the Second World War. McCurdy

(1947) also emphasised the importance of understanding the area being mapped, having secondary material such as field notes, surveying notes, ordinary photographs, and experience with photogrammetry, in order to create more accurate maps and charts in the future. Similarly, McBeth (1956) further explored photogrammetric methods of delineating the shoreline from stereo pairs of aerial photographs by analysing colour, tone and texture to differentiate between sandy beaches, coastal vegetation and rocky shorelines. This methodology includes the process of delineating the high water line by comparing tonal changes in wet versus dry sand and the possible errors that can be incurred by the photogrammetrist (McBeth, 1956).

Apart from using aerial photography, historical maps and nautical charts were other data sources that early coastal researchers utilised (de Boer and Carr, 1969; Hapke *et al*., 2011; NOAA, 2016; Burningham and Fernandez-Nunez, 2020). The Ordnance Survey in the UK has an extensive history of mapping Britain's coastlines from as far back as the late 18th and early 19th century (de Boer and Carr, 1969; Burningham and Fernandez-Nunez, 2020). While in the United States, *'The Survey of the Coast*' project was founded in the 1830s to accurately map the land and nautical features around the US to provide vital information for international and inter-state shipping routes (NOAA, 2016). These maps are referred to as NOS T-Sheets (National Ocean Survey Topographic-Sheets) and have provided a rich source of shoreline data for more than 180 years (Hapke *et al*., 2011). De Boer and Carr (1969), have used even older historical maps and charts to show how the coastlines around Yorkshire and Suffolk in the UK have changed over hundreds of years, with some records dating back to the 14th, 15th and 16th centuries.

By the 1970s, large portions of the US East Coast had been photographed by aircrafts on multiple occasions, leading to an accumulation of at least 30 years' worth of aerial photographs that could be studied (Stafford and Langfelder, 1971; Dolan *et al*., 1978). Coastal researchers began documenting the complex feedback and linkages of coastal systems and the term 'morphodynamics' was coined in the 1970s to describe the landforms and processes within coastal environments (Jackson and Short, 2020). Additionally, coastal researchers were becoming increasingly aware of the risks posed by coastal erosion, with the International Geographical Union creating working groups on the Dynamics of Coastal Erosion (197 –1976) and the Commission on the Coastal Environment (1976–1984) (Luijendijk and de Vries, 2020). This led to the drafting of various national coastal management acts and policies in both the United States and United Kingdom (Ellis, 1978; Burningham and Fernandez-Nunez, 2020). Therefore, standard practises and methodologies were created which provided the foundations for the field of shoreline change analysis to develop into what it is today (Burningham and Fernandez-Nunez, 2020).

Stafford and Langfelder (1971), Dolan *et al*. (1978) and Ellis (1978) are considered to be among the main authors who established standard sets of methodologies to best delineate and map shoreline positions. Ellis' (1978) *Coastal Mapping Handbook* served as a comprehensive guide for coastal managers to consolidate the different shoreline definitions used by different states in the US; and how to access coastal data and resources from various federal agencies and departments. Stafford and Langfelder (1971) and Dolan *et al*. (1978) specifically focus on how to delineate shoreline positions from multiple aerial photographs and all claim that using aerial photography is the most timeous and cost effective method of measuring erosion along the US East Coast. Moreover, they outline the advantages and disadvantages of using aerial

photographs as compared to repeated field surveys, maps and charts, or manual photography.

One of the main limitations of using hard copy aerial photographs during this time was the difficulty of resizing and repositioning the images in such a way that they could be compared. Computers and basic geographic information systems were not widely available, nor sufficiently advanced to perform georectification techniques. Stafford and Langfelder (1971) created punch cards to operate in a specially made computer programme that could then calculate the average distances between two shorelines. While Dolan *et al*. (1978) implemented the Orthogonal Grid Address System (OGAS) to overlay different images to the same scale and trace their respective high-water lines and dune lines, then cast 100 m transects across the lines to calculate the average rates of change. As computational capacity and technologies improved, other models started to be developed, such as GENESIS (GENEralized model for Simulating Shoreline change), created by Hanson (1989).

During the 1990s, Thieler and Danforth developed the Digital Shoreline Mapping and Analysis Systems (DSMS / DSAS), which could be applied freely on most major GIS software to geo-rectify images and calculate the rate of shoreline changes (Thieler and Danforth, 1994a and 1994b). It was later acquired by the United States Geological Survey (USGS) to form part of their '*National Assessment of Coastal Change Hazards*' to calculate rates of shoreline change along the US coast, as well as assist other national and state governments worldwide in coastal hazard decision-making (Oyedotun, 2014; Himmelstoss *et al*., 2018; USGS, 2021a). DSAS proved to be a very efficient and popular software for coastal researchers and its methods and calculations became standard-practice in SCA studies over the following

decades (Oyedotun, 2014; Himmelstoss *et al*., 2018; Burningham and Fernandez-Nunez, 2020). Section 3.5 explores DSAS in further detail.

3.4 Debates within shoreline change analysis

Throughout the 1990s and 2000s, numerous researchers improved upon and critiqued the methods of SCA. These included investigating different statistical and geostatistical approaches to calculating rates of shoreline change (Dolan *et al*., 1991; Dolan *et al*., 1992) and evaluating errors within the data and methods that decrease the accuracy of the results (Crowell *et al*., 1991; Fisher and Overton, 1995; Moore, 2000; Crowell *et al*., 2005; Ruggiero and List, 2009). This is highlighted by Moore (2000: 111) who states that "erosion rates can only be as accurate as the data from which they are derived and the methods by which they are calculated".

Errors can arise from multiple sources such as from the raw data where historical maps may be inaccurately plotted, or aerial photographs that are physically damaged or distorted by the camera lens, tilt of the aircraft, backscattering of light, or relief displacement (Crowell *et al*., 1991). Human errors arise from geo-rectifying aerial photographs to very few or inaccurate ground points, and when manually digitising the shoreline indicator (Thieler and Danforth, 1994b). Finally, external effects of tidal stages, wave run-up, weather conditions and seasonality need to be considered (Crowell *et al*., 1991; Hapke *et al*., 2011). All these errors can influence the horizontal accuracy of the shoreline position and so an uncertainty value needs to be calculated for these error sources. Most calculations for uncertainty follow a similar equation, which is the square root of the sum of squares for different variables that affect the shoreline's position (Hapke *et al*., 2011; Burningham and Fernandez-Nunez, 2020).

Many debates within the field of SCA are centred on quantifying and reviewing these uncertainties. For example, Fenster *et al*. (2001) and Honeycutt *et al*. (2001) both investigate the statistical impact of including shoreline data from storm events in long-term analyses. Additionally, there are debates on which shoreline indicator (proxy) is the best to use, as all have different advantages and disadvantages which need to be carefully evaluated before selection (Boak and Turner, 2005; Del Río and Gracia, 2013; Burningham and Fernandez-Nunez, 2020). Ruggiero and List (2009) and Moore *et al*. (2006) critique the differences in using the high water line (HWL) proxy against the datum-based approach of a mean high water line (MHWL). Moore *et al*. (2006) argue that the HWL is more complex than originally laid out by previous researchers since it is influenced by wave conditions, seasonality and the daily weather, whereas, the MHWL is a more stable indication of the shoreline but requires detailed information to record it such as tidal records and elevation profiles. On the other hand, the HWL is the most popular and simplest indicator as it can be easily identified from historical aerial photographs, high spatial resolution satellite or drone imagery and field surveys (Pajak & Leatherman, 2002; Boak and Turner, 2005; Moore *et al*., 2006; Del Río and Gracia, 2013 Pollard *et al*., 2019).

The dune toe or dune crest are other indicators which may prove more useful for investigating direct effects of wave run-up and sediment supply dynamics along a beach profile, but the limitations are that light reflection off the dune and their two-dimensional shape make it difficult to visually identify them (Del Río and Gracia, 2013). Conversely, the coastal vegetation line is easier to identify in historical imagery as it stands out from the backshore and dune area. However, this feature can change due to other factors separate from beach dynamics

(e.g. invasive species growth or seasonal vegetation types) (Del Río and Gracia, 2013; Pollard *et al*., 2019). Apart from manually digitising these shoreline indicators through visual inspection, the use of remote sensing imagery and techniques allow for automation of these processes. This has greatly advanced the field of SCA, as discussed below.

3.5 Remote sensing for mapping and monitoring shorelines changes

Remote sensing has always been a central component of shoreline change analysis and has driven advancements in how we map, measure and monitor shorelines as different technologies and techniques have evolved over time. Principally, remote sensing is defined as "the process of detecting and monitoring the physical characteristics of an area by measuring its reflected and emitted radiation at a distance" (USGS, 2021b). The first remotely-sensed data of shorelines date back to the invention of the photographic lens and aircraft in the early 1900s where black and white photographs captured the light reflecting off the land and sea below (NOAA, 2016).

Aerial photography grew in popularity after proving to be a useful tool for reconnaissance missions during the First World War and started to become more standardised in the 1930s (Stafford and Langfelder, 1971). In the US, aerial photographs were frequently collected to assess storm and hurricane damage as well as to better map features along its coast from the 1930s to the present (Stafford and Langfelder, 1971; Hapke *et al*., 2011). With the advancement of colour photography, coastal features could be even better distinguished, as they looked more natural (NOAA, 2016). Then in the 1950s, cameras with near infrared sensors were created which allowed for researchers to view landscapes from beyond the

visible section of the electromagnetic spectrum which enhanced the images even more (Boak and Turner, 2005; NOAA, 2016).

However, from the 1960s onward, the 'Satellite Era' revolutionised coastal mapping beyond just the use of aerial photography. Firstly, meteorological satellites could be used to track storm systems before, and while, they battered coastlines (Klemas, 2011). Secondly, global positioning system (GPS) satellites were launched to aid with conducting field surveys and to create accurate elevation models (Splinter *et al.*, 2018). Thirdly, satellites such as SeaSat (launched in 1978) were specifically designed to monitor various oceanographic phenomena using synthetic-aperture radar (SAR) (Gens, 2010). Above all, multispectral satellite sensors have offered coastal researchers the most versatile range of data in terms of what kind of information can be extracted from them and how their historical data archives of more than 40 years can be applied (Klemas, 2011).

Multispectral sensors are able to record emitted and reflected energy at different wavelengths along the electromagnetic spectrum. The most well-known multispectral satellite sensors are the Landsat series which have continuously provided global Earth observation imagery since the launch of Landsat 1 in 1972 (USGS, 2021b). This was followed by seven further Landsat launches over the following decades. The early sensors (Landsat 1 - 4) had coarse spatial resolutions (30 to 120 m). The spatial resolution was then improved to the standard 30 m pixel sizes for Landsat 5, 7 and 8. In 2008, the USGS enabled open-access to the entire Landsat collection, which led to more researchers being able to conduct multispectral SCA studies (Burningham and Fernandez-Nunez, 2020). The European Space

Agency (ESA) has subsequently launched their own multispectral satellite, Sentinel-2, in mid-2015 with four more spectral bands and a higher spatial resolution of 10 m (ESA, 2021).

The significance of these multispectral sensors is that large-scale areas of coastal environments could subsequently be classified into spectral classes to differentiate between land and water. Edge-detection algorithms, supervised and unsupervised techniques, and water indices were developed to identify these land/water differences (Gens, 2010; Teodoro, 2016). These methodologies provide researchers with much more objective approaches to delineate the shoreline position as opposed to the manual methods of drawing shoreline positions on historical aerial photographs. However, multispectral imagery delineations are limited to their pixel sizes and so identifying erosion or accretion of the shoreline is only possible if the change is larger than the pixel size (Vos *et al*., 2019a; Burningham and Fernandez-Nunez, 2020; Luijendijk and de Vries, 2020).

Apart from just monitoring the shoreline from multispectral satellite imagery, the wider coastal system can also be monitored. These include conducting land-cover change studies on urbanisation, changes to river-courses, dam constructions, sand mining, and wetland health or mangrove degradation (Klemas, 2011; Callaghan, 2014; Callaghan *et al*., 2015; Teodoro, 2016; Amrouni *et al*., 2019). Additionally, hydrodynamics can be studied such as swell patterns, wave heights and currents using SAR, or ocean temperature using thermal infrared (Gens, 2010; Klemas, 2011). Pollution, eutrophication (algae blooms) and oil spills can also be monitored with multispectral satellite imagery.

Advancements in remote sensing such as Light Detecting and Ranging (LiDAR) and the use of drones have also allowed for highly accurate (sub-metre) digital shoreline modelling to be conducted along beaches to better understand how their morphodynamics change over storm events and over longer time periods (Splinter *et al*., 2018). In addition, high resolution satellites have also been launched which supply detailed imagery of coastal settings, however, many of these satellites (such as WorldView, GeoEye, and IKONOS) are managed by private companies and their imagery are only available at high costs (Teodoro, 2016). Google Earth and Google Earth Pro offer free, global, easily accessible high resolution colour imagery, with certain sections of the world containing historical high-resolution images covering more than a decade. For example, Warnasuriya *et al*. (2020) promotes the use of Google Earth Pro as an efficient tool for coastal researchers and educators to study the shoreline dynamics of relatively small study sites.

Google has subsequently launched Google Earth Engine (GEE), a cloud-based platform that stores a myriad of remote sensing and earth observation data, allowing users to perform planetary-scale investigations (Gorelick *et al*., 2017). Thus, researchers such as Mentaschi *et al*. (2018) and Luijendijk *et al*. (2018) have been able to conduct shoreline change analyses at global scales. They both used Landsat 5, 7 and 8 imagery spanning more than 30 years. Mentaschi *et al*. (2018) examine changes in land and water bodies, and links this to coastal morphodynamics, stating that 28,000 km^2 has eroded between 1984 and 2015. In comparison, Luijendijk *et al*. (2018) specifically focus on changes to sandy beaches and calculate the global rates of erosion and accretion; finding that 48% of the world's beaches are stable, while 24% are eroding at significant rates (>0.5 m/yr). Luijendijk *et al*. (2018) have also published their findings as an interactive web-GIS where users can explore the varying

rates of erosion and accretion at every 500 m interval along the world's beaches (accessible at: https://aqua-monitor.appspot.com/?datasets=shoreline).

Another recent development to SCA is *CoastSat*, which is an open-source software toolkit that automatically detects and extracts shoreline positions from Landsat (5, 7, 8) and Sentinel-2 satellite imagery that are accessed through GEE (Vos *et al*., 2019b). *CoastSat* was created by Vos *et al*. and the Water Research Laboratory at the University of New South Wales, Australia. First released in 2019, this Python-based software was developed to provide a fast and efficient way to collect highly temporal datasets of shoreline positions over the past +35 years. This is achieved through multiple automated steps of satellite imagery being downloaded from GEE, pre-processed and classified into land cover types, then the position between the sand and breaking waves is delineated as a vector polyline that can be exported to any GIS (see Vos *et al*., 2019b and Chapter 4 for further details). *CoastSat* is drastically different from the standardised SCA methodologies set out five decades ago whereby shorelines would be manually drawn on aerial photographs; and more efficient than other modern methods of downloading entire Landsat tiles and running the data through multiple programmes to pre-process and classify land cover types.

CoastSat has subsequently been updated to include an extension called CoastSat.slope, which utilises the satellite-derived shoreline positions to calculate the slope of the beach and the tidal variations (Vos *et al*., 2020). The Water Research Laboratory has also launched CoastSnap, which is a different type of remote sensing shoreline mapping initiative whereby members of the public take photographs of the beach from designated locations and upload them to social media (Splinter *et al*., 2018; Harley *et al*., 2019). CoastSnap is an effective way

to gather highly spatial and temporal crowd-sourced data to track how specific shoreline sites change over hourly to monthly periods (Splinter *et al*., 2018; Harley *et al*., 2019).

3.6 The Digital Shoreline Analysis System

As previously stated in Section 3.3, the Digital Shoreline Analysis System (DSAS) (developed by Thieler and Danforth in the early 1990s) has contributed greatly to the advancement of coastal morphology and spatial sciences by creating a standardised methodological procedure and statistical outputs that can be applied to various coastal management projects (Oyedotun, 2014; Himmelstoss *et al*., 2018). Over the last three decades, the DSAS software has been continuously updated and improved to be fully integrated into ESRI's ArcGIS programme, and is freely-available through the USGS Woods Hole Coastal and Marine Science Center (USGS, 2021a).

DSAS operates within ArcGIS to calculate the amount of horizontal shoreline movement and linear rate of change by taking multiple shoreline positions from different times and a baseline position, and then intersects these with equally spaced perpendicular transects (Himmelstoss *et al*., 2018). In the latest version of DSAS (v 5.0), users can also model where the shoreline is forecast to move in the next 10 and 20 years. However, the modelling is only based on the linear regression rates of change and does not take into account the underlying geology, beach morphodynamics or beach profile, which makes it a very limited model (Himmelstoss *et al*., 2018).

DSAS has been applied to numerous SCA studies across the world to investigate a variety of different coastal settings, all with different research objectives. These objectives can be

classified into two main categories, either to investigate the impact of climate change, changes to ocean conditions, the geomorphology of the area and sediment budget, or to investigate direct anthropogenic impacts on sandy beaches. For example, Amrouni *et al*. (2019), Nassar *et al*. (2019), Benkhattab *et al*. (2020), El-Gamal *et al*. (2020), Nazeer *et al*. (2020) and Niang (2020) found that shoreline changes along different sections of the North African and Middle Eastern coasts could be attributed to increased urbanisation and human impact. Whereas studies by Irrgang *et al*. (2018) and Zagórski *et al*. (2020) found increasing rates of erosion along separate beaches in the Arctic Circle, which could be attributed to climate change. Other DSAS studies have investigated shoreline change along river deltas (Özpolat and Demir, 2019), barrier islands (Nebel *et al*., 2012; Pollard *et al*., 2020), atoll islands (Ford, 2013) and coral reefs (Bheeroo *et al*., 2016).

Callaghan (2014), Callaghan *et al*. (2015) and Fourie *et al*. (2015) have also conducted DSAS studies along False Bay in Cape Town. False Bay is approximately 80 km south of this project's study site and is composed of the same aeolian deposits (the Witzand Formation) and is subject to similar climate and ocean forces (see Figure 2.4). Callaghan (2014) and Callaghan *et al*. (2015) investigated shoreline changes at four locations along False Bay from 1944 to 2010 using historical aerial photographs. They found that these four beaches experienced net erosion, with average erosion rates varying between 0.14 and 1.46 m/yr. Additionally, the researchers undertook a Landsat land-use land-cover investigation of False Bay between 1985 and 2011 to identify drivers of coastal erosion such as decreased vegetation and coastal dunes coverage (Callaghan, 2014; Callaghan *et al*., 2015). In comparison, Fourie *et al*. (2015) focused on one specific site along False Bay, Monwabisi Beach, where the coastal road continues to be eroded and damaged. They used DSAS to measure this erosion between 2003 and 2014

and then compared these measurements with wave data, concluding that strong wave events caused the most erosion (Fourie *et al*.,2015).

In order to conduct studies using DSAS, shoreline positions first have to be extracted from source data. This can be achieved through either by manually digitising aerial photographs (Fourie *et al*., 2015; Bheeroo *et al*., 2016; Benkhattab *et al*., 2020), or extracting their positions from Landsat imagery (Nassar *et al*., 2019; El-Gamal *et al*., 2020; Godwyn-Paulson *et al*., 2020; Niang, 2020; Yasir *et al*., 2020). However, a common approach has been to combine different imagery sources, such as aerial photographs and medium-resolution satellite imagery (Callaghan, 2014; Callaghan *et al*., 2015; Özpolat and Demir, 2019), or aerial photographs and high-resolution satellite imagery (Del Río *et al*., 2013; Ford, 2013; Irrgang *et al*., 2018). Furthermore, authors such as Nebel *et al*. (2012), Burningham and French (2017), Pollard *et al*. (2020), and Zagórski *et al*. (2020) combine various datasets of historical maps, aerial photographs, GPS ground surveys, LiDAR data and high-resolution satellite imagery to a create more integrated understanding of their respective study sites.

There are some critiques of DSAS in terms of its accessibility and the statistical relevance. The software is freely accessible from the USGS; however, it can only operate in ArcGIS, which is a licensed software. Therefore, open-source alternatives have been made such as AMBUR (Analyzing Moving Boundaries Using R), which offers similar statistical outputs to DSAS but operates using R (Jackson *et al*., 2012; R Core Team, 2021). Moreover, a new plugin has been developed for QGIS to calculate shoreline change rates (Terres de Lima *et al*., 2021). DSAS quantifies the linear rates of shoreline change, however, Burningham and French (2017) argue that shoreline changes are usually not linear but follow complex trends over time and

thus need to be differently examined. Therefore, these researchers developed a cluster-based segmentation to study shoreline changes. Burningham and Fernandez-Nunez (2020) follow on with an investigation into utilising multivariate approaches that can be adopted such as principal component analysis, Bayesian Modelling and machine learning. Beuzen and Splinter (2020) also offer a detailed analysis of how machine learning can be applied to understanding coastal processes.

3.7 Summary

This literature review has provided an overview of the field of shoreline change analysis (SCA). Firstly, the general coastal processes and drivers of coastal erosion were examined. Then the history, developments, and debates within the field of SCA were reviewed. The review then focused on remote sensing as a key component of SCA in terms of the types of satellite and aerial data that has become available over time and the development of technologies to process these remote sensing data. Finally, the literature review focused on DSAS as the most popular software for studying SCA. Examples of these studies were provided and critiques of DSAS were also discussed.

Chapter 4:

METHODOLOGY

4.1 Introduction

This chapter outlines the different remote sensing data types and methodologies used to delineate shoreline positions along the Yzerfontein coast in order to analyse long-term and short-term changes, and predict future shoreline dynamics. The two different data acquisition, pre-processing and analysis methodologies are presented. Descriptions of these methodologies also include samples of the intermediate results to best illustrate the steps take to reach the results.

4.2 Shoreline extraction from historical aerial photography

4.2.1 Data acquisition and pre-processing

Historical aerial photographs were acquired from the National Geo-spatial Information (NGI) agency, a component of South Africa's Department of Rural Development and Land Reform (NGI, 2021). These historical data consist of scanned, grayscale aerial photographs with their accompanying flight paths referencing the date, time, altitude, coverage, and ground-scale of the photographs. The data selection process was based on the availability of photographs and full coverage of the study site, resulting in three selected time periods: 1937, 1960 and 1977 (Table 4.1).

Table 4.1: Summary of the historical aerial photographs data.

Year	Month	Scale	Number of photographs
1937	April	1: 22 000	11
1960	December	1: 36 000	6
1977	March	1: 60 000	3

In order to assess the historical aerial photographs in a spatial context, they were georeferenced, which is the process whereby photographs are aligned to a projected satellite image or map by matching the location of ground control points to features in the photographs (Novak, 1992; ESRI, 2021). This was done using ArcMap 10.6. The aerial photographs were aligned with a sub-metre high-resolution Maxar Technologies© ESRI online satellite imagery basemap projected to WGS 1984 UTM Zone 34 South, as it is the most appropriate map projection for this region (ESRI, 2021). Suitable ground control points were identified for the entire study area before georeferencing, such as roads, rock outcrops, pans, farm boundaries and other 'permanent' features that have remained visible on the landscape over the last 80 years. These were then matched to the aerial photographs and transformed using a second-order polynomial transformation which also decreased any distortions within the images such as tilt, lens distortion and relief displacement (Novak, 1992; Del Río and Garcia, 2013; ESRI, 2021). Figure 4.1 illustrates an example of the georeferencing process being conducted on a 1977 historical photograph of Yzerfontein.

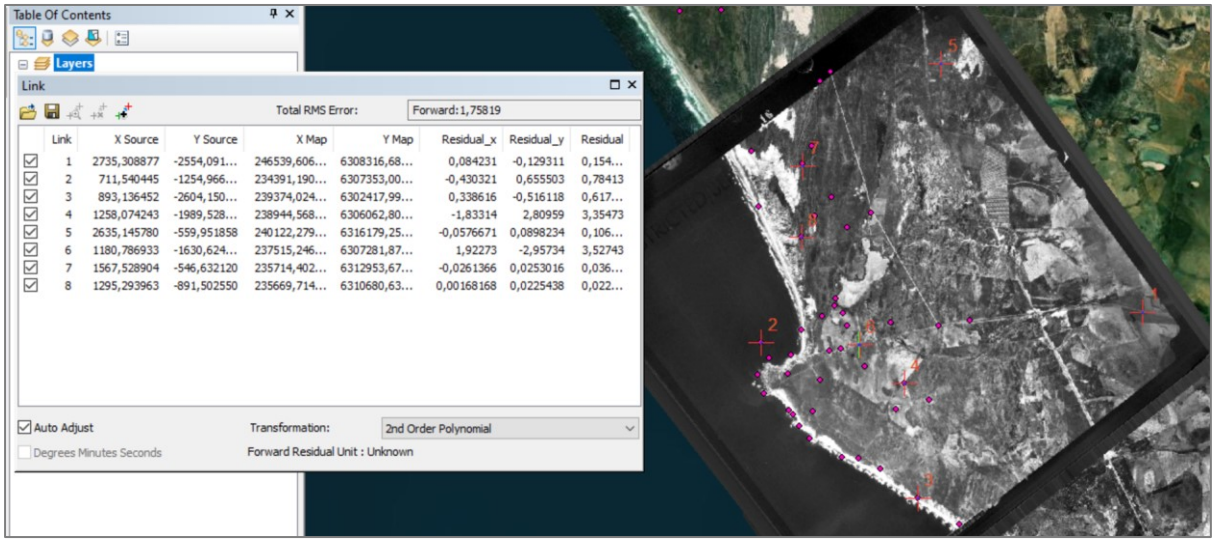


Figure 4.1: Screenshot of the georeferencing process within ArcMap (v10.6) showing the historical aerial photograph overlayed onto an ESRI high-resolution imagery basemap, the eight ground control points, and root mean square error table.

The same base image and similarly-positioned ground control points were used throughout the georeferencing process to minimise the error and ensure that the results could be comparable. Overall, each of the 20 aerial photographs had total root mean square errors (RMSE) averaging to less than 3 m. The georeferenced images were mosaiced to create a continuous single 8-bit unsigned raster for each of the three time periods, covering the entire stretch of study site shoreline.

4.2.2 Digitisation of shoreline indicator

The next process was to delineate the shoreline position onto the historical aerial photographs using the High Water Line (HWL) as the main shoreline indicator. This marks the extent of the previous high tide and is indicated by the dark grey boundary in the saturated sand where the water has decreased the reflectance of light (Dolan *et al*., 1978; Pajak & Leatherman, 2002; Moore *et al*., 2006). The most common method of marking this indicator is by manually digitising the wet-dry boundary as it is considered to be the simplest delineation technique when working with non-extensive sites (Dolan *et al*., 1978; Pollard *et al*., 2019). Thus, the HWL was digitised by carefully tracing the visible grey boundary features on the georeferenced aerial photographs into polyline shapefiles in ArcMap 10.6.

However, as previously discussed in Chapter 3.4, when a shoreline position is delineated from a remotely sensed data source or from a field survey, it may contain an associated error or uncertainty in its position (Crowell *et al*., 1991; Moore, 2000; Crowell *et al*., 2005; Hapke *et al*., 2011). These errors include human error (or bias) when manually digitising, sensor distortions, georeferencing errors, the errors associated with the image's scale or pixel size, and external effects of the tidal cycle (Crowell *et al*., 1991; Fisher and Overton, 1995; Hapke

et al., 2011; Burningham and Fernandez-Nunez, 2020). Most calculations for uncertainty follow a similar equation, which is the square root of the sum of squares for different variables that affect the shoreline's position (Hapke *et al*., 2011; Burningham and Fernandez-Nunez, 2020). These variables all represent the horizontal distance within which the shoreline could be located.

The three particular variables selected in this study were based on Hapke *et al*. (2011) and Niang (2020) where: 1) E_g is the georeferencing error, which is the Average Total RMSE for all the images. 2) E_p is the pixel error, which is the minimum pixel size for the image based on its scale. 3) And E_d is the digitisation error, which can be approximated to at least half the pixel size (see Equation 1, from Niang, 2020). These variables result in total horizontal uncertainty values of 4.09, 5.13 and 6.05 m for the three respective time periods (see Table 4.2).

$$U = \sqrt{{E_g}^2 + {E_p}^2 + {E_d}^2} \qquad (Equation\ 1)$$

Table 4.2: Estimated total shoreline uncertainty for each of the historical aerial photographs (based on Niang, 2020).

Measurement uncertainty (m)	**1937**	**1960**	**1977**
Georeferencing error (E_g) (Average Total RMSE)	2.35	2.52	2.32
Pixel error (E_p)	3.00	4.00	5.00
Digitisation error (E_d)	1.50	2.00	2.50
Total shoreline uncertainty (U)	4.09	5.13	6.05

4.3 *CoastSat* shoreline extraction

The second method for shoreline extraction was performed using the novel open-source software, *CoastSat*, which operates in an online Python coding visualization environment (Jupyter Notebook) and uses Google Earth Engine (GEE) and supervised image classification techniques to automatically extract the shoreline position from all publicly-available Landsat and Sentinel-2 imagery (Vos *et al*., 2019b). This research report uses Version 1.0.5, downloaded from GitHub (https://github.com/kvos/CoastSat).

4.3.1 Satellite data acquisition and pre-processing

The initial step to acquiring the satellite imagery data was to link the *CoastSat* Python toolkit to an existing Google Earth Engine account to gain access to its vast cloud-storage of remote sensing data. From here, the entire Landsat 5, 7 and 8 catalogues of 35+ years of data could be accessed as well as the 5+ years of Sentinel-2 imagery. *CoastSat* then downloaded the selected data from GEE based on the user-defined parameters such as the study period, the satellite mission and study area geometry.

CoastSat only requires four spectral bands to perform the supervised classification which are blue, green, red, and shortwave infra-red (SWIR 1), as well as the panchromatic band to pre-processes the imagery. Therefore, only these five bands needed to be downloaded from GEE. Selecting only the necessary spatial and spectral information from the imagery greatly decreased the data size and computational capacity compared to downloading the entire imagery tile, which is one of the main advantages of GEE (Gorelick *et al*., 2017; Vos *et al*., 2019b).

The *CoastSat* code also pre-processed the images by performing cloud-masking and enhanced the spatial resolution of imagery to improve the accuracy of the shoreline detection. For Landsat 7 and 8, this was done by pan-sharpening the 30-metre bands with the 15-metre panchromatic band. Landsat 5 bands were decreased to 15 m using down-sampling techniques as Landsat 5 does not have a panchromatic band (Vos *et al*., 2019b; USGS, 2021b). Additionally, the Sentinel-2 20-metre SWIR 1 band was down-sampled to the same resolution as its colour bands (10 m). By enhancing the spatial resolution of the imagery, the accuracy of the shoreline detection was improved, and it made the Landsat and Sentinel-2 imagery more compatible with each other (Vos *et al*., 2019b). See Table 4.3 for a summary of the different satellite imagery and their characteristics.

In order to analyse both the long-term and short-term shoreline changes, different data selection strategies were chosen for the Landsat and Sentinel-2 data. The Landsat series were chosen for the long-term analysis because of their extensive historical archives (Landsat 5 launched in 1984), while the Sentinel-2 mission was chosen for the short-term analysis because of its more frequent revisit time of 5 days (Table 4.3). The Landsat data were sampled at 5-year intervals to capture the medium-term variation of the shoreline from 1985 to 2020. Thus, all available Landsat 5, 7 and 8 imagery were downloaded for at 5-year intervals, depending on the satellite's lifespan. All Landsat 5 imagery from 1985, 1990, 1995, 2000, 2005 and 2010 were selected and downloaded from GEE. Additionally, all Landsat 8 imagery from 2015 and 2020 were also downloaded. The Landsat 5 and 7 missions overlapped with their data collection from 1999 to 2003, when Landsat 7 then experienced a failure with its Scan Line Correction (USGS, 2021b). Therefore, Landsat 7 imagery were only downloaded from 2000 to add to the available Landsat 5 data from that year. This amounted to 164 images

being downloaded from the eight years, which was then reduced to one image per year during to post-processing (see section 4.3.4).

Table 4.3: Summary of satellite imagery used by *CoastSat* (Source: Vos *et al*., 2019b; ESA, 2021; USGS, 2021b). *Note SLC: Scan Line Correction.

		Satellite characteristics				
Satellite mission	**Sensor**	**Timespan**	**Maximum revisit time**	**Bands**	**Wavelength (µm)**	**Pixel size (m)**
Landsat 5	Thematic Mapper (TM)	1984 – 2013	16 days	Blue	0.45 - 0.52	30
				Green	0.52 - 0.60	30
				Red	0.63 - 0.69	30
				NIR	0.76 - 0.90	30
				SWIR 1	2.08 - 2.35	30
Landsat 7	Enhanced Thematic Mapper Plus (ETM+)	1999 – 2003, SLC – Present	16 days	Blue	0.45 - 0.52	30
				Green	0.52 - 0.60	30
				Red	0.63 - 0.69	30
				NIR	0.77 - 0.90	30
				SWIR 1	1.55 - 1.75	30
				Pan	0.52 - 0.90	15
Landsat 8	Operational Land Imager (OLI)	2013– Present	16 days	Blue	0.45 - 0.51	30
				Green	0.53 - 0.59	30
				Red	0.64 - 0.67	30
				NIR	0.85 - 0.88	30
				SWIR 1	1.57 - 1.65	30
				Pan	0.50 - 0.68	15
Sentinel-2 (A and B)	Multispectral Instrument (MSI)	2015– Present	5 days	Blue	0.45 - 0.52	10
				Green	0.54 - 0.58	10
				Red	0.65 - 0.68	10
				NIR	0.78 - 0.90	10
				SWIR 1	1.56 - 1.65	20

To evaluate the variability of the shoreline position over a short-term period, all available Sentinel-2 A and B imagery were downloaded between August 2015 (when the satellites launched) to the end of 2020 to create a highly-temporal dataset. This resulted in a total of 601 images captured over the 5-year period. However, not all these downloaded Sentinel-2 and Landsat imagery were used in the final analysis, as they had to first be processed and post-processed.

4.3.2 Automatic shoreline extraction

CoastSat uses a combination of a neural network supervised classification, the modified normal difference water index (MNDWI) and Otsu's threshold algorithm to detect the shoreline position (Vos *et al*., 2019a and 2019b). First, all images were automatically classified into water, sand, white-water (e.g., breaking waves) and 'other' based on pre-existing training data models. Second, the pixels were converted to MNDWI values, which differentiates between water and non-water. Then, Otsu's thresholding algorithm was applied to identify the maximum variance between the sand and water classes (see Vos *et al*., 2019a and 2019b for further details).

Additionally, a reference shoreline was manually digitised to its approximate position on the satellite images and a maximum search distance was selected. This tool was used to make sure that only the shorelines along the study site were created and not around the Yzerfontein Salt Pan, Rooipan, or Langebaan Lagoon (Figure 4.2). Figure 4.2 illustrates an example of how the *CoastSat* classification operates and how the shoreline position is delineated within a section of the study site.

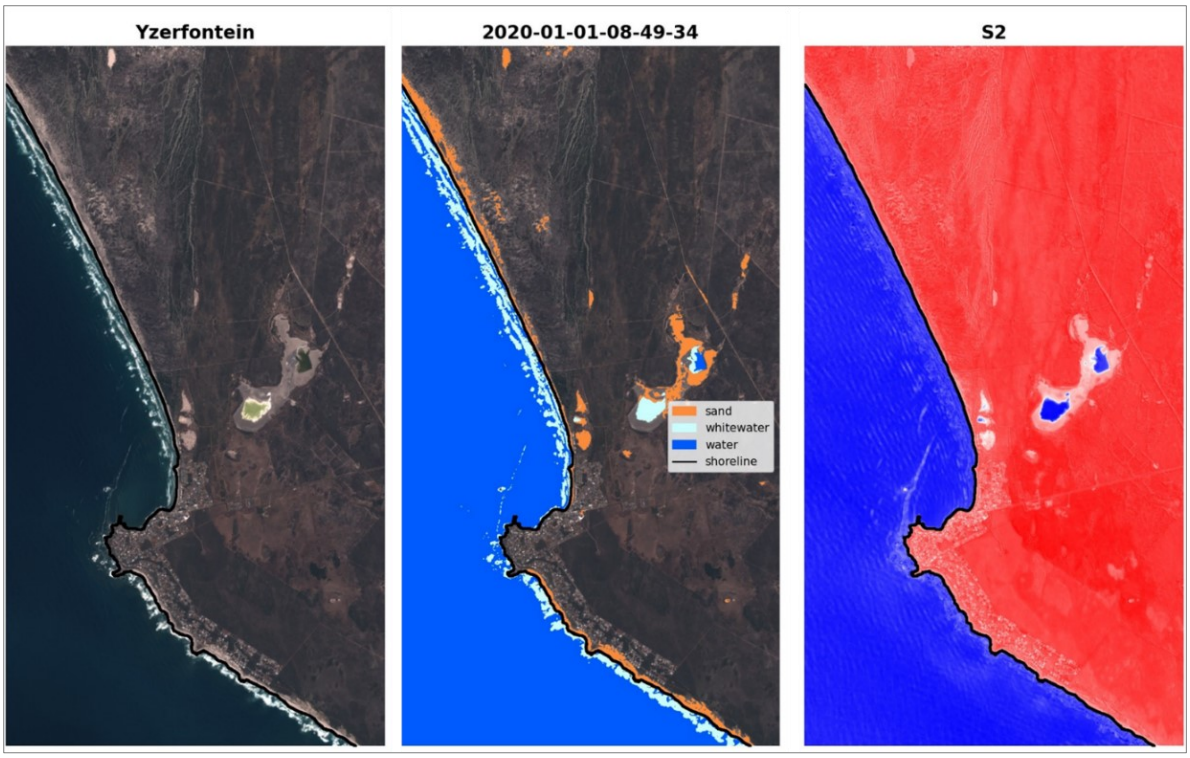


Figure 4.2: Example of *CoastSat* shoreline detection process, indicating the shoreline in black on a Sentinel-2 true colour image (left), the classified image of sand, white-water, water and other (centre), and the MNDWI values showing low values in blue and high values in red (right).

CoastSat performs optimally with smaller study areas (e.g., 5 km^2), and the creators advise that extensive study areas (e.g., 100 km^2) are divided into sub-areas to better handle the data computations (Vos *et al*., 2019b). Therefore, the 30 km stretch of coastline was divided into four equal parts and the code was run four times per period. After the land-cover classification and shoreline delineation was completed, each image was subsequently visually inspected and approved by the researcher. This was to ensure that there were no major misclassifications or cloud-cover that incorrectly place the shoreline position. All shorelines were then saved and exported as a vector polyline GeoJSON file.

4.3.3 Post-processing of shorelines

From all the different Landsat data downloaded and processed through *CoastSat* for each 5-year interval, only one image acquisition date was selected from the specified years. This was based on various criteria; the main criteria being that no clouds obstructed the study site, and that the classified shoreline position had no visible errors or missing areas for all four of the shoreline sub-areas. Additionally, in order to not have any seasonal influence over the data (and to be comparable with the historical photographs), only images from the summer months were chosen (October to March). Thus, one image and its extracted shoreline position from each of the five-year intervals between 1985 to 2020 were selected (Table 4.4).

Table 4.4 Landsat image selection dates for the long-term analysis.

Year	Acquisition Date	Satellite Mission
1985	9 April	Landsat 5
1990	19 December	Landsat 5
1995	30 October	Landsat 5
2000	20 November	Landsat 7
2005	9 October	Landsat 5
2010	29 March	Landsat 5
2015	22 November	Landsat 8
2020	9 October	Landsat 8

In comparison, for the short-term analysis, the Sentinel-2 dataset were also post-processed by manually inspecting the automated shoreline positions and ensuring that no cloud-cover obscured the classification, and that the shoreline was correctly classified for the four sub-

areas for each image acquisition date. This resulted in the original 601 Sentinel-2 images being reduced to 304 images (full list in Appendix Table A2).

The Landsat and Sentinel-2 extracted shoreline GeoJSON files were then converted to shapefiles and edited in QGIS (v 3.10). The four sub-areas were merged together to form one continuous shoreline in the study site for each of the image dates (8 and 304 respectively). Finally, the vector polylines were clipped to remove all the rock outcrops such as *Gabbro Point*, *Yzerfontein Point*, *Skaap Island* and *Bakoond,* thereby leaving only the sandy beaches (see Figure 2.2a for visual reference).

Similar to the shorelines extracted from the historical aerial photographs, these shorelines also contain a positional uncertainty (U) based on the satellite imagery geo-accuracy (georeferencing: E_g) and pixel size (E_p) (Vos *et al*., 2019a). Therefore, the total horizontal uncertainty (Equation 2) follows the same formula as Equation 1 but does not include a digitisation error. Every Landsat image contains a geometric RMSE value in its metadata and Table 4.5 summarises these error values. However, the Sentinel-2 metadata does not contain any georeferencing or geo-accuracy values, so their positional uncertainty can only be approximated to their 10-metre pixel size (Equation 3). Figure 4.3 Provides a summative flowchart of the *CoastSat* automatic shoreline extraction and processing.

$$Landsat \quad U = \sqrt{{E_g}^2 + {E_p}^2} \qquad (Equation\ 2)$$

$$Sentinel\ 2 \quad U = \sqrt{{E_p}^2} = 10 \qquad (Equation\ 3)$$

Table: 4.5 Estimated total shoreline uncertainty for each of the Landsat images.

Measurement uncertainty (m)	**1985**	**1990**	**1995**	**2000**	**2005**	**2010**	**2015**	**2020**
Georeferencing error (E_g) (RMSE)	5.18	8.06	5.07	6.15	5.68	4.99	8.88	7.43
Pixel error (E_p)	15	15	15	15	15	15	15	15
Total shoreline uncertainty (U)	15.87	17.02	15.83	16.21	16.04	15.81	17.43	16.74

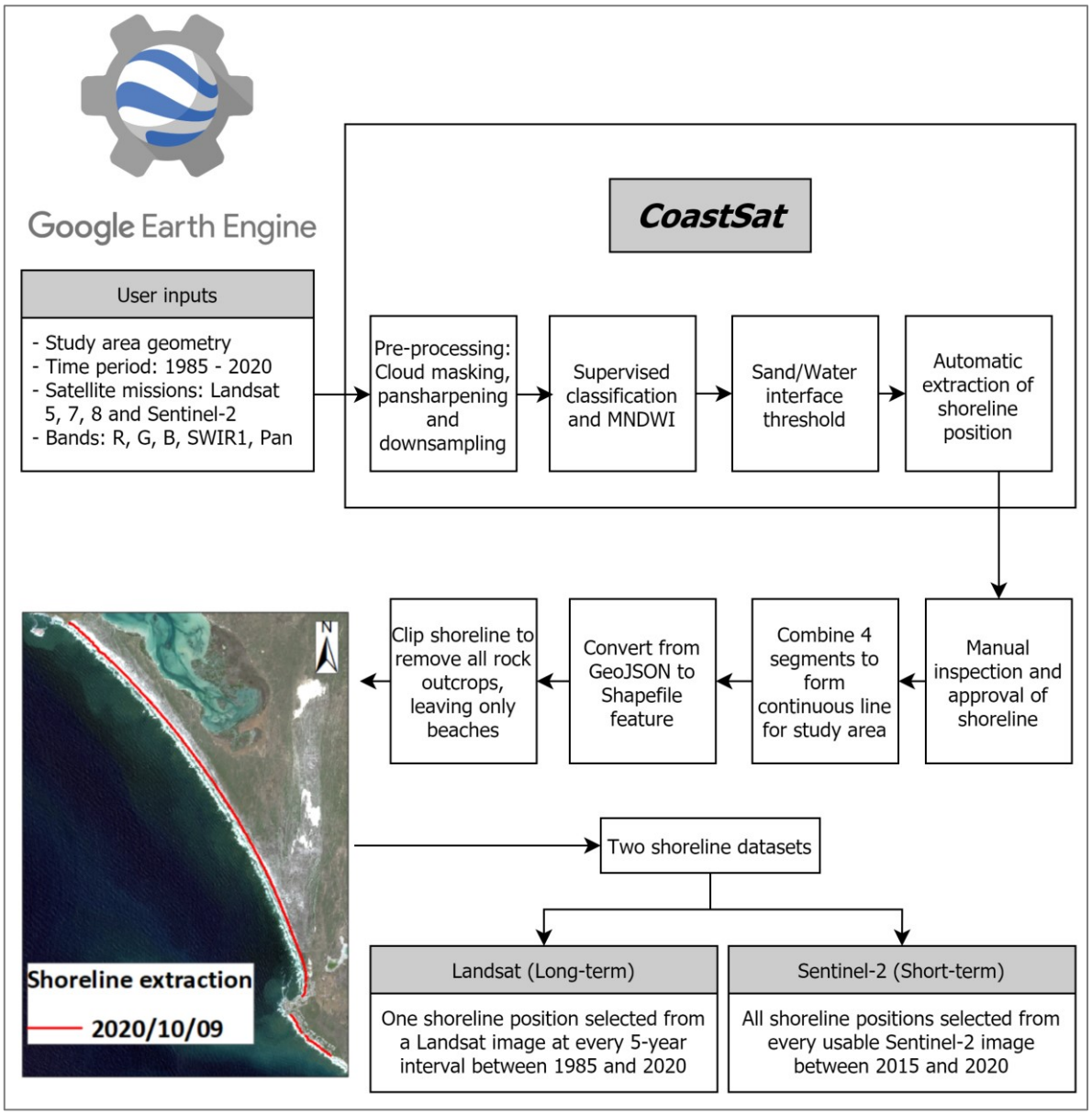


Figure 4.3: Flowchart of processes conducted within the CoastSat toolkit (Adapted from Vos *et al.,* 2019a and 2019b).

4.4 Long-term analysis

The third stage of this research was to use the Digital Shoreline Analysis System (DSAS) to quantify the amount and rates of shoreline change at a long-term perspective (84 years). The long-term dataset combined the manually digitised historical shoreline data from 1937, 1960 and 1977 with the *CoastSat* shorelines from 1985, 1990, 1995, 2000, 2005, 2010, 2015 and 2020. Version 5 of the DSAS software was freely downloaded from the USGS website (https://www.usgs.gov/centers/whcmsc/science/digital-shoreline-analysis-system-dsas?qt-science_center_objects=0#qt-science_center_objects) and added as an extension to ArcMap 10.6. The digitised and automatically extracted shoreline polylines were then added to a personal geodatabase, and the feature date attributes were converted from International Organization for Standardization date and time to United States short date formats (as DSAS is an American programme). Another attribute column was also added to input the positional uncertainty values for each shoreline listed in Table 4.2 and Table 4.5.

Following on, a baseline was manually digitised approximately 150 m towards the sea to represent an independent marker off which the shorelines were measured from (Himmelstoss *et al*., 2018). Using DSAS, perpendicular transects were then cast from the baseline at 100 m equal intervals to the different polylines, with a smoothing distance of 200 m (see Figure 4.4a). The software then calculated the distances between each point of intersection with the transects and recorded these attributes. The raw data attributes were transformed into statistical outputs to show the horizontal changes and the rates of change of the shoreline. These include:

1. Net Shoreline Movement (NSM): the horizontal distance between the oldest and the youngest shorelines.

2. Shoreline Change Envelope (SCE): a measure of the greatest horizontal change in shoreline movement irrespective of the dates.
3. End Point Rate (EPR): the distance of shoreline movement between the oldest and the youngest shoreline positions divided by the time elapsed.
4. Linear Regression Rate (LRR): an ordinary least square regression of shoreline change over time.
5. Weighted linear regression (WLR): a least square regression of the transects which considers the uncertainty of the shoreline position, with the weight equal to the inverse squared of the uncertainty (Oyedotun, 2014; Himmelstoss *et al*., 2018).

The five measurements calculated by DSAS were used to visualise the shoreline changes in ArcMap and to identify which locations have experienced chronic erosion or fluctuations over time. Comparisons between the measurement statistics and the three beaches were also made to assess if the beaches all underwent similar rates of change or not.

Particular attention was paid to the weighted linear regression rate of change (WLR) as this rate considers the positional uncertainties of the shoreline and can therefore be considered a more accurate representation of erosion and accretion trends compared to the ordinary least squares regression (Himmelstoss *et al*., 2018) (Figure 4.4b). The WLR output also provides a 95% confidence interval (C.I.) which tests whether the rates of erosion are significant or not, based on the null hypothesis that the rates are equal to zero; versus the alternative hypothesis that the rates are not equal to zero.

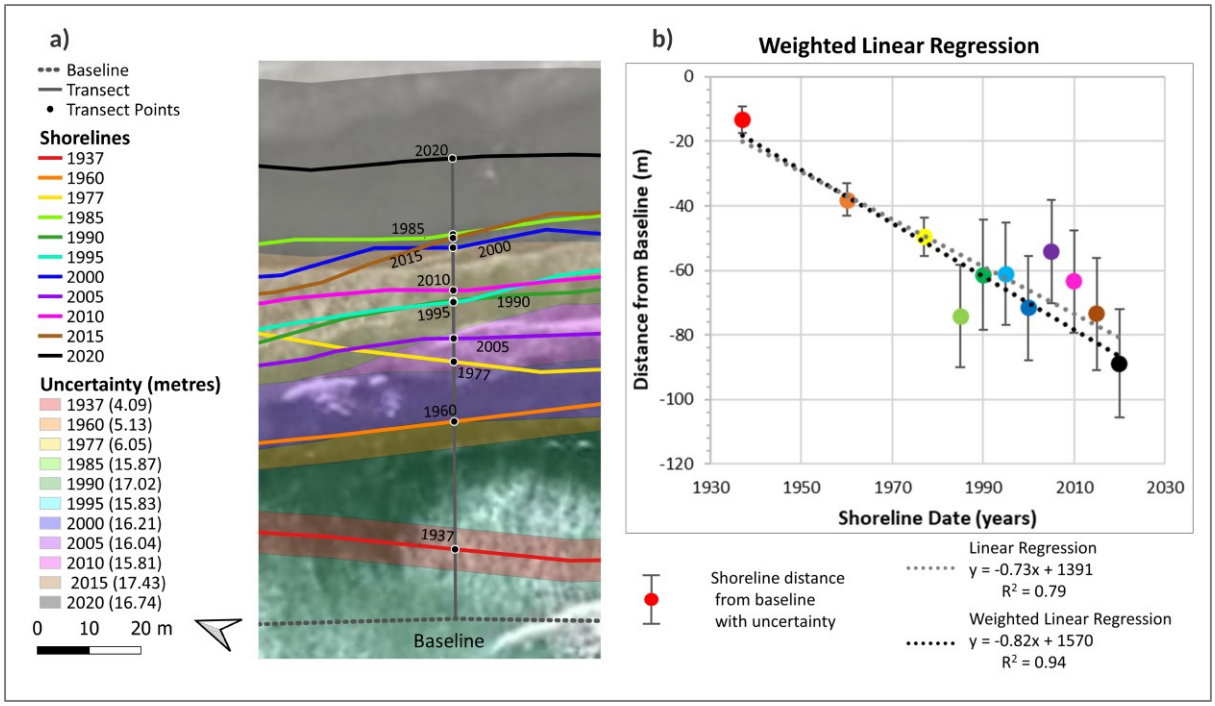


Figure 4.4: a) Map of a perpendicular transect through the shoreline positions from the different time periods and their respective uncertainty values as buffers. b) Plot of the linear regression and weighted linear regression for distance from the baseline versus time (Adapted from Himmelstoss *et al.,* 2018: 50).

In addition to visualising the DSAS trends as maps and summative tables, a multivariate heat-matrix was also produced to show the dynamics of the shoreline over space and time. This timeseries heat-matrix graphing method was adopted from Burningham and French (2017) and was created using R and the Lattice Package (Sarkar *et al*., 2020; R Core Team, 2021).

4.5 Short-term analysis

The next component was to analyse the dynamics of the study site shoreline at a finer temporal-scale to see if any seasonal variations could be detected or how major storm events affected the shoreline. This was conducted using the shoreline positions automatically extracted from Sentinel-2 with the use of *CoastSat* (as explained in Section 4.2). This dataset consisted of 304 different shoreline vector polylines extracted from Sentinel-2 imagery

between August 2015 and December 2020 (Appendix Table A2). The dataset was deemed too large to use DSAS for further investigation, and instead, a case-study approach was used to allow for deeper insight into specific cross-sections along the study site.

Six locations were selected as case-studies along the different sandy beaches as seen in Figure 4.5. The first site selected was the mid-point of Pearl Bay, near *De Goede se Baai* and *Bakoond* (Figure 2.2a), and the second location was the mid-point of Yzerfontein Main Beach. Since these beaches are relatively small, one transect per beach was deemed sufficient to gauge the general trends experienced, whereas Sixteen-Mile Beach is much longer and so four locations were distributed across it. One site is 600 m north of the Gabbro Point outcrop, near Rooipan, where the dune cordon and surrounding infrastructure were significantly damaged during the June 2017 storm and continue to experience erosion. The fourth location is situated 6 km from Gabbro Point and was selected for further investigation as the long-term change analysis revealed that this section has experienced the largest amount to erosion between 1937 and 2020. For the purpose of this project, this location has been named an 'erosion hotspot' (Figure 4.5). The fifth location was selected at the mid-point of Sixteen-Mile Beach, near the section of the West Coast National Park, which is knows at Abraamskraal. The final location was selected at the northern end of Sixteen-Mile, between Tsaarbank and Black Rock. These various locations were chosen to investigate how the middle and outer portions of this log-spiral beach dynamics differ.

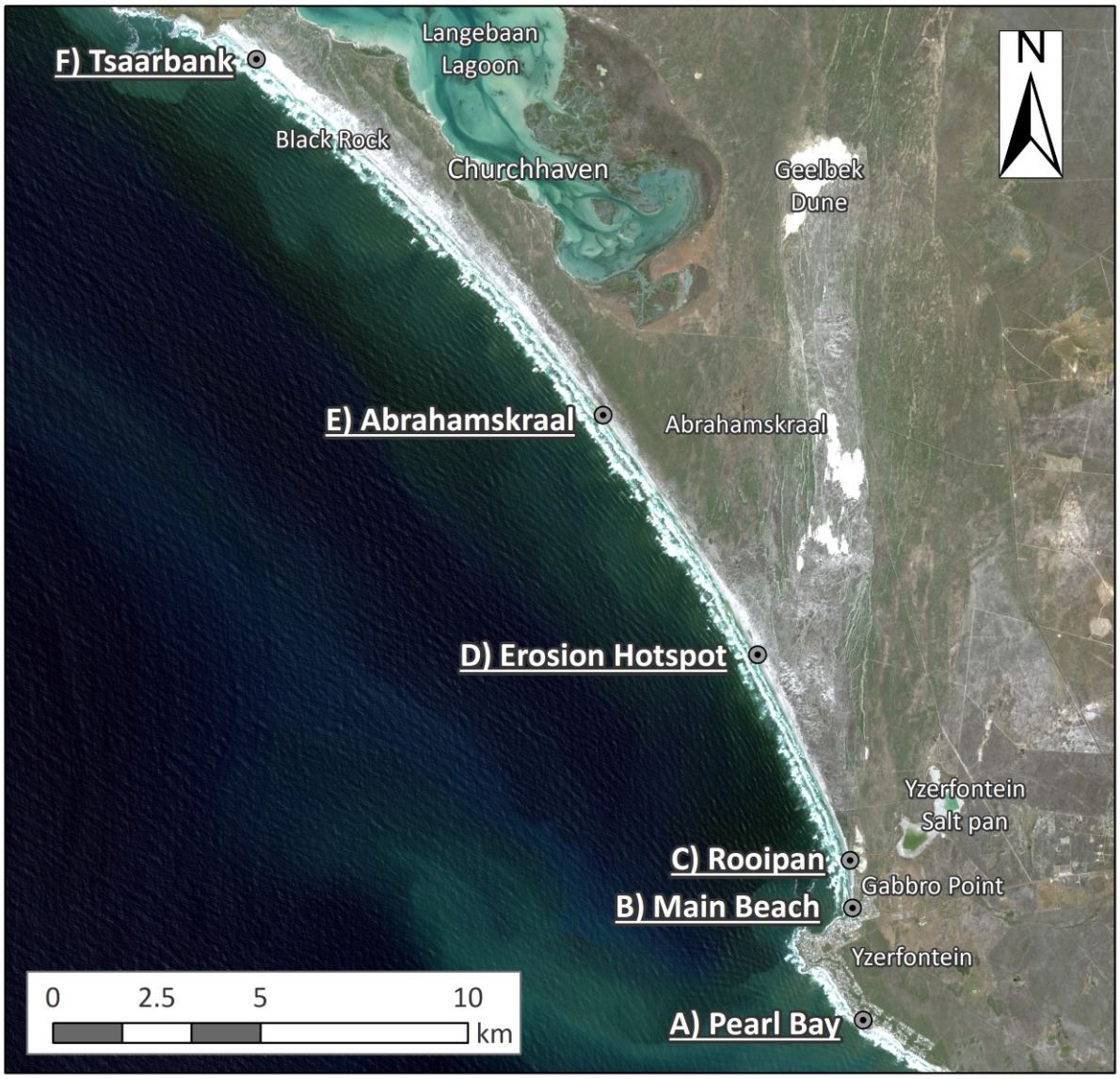


Figure 4.5 Location of six case-study sites selected for the short-term analysis.

Thus, the post-processed Sentinel-2 shoreline dataset was imported into QGIS and transects were drawn perpendicularly across these lines at each of the six locations. The intersection tool was used to record the coordinates of where each of the shorelines crossed the transect. Then, the distances between all the points and the most landward point of intersection were calculated using the 'Distance to Nearest Hub' tool. Finally, these distances were de-mean as to show the cross-shore change (e.g., the more landward shorelines recorded negative values while the more seaward shorelines have positive change values) (Figure 4.6). These attribute

distances were then exported from QGIS as a CSV file and plotted as cross-shore change distance versus time for each of the six locations using *iNZight for Data Analysis* programme (inzight.nz/). An ordinary least squares regression was conducted on the datasets to investigate the strength of any linear trends, and the impact of the June 2017 storm on the shoreline position was examined.

The above method of constructing cross-shore change analyses on shoreline positions is a component of the *CoastSat* programme and can be conducted using Jupyter Notebook. The *CoastSat* website provides an interactive web-GIS page (http://coastsat.wrl.unsw.edu.au/) which shows cross-shore change plots for 100 m-transects of the east coast of Australia and west coast of the US (Vos et al., 2020). This is where the methodology for the short-term analysis orginiates from, however, QGIS and InZight were used to create the plots instead of *CoastSat*, because of their simpler data management of visualisation tools.

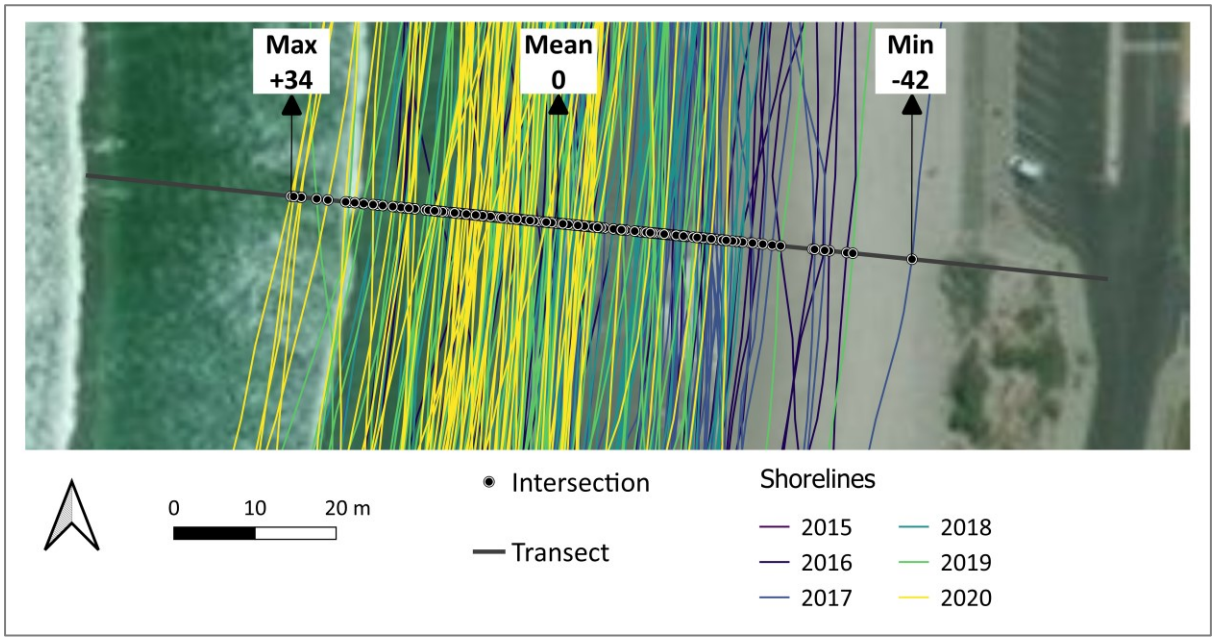


Figure 4.6: Transect intersecting with the short-term shorelines at Yzerfontein Main Beach.

4.6 Future shoreline forecasting

Lastly, the final stage of analysis was to investigate how the shoreline may change in the future based on statistical trends from the long-term dataset (1937 to 2020). The latest version of DSAS (v5.0, 2018) has a beta function which can be used to make a future projection of the shoreline position based purely on the statistical trend and weighted linear regression rates, called the 'Kalman Filter' (Himmelstoss *et al*., 2018). This function is used to generate the possible shoreline position of Pearl Bay, Yzerfontein Main Beach and Sixteen-Mile Beach in the next 10 and 20 years, as well as the positional uncertainty of these forecast lines. The forecasting was conducted on three study site beaches to investigate whether there are regions of concern for where possible erosional trends could impact on the foredune or coastal infrastructure, or if there are sections of coastline which could accrete over time. These forecast shorelines and their respective uncertainty buffers were visually inspected against a recent high resolution (sub-metre) satellite image along the 30 km study site. However, these were best visualised as ~1 km case-study examples along the coast, similar to section 4.5.

Additionally, it must be emphasised that the forecasting model is only based on statistical trends in the data, and that it must therefore be used with caution since it cannot take into account further parameters such as underlying geology, beach profile or wave conditions, to name a few (Himmelstoss *et al*., 2018).

4.7 Summary

Chapter 4 laid out the methodologies undertaken in this research report to firstly collect and process the remote sensing data, and then to extract shoreline positions from the imagery

either through manual digitisation or using *CoastSat*. Thirdly, the methodologies for calculating the long-term, short-term, and future shorelines trends were presented. Figure 4.7 summarizes the entire workflow of this report's methodologies.

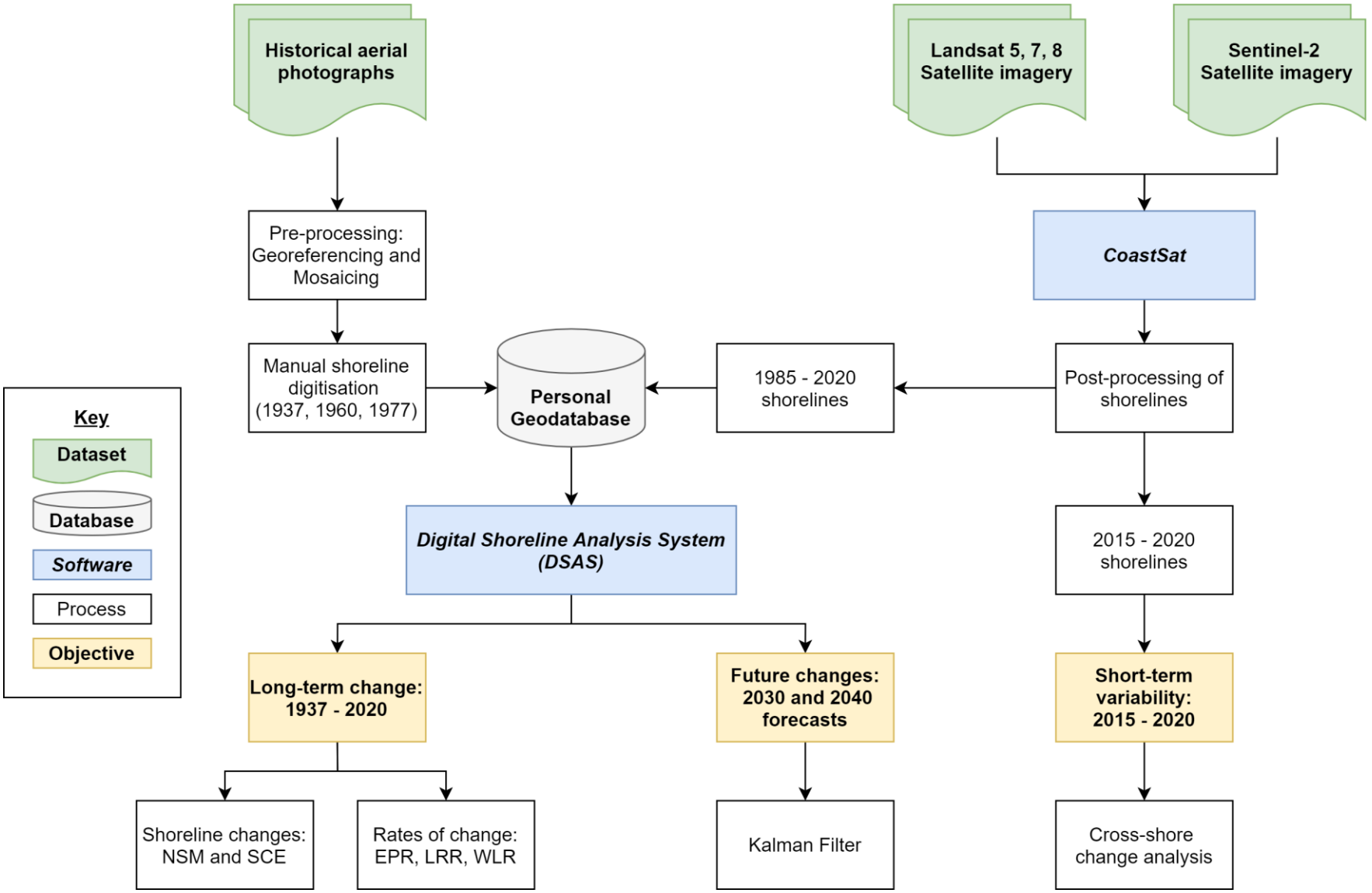


Figure 4.7: Summary flowchart of the entire research report methodologies.

Chapter 5:

RESULTS

5.1 Introduction

This chapter presents the main findings of the research report in line with its objectives. Firstly, the long-term shoreline changes are presented as a series of maps, graphs, and tables to illustrate the shoreline trends between 1937 and 2020. Secondly, the short-term shoreline changes between 2015 and 2020 are presented for specific locations within the study site to better understand the seasonal variability and storm surge impact. Thirdly, future shoreline positions for the next 10 and 20 years are modelled and illustrated as map overlays against the current coastline.

5.2 Long-term shoreline change

Long-term shoreline changes for the study area were calculated by extracting shoreline proxy positions from eleven time periods between 1937 and 2020 using manual and automated methods. The Digital Shoreline Analysis System (DSAS) was then used to calculate and visualise the amounts and rates of change between the different shoreline positions.

The first findings from DSAS are the net shoreline movement (NSM), which represents the total horizontal change in shoreline position between 1937 and 2020 (Figure 5.1). Figure 5.1 illustrates these changes as a map and colour legend showing the location of where varying amounts of total erosion or accretion have occurred alongside a graph showing the exact amount of NSM at each 100 m-transect. From Figure 5.1, it is apparent that the majority of the study site has experienced a negative NSM over the last 83 years. Overall, 95% of the study site has experienced a negative NSM with an average movement of -38 m (Table 5.1).

The largest NSM amounted to -99.29 m, which occurred along Sixteen-Mile Beach between Abrahamskraal and Gabbro Point; whereas the largest positive (seaward) movement amounted to 13.8 m and occurred three km south of Black Rock.

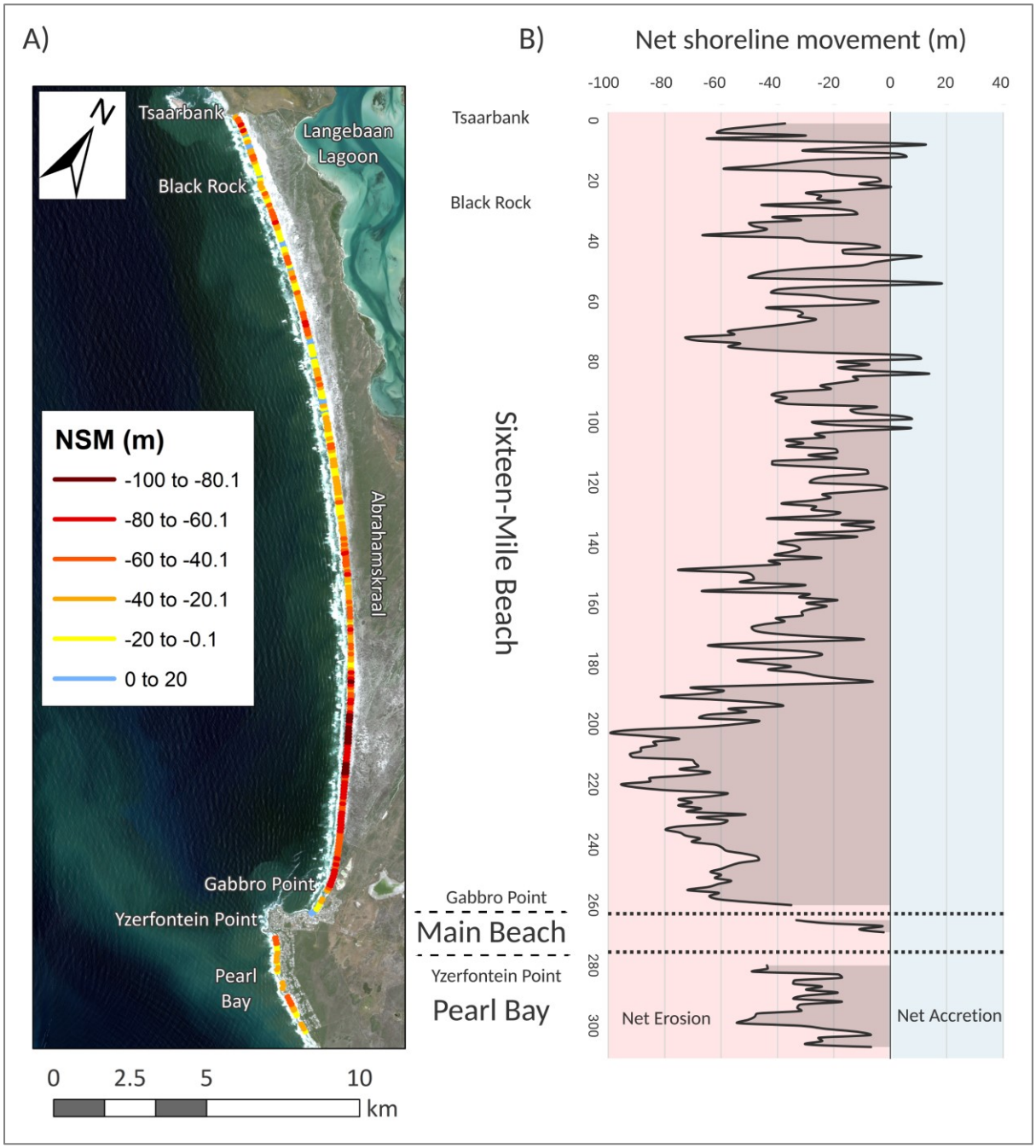


Figure 5.1: A) Map of net shoreline movement (NSM) along the study site with warm colours representing erosion and cool colours representing accretion. B) Graph of NSM vs. the 100 m-transects along the coast.

Table 5.1: Summary of Net Shoreline Movement (NSM) to the study site shoreline and its three beaches with landward movement as negative and seaward movement as positive.

	Net Shoreline Movement (m)				
Shoreline	Average	Percent of net erosion (%)	Maximum erosion	Percent of net accretion (%)	Maximum accretion
Sixteen-Mile Beach	-39.36	95	-99.29	5	+18.30
Yzerfontein Main Beach	-8.58	71	-32.29	29	+6.72
Pearl Bay	-30.44	100	-54.86	0	NA
Total Study Site	**-37.79**	**95**	**-99.29**	**5**	**+18.30**

All three beaches experienced differing NSM, with Sixteen-Mile experiencing the largest amounts of erosion (-99.29 m) and accretion (+18.3 m) for individual transects, whereas Yzerfontein Main Beach experienced the least amount of change, averaging to -8.58 m. Approximately one-third of Main Beach (29%) had moved marginally landward (maximum accretion of 6.72 m), compared to Pearl Bay where all the embayments had moved landward at an average distance of -30.44 m (Figure 5.1 and Table 5.1).

In addition to the NSM, DSAS was also used to calculate the Shoreline Change Envelope (SCE), which represents the greatest distance between the shorelines, irrespective of time or direction. Thus, the SCE shows the extra variability and dynamics of the shoreline movement. Only 38% of transects showed the NSM to be the same as the SCE, meaning that 62% of the shoreline experienced its largest amount of change during a different time period, other than 1937 to 2020 (for example 1960-2005 and 1977-2020). Table 5.2 summarises the SCE statistics, which indicate that the maximum amount of change is the same as the maximum and minimum NSM of 99.29 m and 13.81 m, respectively. Once again, Yzerfontein Main Beach

underwent the least total change (average = 22.73 m), followed by Pearl Bay (average = 40.23 m), while Sixteen-Mile Beach underwent the greatest average change of 52.13 m.

Table 5.2: Summary of Shoreline Change Envelope (SCE) along the study site shoreline and its three beaches irrespective of the direction of movement.

	Shoreline Change Envelope (m)		
Shoreline	Average	Maximum	Minimum
Sixteen-Mile Beach	54.21	99.29	18.69
Yzerfontein Main Beach	22.73	38.52	13.81
Pearl Bay	40.23	25.12	57.25
Total Study Site	**52.13**	**99.29**	**13.81**

DSAS calculates three different statistics to represent the rate of horizontal shoreline change over time (m/yr). These are the End Point Rate (EPR), the Linear Regression Rate (LRR) and the Weighted Linear Regression Rate (WLR). The EPR is simply the NSM divided by the total period (83 years). Hence, the maximum EPR was the NSM value of -99.29 m divided by 83 years, which equates to -1.19 m/yr (Table 5.3). Similar to the NSM results (Table 5.1), 95% of the study site transects have negative rates of erosion, while 5% have positive rates of accretion. All of the Pearl Bay Beach transects have negative EPRs, averaging to -0.36 m/yr, whereas Yzerfontein Main Beach has the smallest average EPR of -0.10 m/yr.

Since every delineated shoreline position had an associated uncertainty value, these rates also had an associated uncertainty. This was calculated as the square root of the sum of the 1937 and 2020 squared uncertainty values (4.09 m and 16.74 m correspondingly (see Chapter 4.3)), divided by the time period difference (83 years) which equates to 0.21m/yr. Thus, all the EPRs were tested for their statistical significance (if the rate ± 0.21 contains zero).

This null hypothesis test revealed that only 82% of all EPRs had statistically significant rates of erosion, and almost none of the prograding rates were statistically significant (Table 5.3).

Table 5.3: Summary of End Point Rates of change (EPR) to the study site shoreline and its three beaches with erosional rates as negative and accretional rates as positive.

	End Point Rate (m/yr)						
Shoreline	Overall rate	Average erosion rate	Percent of negative rates (Statistically significant) (%)	Maximum rate of erosion	Average accretion rate	Percent of positive rates (Statistically significant) (%)	Maximum rate of accretion
Sixteen-Mile Beach	-0.47 ±0.21	-0.50 ±0.21	95 (85)	-1.19 ±0.21	+0.09 ±0.21	5 (0.4)	+0.22 ±0.21
Yzerfontein Main Beach	-0.10 ±0.21	-0.17 ±0.21	71 (29)	-0.40 ±0.21	+0.07 ±0.21	29 (0)	+0.08 ±0.21
Pearl Bay	-0.36 ±0.21	-0.36 ±0.21	100 (82)	-0.65 ±0.21	N.A.	N.A.	N.A.
Study Site	**-0.45 ±0.21**	**-0.48 ±0.21**	**95 (82)**	**-1.19±0.21**	**+0.09 ±0.21**	**5 (0.3)**	**+0.22 ±0.21**

The second rate of change is the Linear Regression Rate (LRR), which is different from the EPR in that it uses all the shoreline dates to calculate linear trends over time based on the Least Sum of Squares method. The LRR revealed that the dominant trend along the coastline is landward movement, with 86% of the study site having negative rates and an average rate of -0.28 m/yr (Table 5.4). However, when taking the data confidence intervals into consideration, only 34% of the study site transects have significant negative rates of change and none of the positive

LRR are considered statistically significant for any of the beaches. The maximum negative LRR was found to be -0.89 ±0.50 m/yr and the maximum positive rate equal to +0.10 ±0.39 m/yr; both of which were recorded along Sixteen-Mile Beach. Sixteen-Mile Beach and Pearl Bay had similar overall LRRs of -0.28 ±0.40 m/yr and -0.27 ±0.30 m/yr, respectively. Yzerfontein, in contrast, had a much smaller average LRR and confidence interval of -0.05 ±0.19 m/yr (Table 5.4).

Table 5.4: Summary of Linear Regression Rates of change (LRR) to the study site shoreline and its three beaches with erosional rates as negative and accretional rates as positive.

	Linear Regression Rate (m/yr)						
Shoreline	Overall rate	Average erosion rate	Percent of negative rates (Statistically significant) (%)	Maximum rate of erosion	Average accretion rate	Percent of positive rates (Statistically significant) (%)	Maximum rate of accretion
Sixteen-Mile Beach	-0.28 ±0.40	-0.35 ±0.40	85 (32)	-0.89 ±0.50	+0.10 ±0.40	15 (0)	+0.30 ±0.43
Yzerfontein Main Beach	-0.05 ±0.19	-0.11 ±0.18	71 (14)	-0.24 ±0.23	+0.08 ±0.23	29 (0)	+0.10 ±0.23
Pearl Bay	-0.27 ±0.30	-0.27 ±0.30	100 (43)	-0.58 ±0.29	N.A.	N.A.	N.A.
Study Site	**-0.28 ±0.39**	**-0.34 ±0.39**	**86 (34)**	**-0.89 ±0.50**	**+0.10 ±0.39**	**13 (0)**	**+0.30 ±0.43**

Although the LRR contains a 95% confidence interval to test for statistical significance, it does not consider the uncertainty of the input data in the regression model. Therefore, DSAS also calculates a Weighted Linear Regression Rate (WLR) which multiplies all shoreline transect values by

the squared inverse of their respective uncertainty values (Himmelstoss *et al*., 2018). Since the data extracted from the Landsat imagery have large (>15 m) uncertainty values, the WLR provides a more reliable rate of change.

From Table 5.5, the overall WLR is similar to the LRR, at -0.28 ±0.33 m/yr. The majority of overall WLRs for the three beaches are equal (or similar) to their LRRs and the main differences being that the 95% confidence intervals have decreased. This has resulted in the percent of statistically significant negative rates increasing from 34% to 47%, and significant positive rates increasing from 0 to 3% for the study site. However, the maximum erosion and accretion rates are larger for the WLR than the LRR. Sixteen-Mile Beach recorded a maximum erosion rate of -1.19 ±0.47 m/yr and maximum accretion rate of +0.50 ±0.40 m/yr, compared to Yzerfontein's maximum rates of -0.33 ±0.15 m/yr and +0.15 ±0.20 m/yr, and Pearl Bay's maximum rates of -0.62 ±0.15 m/yr and +0.03 ±0.26 m/yr.

Table 5.5: Summary of Weighted Regression Rates of change (WLR) to the study site shoreline and its three beaches with erosional rates as negative and accretional rates as positive.

	Weighted Linear Regression (m/yr)						
	Overall rate	Average erosion rate	Percent of negative rates (Statistically significant) (%)	Maximum rate of erosion	Average accretion rate	Percent of positive rates (Statistically significant) (%)	Maximum rate of accretion
Sixteen-Mile Beach	-0.29 ±0.35	-0.44 ±0.35	77 (46)	-1.19 ±0.47	+0.20 ±0.35	23 (3)	+0.50 ±0.40
Yzerfontein Main Beach	-0.06 ±0.13	-0.19 ±0.12	57 (29)	-0.33 ±0.15	+0.10 ±0.15	43 (0)	+0.15 ±0.20
Pearl Bay	-0.25 ±0.24	-0.26 ±0.24	96 (56)	-0.62 ±0.15	+0.03 ±0.26	4 (0)	+0.03 ±0.26
Study Site	**-0.28 ±0.33**	**-0.41 ±0.33**	**78 (47)**	**-1.19 ±0.47**	**+0.19 ±0.34**	**22 (3)**	**+0.50 ±0.40**

Figure 5.2 visually presents the WLR in greater detail as both a map and graph (similar to Figure 5.1). Here, one can see the sections of the beaches that have the largest rates of change. Along Pearl Bay, the WRL is relatively small, between 0 and -0.5 m/yr, with no significant trends of accretion.

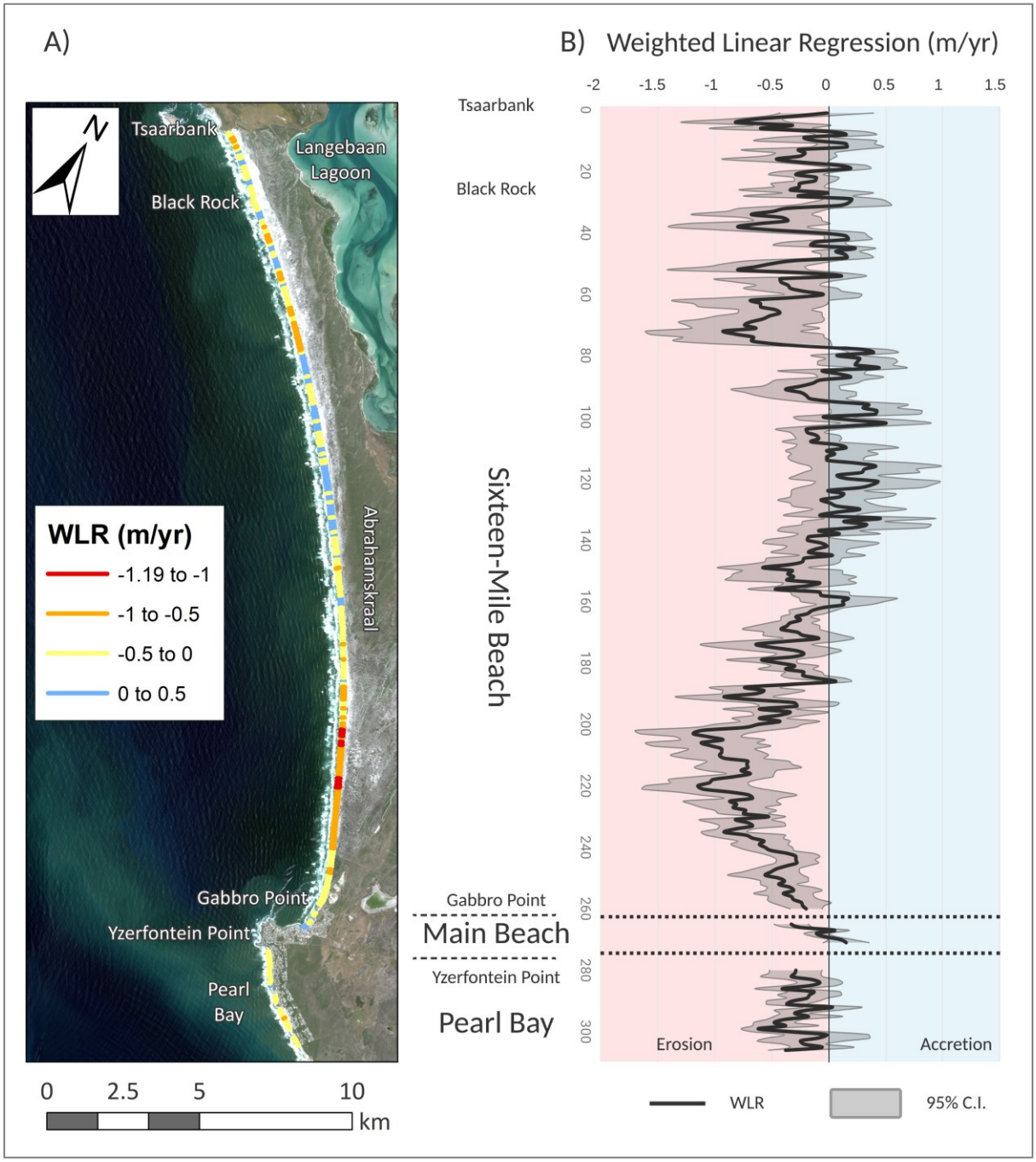


Figure 5.2: A) Map of the Weighted Linear Regression rates along the study site with warm colours representing erosion and cool colours representing accretion. B) Graph of WLR at every 100m transect along the coast and the 95% confidence interval.

Yzerfontein Main Beach shows the least average rate of change and its rates were mainly non-significant (indicating an almost stationary trend). By comparison, Sixteen-Mile Beach shows more complex patterns of shoreline erosion and accretion. Moving north from Gabbro Point, the rate of erosion increases from -0.25 ±0.12m/yr to the maximum rate for the whole site of -1.19 ±0.47 m/yr. This location, approximately 6 km north of Gabbro Point, could be considered an 'erosion hotspot' since the rate is greater than 1 m/yr (Luijendijk *et al.*, 2018). The rate of negative change then decreases between this location and Abrahamskraal, where the rate then becomes positive and reaches its maximum of +0.50 ±0.40 m/yr. Between Abrahamskraal and Tsaarbank, the rates of change fluctuate around -0.4 m/yr.

Figure 5.3 provides a visual summary of all five DSAS statistics represented as different colour-coded transects which have been placed parallel to the shoreline basemap to indicate the relative location of the amounts and rates of change. Here it shows the general trend of erosion and negative shoreline movement along the southern end of Sixteen-Mile Beach, while the midsection of the beach shows slight accretional trends.

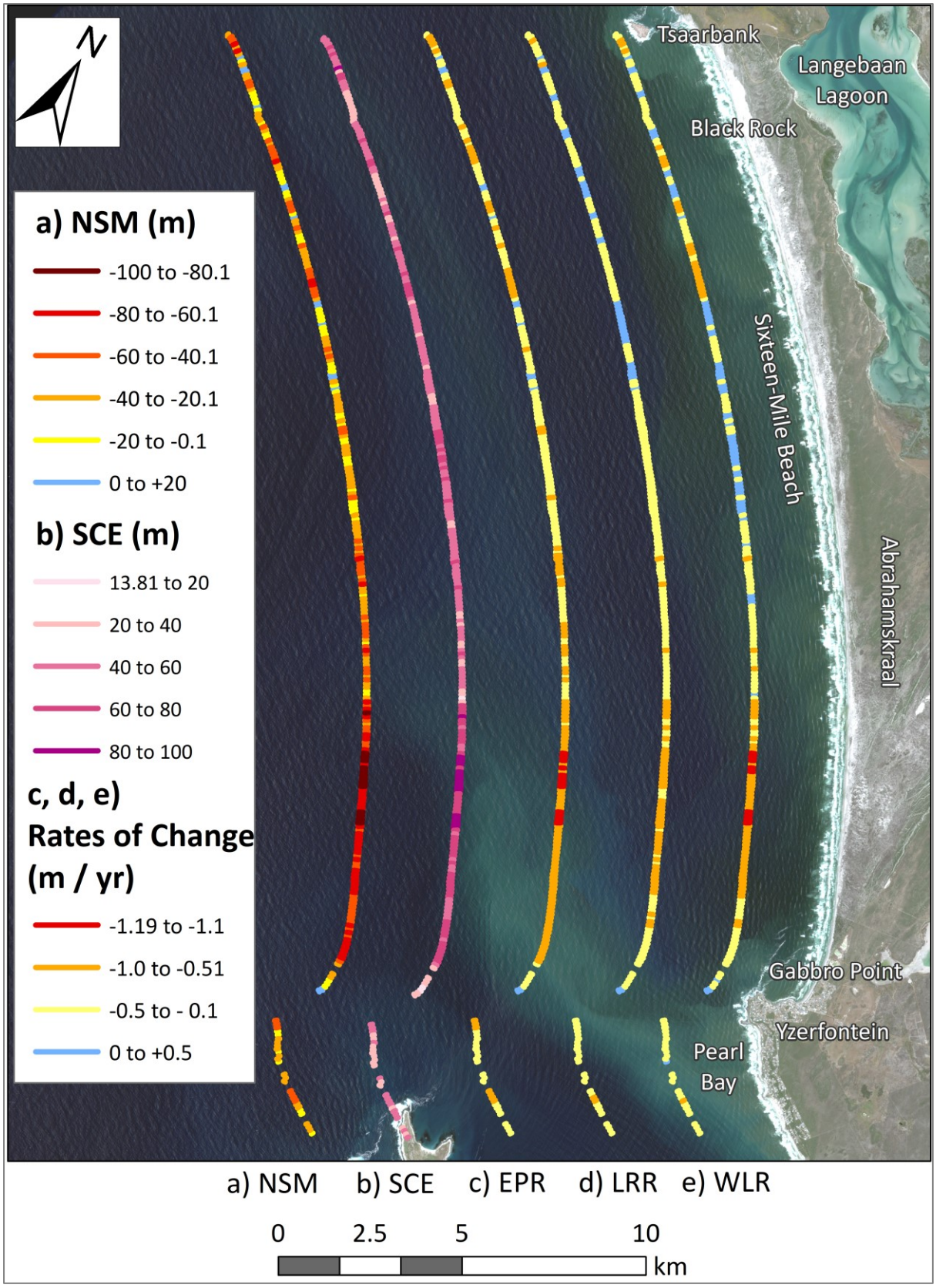


Figure 5.3: Summary of DSAS results showing a) the Net Shoreline Movement (NSM), b) Shoreline Change Envelope (SCE), c) End Point Rate (EPR), d) Linear Regression Rate (LRR), and e) the Weighted Linear Regression (WLR).

The final evaluation of long-term shoreline change was investigated by using a multivariate approach, adopted from Burningham and French (2017), to construct a timeseries heat-matrix. Figure 5.4 shows this timeseries heat-matrix whereby the years are plotted on the x-axis and the 30 km shoreline chainage is plotted on the y-axis from south to north. Within the plot is a choropleth matrix representing the amount of shoreline change (m) with regards to the 1937 shoreline position. These values remain the same until the midpoint of the different time periods and so it appears as a discrete matrix of values, as compared to a smoothed interpolated plot. Shades of blue signify increased seaward movement of the shoreline compared to 1937, while shades of red signify increased landward movement. This allows for greater inspection of the interdecadal trends.

The shoreline has been under a constant state of change between each decade (see Figure 5.4). From 1937 to 1960, sections of shoreline moved between -20 m and +20 m away from their original positions, with slight accretion south of Black Rock and the middle of Sixteen-Mile Beach, while the remaining sections of shoreline moved landward. Then, between 1960 and 1977, greater amounts of accretion occurred along the middle of Sixteen-Mile Beach, while the southern end experienced more erosion. Less extreme changes occurred along the coastline between 1977 and 2015 considering the positional uncertainty values that would be attached to these measurements.

The most drastic changes shown in Figure 5.4 are those between 2015 and 2020, whereby most of the shoreline shows an increased landward movement. All of Pearl Bay, Yzerfontein Main Beach and the southern end of Sixteen-Mile Beach show the largest amount of change within this period, highlighting the previously mentioned ‘erosion hotspot’ area 6 km north

of Gabbro Point and Yzerfontein. Hence, this period of 2015-2020 has been further investigated in the next section.

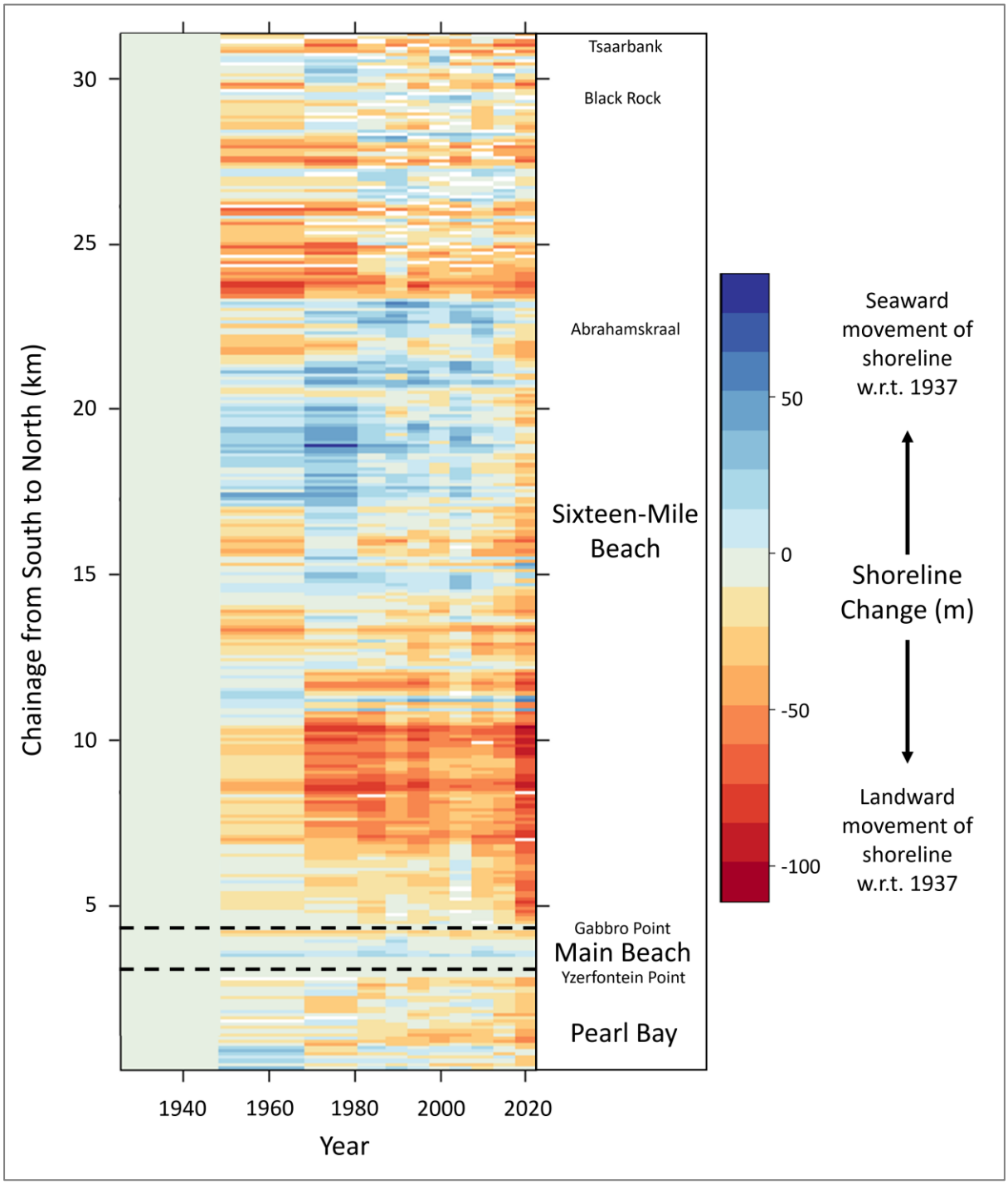


Figure 5.4: Timeseries heat-matrix representing the amount of change to the shoreline with regards to the 1937 shoreline position over the eleven time periods.

5.3 Short-term shoreline change

The second stage of the analysis was to investigate the short-term shoreline changes experienced between 2015 and 2020 by using a highly temporal dataset of 304 shoreline positions extracted from Sentinel-2 imagery using *CoastSat*. A case-study based approach was adopted to investigate six specific locations along the study site, namely at the mid-point Pearl Bay, the mid-point of Yzerfontein Main Beach, near Rooipan, near Abrahamskraal, near Tsaarbank, as well at the 'erosion hotspot' identified in the long-term analysis (refer to Figure 4.5 in Chapter 4).

Transects were drawn through the multiple shoreline positions to calculate the cross-shore changes with respect to the mean distances, which were then plotted against time (Figure 5.5). Figure 5.5 shows the six cross-shore change graphs with a colour key to emphasise the landward (red) and seaward (blue) changes. The graphs also include a simple linear regression trend line through the data and their coefficient of determination (R^2) values, as well as a marker to indicate when the storm surge event of June 2017 occurred (orange line in Figure 5.5).

All six of the case-study locations show a high variability in shoreline position over time with an average range of 77 m. The Erosion Hotspot (D) has the largest range of 91 m, followed by Rooipan (C) with a range of 86 m. Pearl Bay (A) has the smallest range of 50 m. Pearl Bay also has the most cyclical trends in the dataset with cross-shore changes approximating +20 m during the summer months, while decreasing to -20 m from the mean position in the middle each of the five years (winter months). This could indicate a seasonal influence on the beach. On the other hand, none of the other locations show the same cyclical pattern in their data.

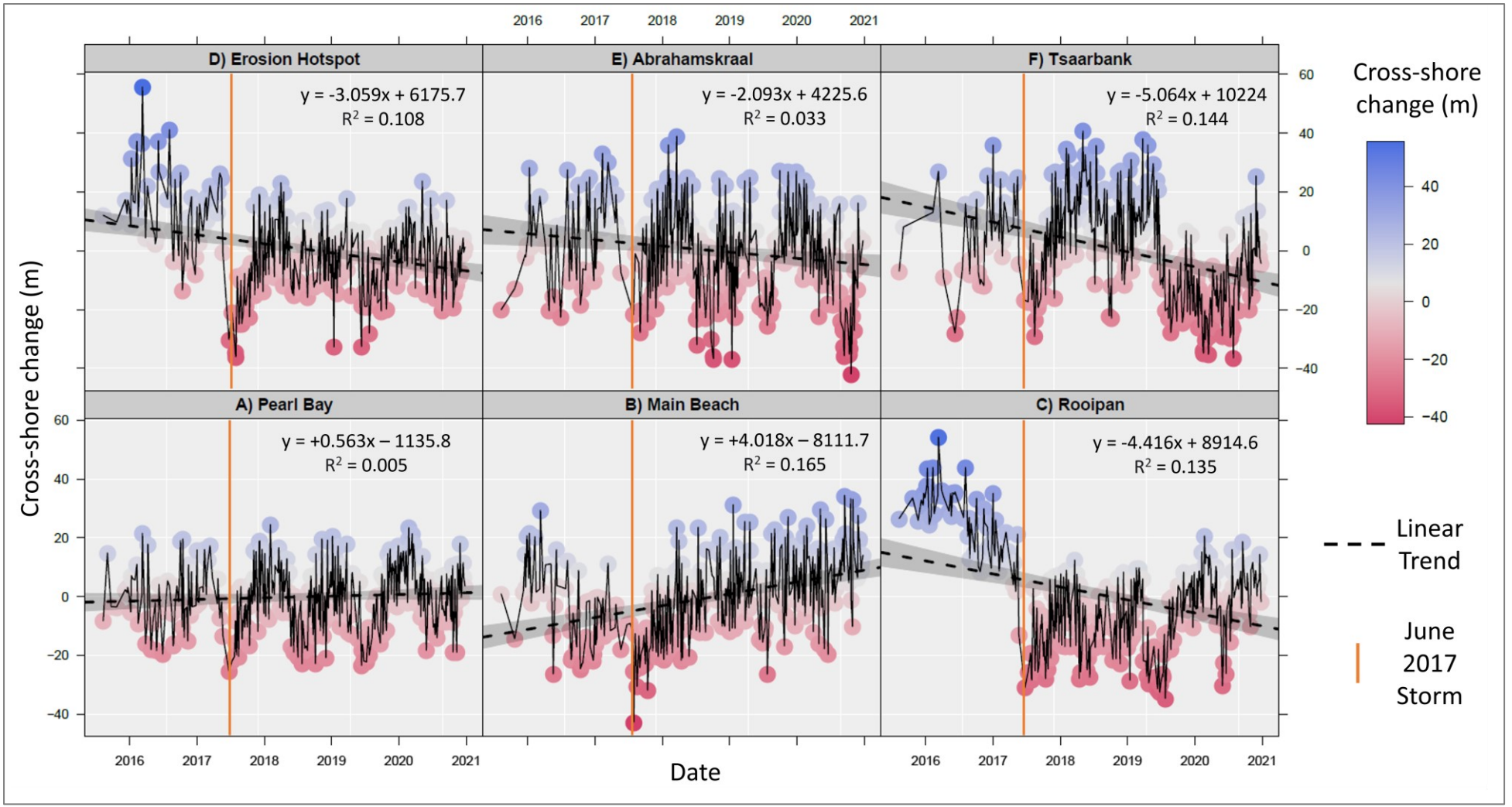


Figure 5.5: Cross-shore change between August 2015 and December 2020, derived from Sentinel-2 data, for six locations along the study site.

Figure 5.5 also highlights when the storm surge of June 2017 took place (the orange line), and the impact that it had on the shoreline position. All six locations show a decrease in cross-shore change compared to before the storm. Rooipan (A) and the Erosion Hotspot (D) show a substantially large movement of more than 50 m landward. Additionally, this was the most landward shoreline position recorded during this period for Rooipan, Yzerfontein Main Beach and Pearl Bay, while the Erosion Hotspot recorded its most landward shoreline position a few days after the storm. The plots also provide insight into how the different section of beach recovered after the storm. Pearl Bay, Yzerfontein Main Beach, Abrahamskraal and Tsaarbank's shorelines extended back to their pre-storm positions, while the shoreline near Rooipan and the Erosion Hotspot experienced less recovery and did not return to their 2015/2016 positions.

As for the overall linear trend in the shorelines, four out of six of the locations have negative rates of change. Tsaarbank (F) has the largest negative rate of -5.064 m/yr, followed by Rooipan (-4.416 m/yr), then the Erosion Hotspot (-3.059 m/yr), and Abrahamskraal (-2.093 m/yr). The trend for Pearl Bay is +0.563 m/yr, which can be approximated to a near-stationary trend. In comparison, Yzerfontein Main Beach (B) has a positive rate of change over this period of +4.018 m/yr. However, the coefficients of determination (R^2) are all less than 0.17 which proves a very weak linear relationship between cross-shore distance and time.

In comparing the short-term linear regression rates with the DSAS long-term rates, it appears that these short-term rates are substantially greater. For example, Sixteen-Mile Beach has an average long-term LRR of -0.28 m/yr (Table 5.4), while the average rate of the four case-study locations along Sixteen-Mile Beach (Figure 5.5 C to F) is equal to -3.66 m/yr. Additionally,

Yzerfontein Main Beach has an average long-term LRR of -0.05 m/yr (Table 5.4) and a much larger accretional short-term rate of +4.018 m/yr. However, Pearl Bay does have the most similar short-term and long-term rates compared to the other five locations of +0.563 m/yr and -0.27 m/yr, respectively.

5.4 Future shoreline changes

The final phase of analysis was to model the future shoreline position for 2030 and 2040 using the statistical trends from the long-term analysis (1937 to 2020) from Chapter 5.2. These models were created using DSAS (v 5.0) and its new 'Beta Shoreline Forecasting' tool which uses a Kalman Filter to calculate the position of the shoreline based on the linear regression rates and uncertainty values in 10 and 20 years' time from the most recent position (Himmelstoss *et al*., 2018). Combined uncertainty values are then also calculated by DSAS to show the horizontal extent within which the new shoreline positions could be situated; these are created as buffer polygons around the 10 and 20-year shorelines.

The model was run for the entire study site to investigate whether there are regions of concern for where possible erosional trends could affect the foredune or coastal infrastructure, or if there are sections of coastline, which could accrete over time. The 10 and 20-year shorelines and their respective uncertainty buffers were then compared to an ESRI basemap / Maxar Technologies high-resolution satellite image from 2020 and visually inspected. Overall, the future shoreline positions did not show substantial movement from the current high-water line and the uncertainty buffers remained within the extent of the foreshore. Figure 5.6 illustrates four case-study examples of ~1 km stretches of coast, showing

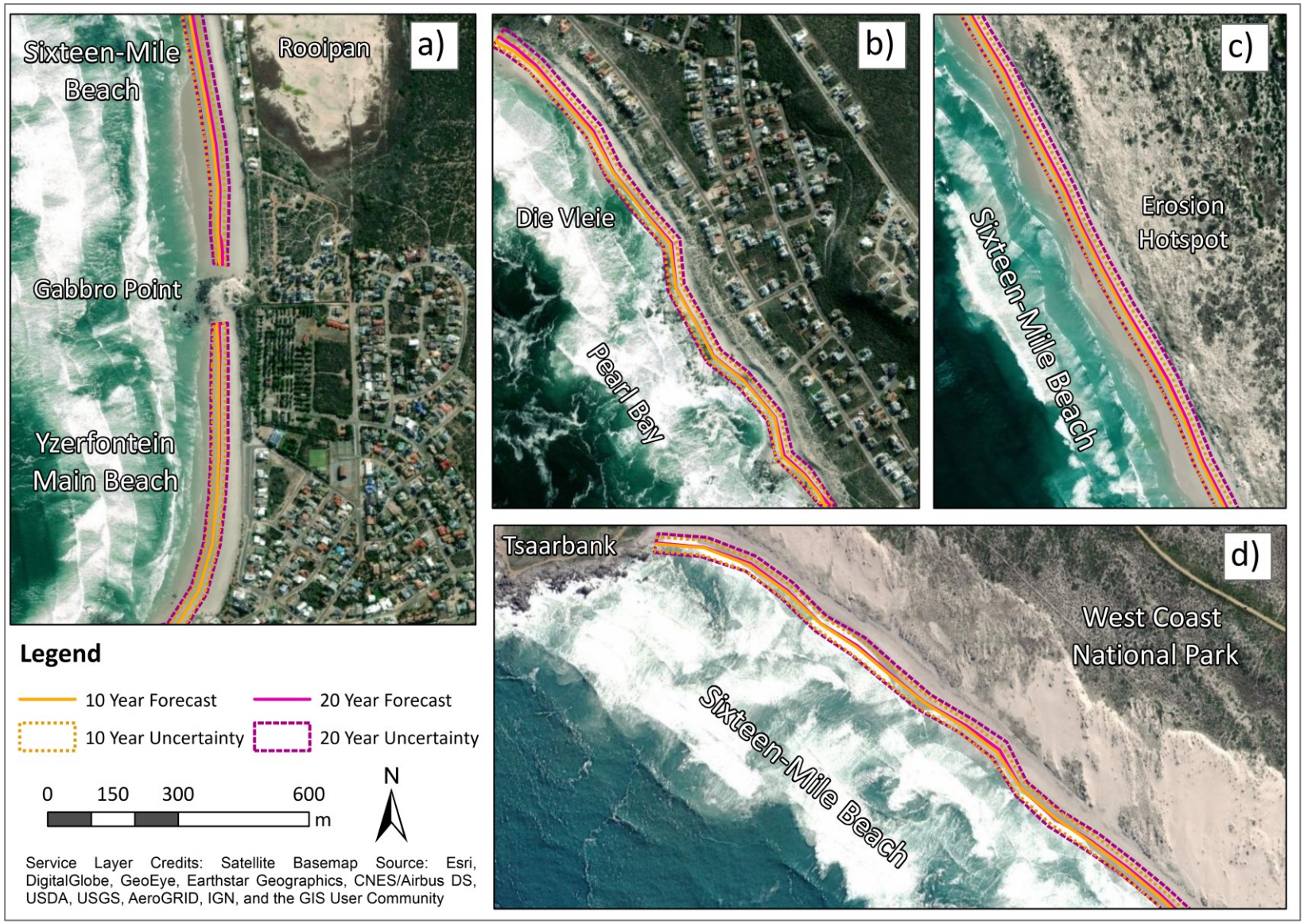


Figure 5.6: Shoreline position forecasts for the next 10 and 20 years with their horizontal uncertainty for four locations along the study site: a) Yzerfontein Main Beach and the southern end of Sixteen-Mile, b) the northern end of Pearl Bay, c) the erosion hotspot located 6 km north of Gabbro Point, and d) the northern end of Sixteen-Mile Beach at Tsaarbank.

the 10 year (2030) shoreline forecast and uncertainty boundaries in orange and the 20 year (2040) in dark pink/purple.

From Figure 5.6, the two shoreline forecasts follow the general curvature of the current foreshore except d) at Tsaarbank. The shoreline at Tsaarbank shows a series of cusps along the beach which have been over-simplified into a straighter line by the model. The 10-year uncertainty area had an average buffer distance of 16 m (width of 32 m) and the 20-year uncertainty had an average buffer distance of 22 m (width of 44 m). These distances fall within the study site's wide backshore and do not appear to cross the dune toe threshold — apart from along the 'erosion hotspot' (Figure 5.6c). At the 'erosion hotspot' (and a small section 1 km north of it), the 20-year uncertainty buffer exceeded the edge of the foredune. Figure 5.6b shows the northern end of Pearl Bay, where the uncertainty buffer is closer to the dune toe than at Sixteen-Mile Beach and Yzerfontein Main Beach (Figure 5.6a).

5.5 Summary

Chapter 5 has presented the results of this research report which are divided into three sections of investigating long-term, short-term, and future shoreline changes. The long-term changes between 1937 and 2020 revealed that there was an overall net landward movement, averaging -38 m (Table 5.1). Yzerfontein Main Beach experienced the least change, followed by Pearl Bay which saw some erosion during 2015 to 2020. As for the rate of shoreline change, only 47% of the shoreline experienced statistically significant rates of erosion and 3% rates of accretion, whereas the other 50% can be classified as not showing any significant trend (Table 5.5).

The short-term analysis revealed that the June 2017 storm had an impact on all case-study locations along the study site (Figure 5.5). Some beaches recovered faster than others after the storm, while near Rooipan and at the 'erosion hotspot', the shoreline has not yet returned to its pre-storm locations and shows a continuing landward trend of movement. Most cross-shore change plots did not show clear seasonal trends, except for Pearl Bay which shows constant fluctuations between the summer and winter seasons. Finally, the future shoreline modelling revealed that the shoreline is forecast to move marginally landward in the next 10 and 20 years, and that the added uncertainty buffers of approximately 16 and 22 m, respectively, are contained within the current wide foreshore area (Figure 5.6). These findings are discussed in further detail in the following chapter.

Chapter 6:

DISCUSSION

6.1 Introduction

This chapter discusses the significance of the results obtained from the investigation. Firstly, the results are analysed and critiqued against similar shoreline change studies and the implications of these results are highlighted. Secondly, the limitations of the study are explained and how these may have influenced the results. Finally, numerous recommendations are provided for how to further expand this research.

6.2 Analysis and critique of results

It has been found in conducting the long-term and short-term analyses of South Africa's south western shoreline, that these beaches have undergone dynamic changes. The main findings of this study are that Sixteen-Mile Beach, Yzerfontein Main Beach, and Pearl Bay have undergone a net landward movement of the shoreline, averaging to 38 m. Between 1937 and 2020 these beaches have undergone differing amounts of erosion and accretion, at different time periods over the eight decades. This was calculated by combining two different datasets and methodologies, namely digitising historical aerial photographs, and automatically extracting shoreline positions from satellite imagery. Overall, Yzerfontein Main Beach was found to have undergone the least amount of shoreline change, followed by Pearl Bay. Whereas, Sixteen-Mile Beach has experienced zones of greater shoreline retreat and advancement. The southern half of Sixteen-Mile Beach has shown a net landward shoreline movement of approximately 50 m, while the northern half has experienced less landward movement (~ 30 m) with small sections showing a seaward progradation (maximum 18.3 m) (refer to Figure 5.1 and Table 5.1).

A possible reason for these differences in erosion trends could be due to how the wave energy is dissipated across this large log-spiral beach system. For example, the rock outcrops along Pearl Bay, the harbour seawall and Meeurots outcrop may provide these beaches with more shelter from the southerly wave swells (see Figure 2.2a). In comparison, Sixteen-Mile Beach is completely exposed to wave energy and longshore drift. However, this would have to be further investigated through hydromorphological analysis of the sea-swell patterns to be confirmed.

The highest recorded net shoreline movement and rate of erosion was found to be six km north of Gabbro Point, measuring 99.29 m and -1.19 m/yr respectively. Interestingly, field surveys conducted by Franceschini (2003) and Franceschini and Compton (2006), found that the beach profile and characteristics changed at six km north of Gabbro Point. The average grain size rapidly changed from fine to medium between the six and nine km mark, the calcium carbonate composition decreased, and height of the pioneer dunes also substantially increased at this location (Franceschini, 2003; Franceschini and Compton, 2006). The researchers also describe this location as having a very wide backshore area (>90 m). This could possibly lead to more variability in tidal runup being recorded by *CoastSat*, which could have influenced the long-term rates of changed of this research report.

Moreover, the increased erosion experienced along the southern section of Sixteen-Mile Beach appears to contradict the theory by Compton (2016) that Dassen Island creates a 'swell barrier' around the southern end of Sixteen-Mile Beach, which allows for sediment to accumulate and be transported inland to form the start of the Yzerfontein-Geelbek dune system (see Figure 2.7). However, these results also confirm the findings of Franceschini and

Compton (2006), Kandel and Conard (2013) and Henrico *et al*. (2020) who all ascertain that the Yzerfontein-Geelbek dune system has shifted northwards and decreased in size over the decades. Additionally, this investigation has also been able to identify these trends from the historical aerial photographs, which clearly show that the dunes have decreased, as well as the shoreline moving landwards (Figure 6.1). Quantifying the changes in the dune system was beyond the scope of this research report but could be further investigated by manually digitising these changes in dune size or through object-based image classification techniques.

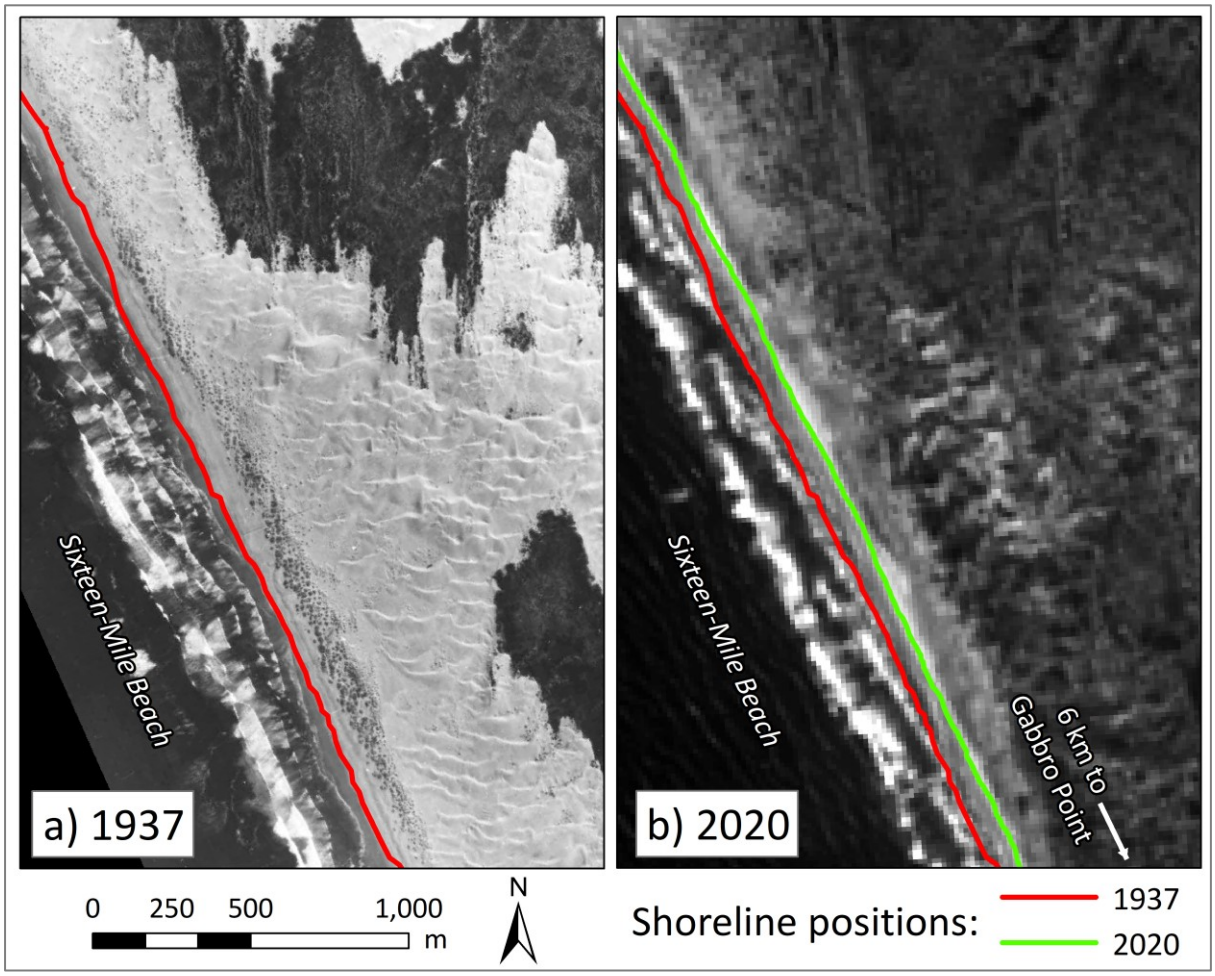


Figure 6.1: A comparison between the historical aerial photograph from 1937 and the panchromatic Landsat 8 image from 2020 showing the change in shoreline position and coastal dune distribution.

The results of this research can also be compared and contrasted to that of Luijendijk *et al*. (2018) who conducted a global-scale study of shoreline change by calculating rates of erosion and accretion at every 500 m interval of sandy beach. The researchers used Landsat satellite imagery between 1984 and 2016 to extract the shoreline positions and have published their results as a web-GIS site where users can click on each transect to view its rate of change (https://aqua-monitor.appspot.com/?datasets=shoreline). Figure 6.2 illustrates their results for Yzerfontein and Sixteen-Mile Beach. The rates of change of the transects covering the study site range between -2.9 ±0.6 m/yr and +0.5 ±0.6 m/yr, with an average rate of -1.71 ±0.44 m/yr.

These rates of change are greater than the linear regression and weighted linear regression rates found in this study (with an average WLR of -0.28 ±0.33 m/yr). All but one of their 500 m transects have negative rates of change, whilst this study found 78% of the 100 m transects have negative WLR rates. Additionally, Luijendijk *et al*. (2018) indicate that the highest rates of erosion occurred immediately north of Gabbro Point, near Rooipan. These results are surprising, since the trends are from 1984 to 2016, before the strong storm surge of 2017, and show shoreline erosion. Yet, this project's findings show that the 2017 storm was a significant driver in erosion north of around Gabbro Point, which was less dynamic between 1985 and 2015 (see heat-matrix Figure 5.3).

In Figure 6.2, it is noted that extreme erosional transects are labelled on the eastern bank of Langebaan Lagoon (visualised by the long red lines). These are most likely due to tidal fluctuations in the saltmarsh vegetation. This highlights the limitations to Luijendijk *et al*.'s (2018) global model.

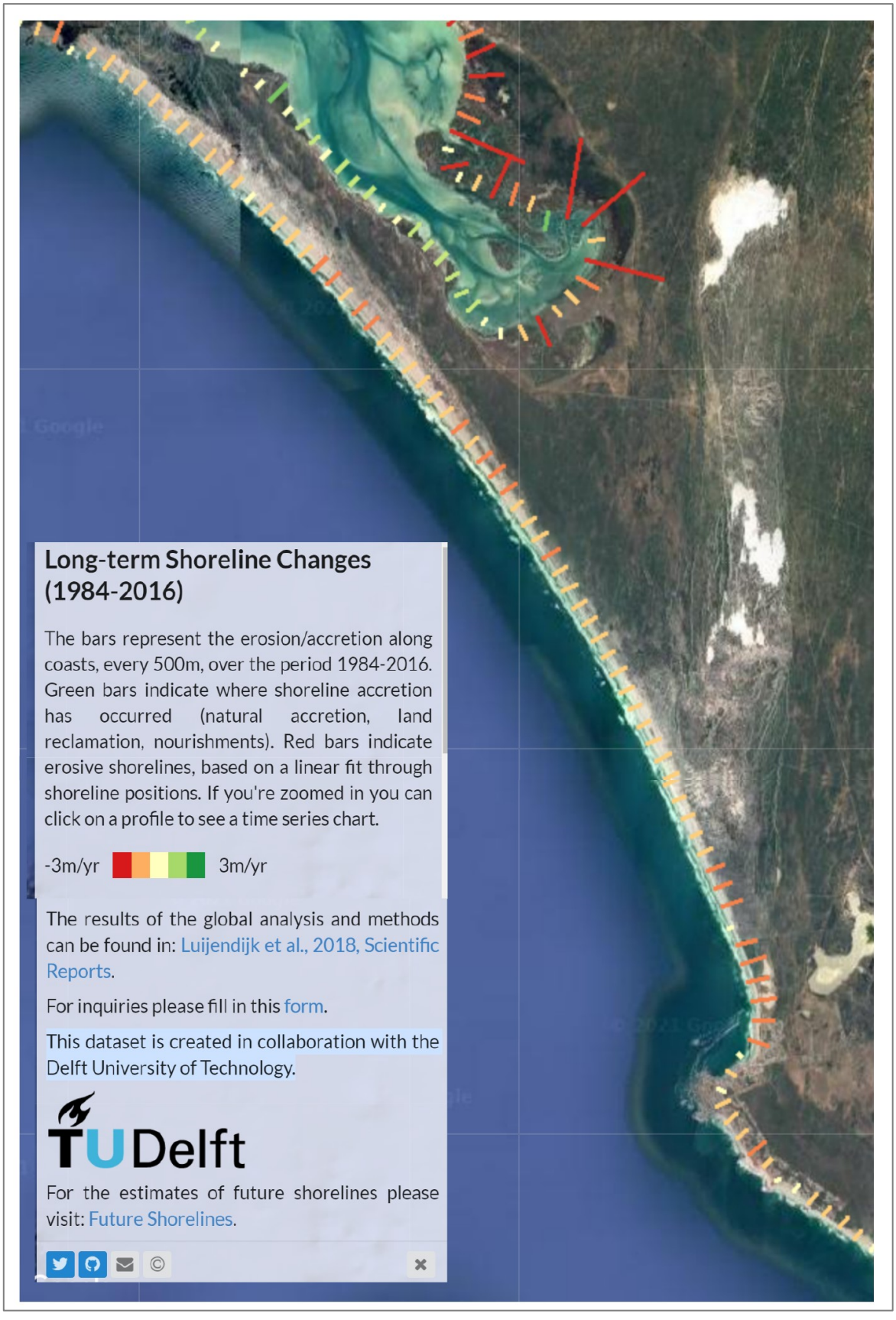


Figure 6.2: Screenshot of the results obtained from the global study on long-term shoreline change conducted by Luijendijk *et al*. (2018) for Yzerfontein and Sixteen-Mile Beach (source: https://aqua-monitor.appspot.com/?datasets=shoreline).

Furthermore, the results of this study are comparable with those of Callaghan (2014) and Callaghan *et al*. (2015) who investigated shoreline changes along False Bay, in Cape Town, between 1944 and 2010 using historical aerial photographs. False Bay experiences similar swell patterns and climatic conditions, and is composed of the same Witzand Formation, thus one would expect rates of erosion to be similar. Callaghan (2014) and Callaghan *et al*. (2015) calculated average linear regression rates (LRR) of between -0.14 and -1.46 m/yr along four of False Bay's beaches, which signifies a net erosion of these beaches over the 66-year study period. These LRR are similar to those of this study whereby Sixteen-Mile Beach, Yzerfontein Main Beach and Pearl Bay experienced LRR of -0.28 ±0.40, -0.05 ±0.19 and -0.27 ±0.30 m/yr, respectively, over the 83-year time period. However, the researchers attribute these erosion trends to increased climapogenic activities along the coast, noting increased urbanization, construction of coastal barriers and controlling rivers. Yzerfontein and the West Coast National Park have not experienced such anthropogenic pressures and do not have any river mouths directly changing the sediment budget.

The linear regression and weighted linear regression rates of this research report were subsequently used to model future changes to the shoreline positions with the new DSAS forecasting function. This model produced shoreline positions for 10 and 20 years' time (2030 and 2040) and their respective uncertainty boundaries (see Figure 5.6). The main findings of these forecasts were that the shoreline positions were estimated to retreat one to five m away from the current high water line, and that the uncertainty boundaries remained within the current extent of the backshore. It was only at the 'erosion hotspot' that the 20-year uncertainty boundary was shown to extend over the foredunes (see Figure 5.6c). Therefore, these results indicate that future shoreline changes may not severely impact the housing and

infrastructure along Yzerfontein and Pearl Bay, as well as not extensively erode the foredunes of Sixteen-Mile beach and its coastal ecosystems.

Nevertheless, the creators of the DSAS forecasting model (Himmelstoss *et al*., 2018) warn of the limitations to the model as it only considers the statistical rates of change and not the underlying geology, beach profile or wave conditions which may cause increased rates of change in the future. Much like Bruun's Rule of Erosion, the models are only able to provide a general overview of how a beach may respond to increased erosion due to sea-level rise, but they do not account for the full complexities of coastal systems (Cooper and Pilkey, 2004; Masselink *et al*., 2011; Cooper *et al*., 2020). Thus, these 10 and 20-year forecasting models are very limited and do not illustrate how the beach width, beach profile and foredunes will change if the shoreline continues to retreat or if another large storm surge occurs. During the June 2017 'Cape Storm', a combination of extreme wind, rain, and low pressure caused significant swell waves and storm surges around the southwestern Western Cape Province, which was already in a prevailing two-year drought (Barnes *et al*., 2021; Troch *et al*., 2021). Thus, the next vital research question to pose is if this storm can be viewed as a once-off extreme event or if the frequency of these type of climate extremes may increase due to regional and global anth?

6.3 Limitations

The major limitations to this research report are the high levels of uncertainty in the data. By using medium resolution satellite imagery, the results are negatively influenced by the image pixel size, meaning that the Sentinel-2 and Landsat imagery shorelines are only accurate within 10 and 15 m, respectively (Vos *et al*., 2019a and 2019b). For example, Figure 6.1 shows

the 15 m panchromatic band from Landsat 8 compared to the 3 m aerial photograph. In addition, these shoreline positions are influenced by the tidal conditions and variations. *CoastSat* has the option to undertake a tidal correction of the shoreline position data to remove variations caused by the tides (Vos *et al*., 2019a and 2019b). However, there is very limited access to accurate, long-term, publicly available tidal data for this region, therefore, tidal corrections were not conducted for the study which decreases the accuracy of the results.

Another source of uncertainty stems from how the historical aerial photographs were georeferenced. Thieler and Danforth (1994b) state the possible sources of error that can arise from georeferencing and digitising historical aerial photographs. These range from the photographs being distorted by the tilt or steadiness of the aircraft, to the photographs being physically damaged, or there being too few ground control points to match with a georectified source. All the photographs acquired from the NGI for this investigation were clear with little distortion, but a few had been drawn and marked on. However, georeferencing proved difficult due to the lack of consistent and well-defined ground control points as Sixteen-Mile Beach has always remained relatively undisturbed by human activity and its active foredunes and vegetation have changed over the decades. Thus, the historical shoreline positions from 1937, 1960 and 1977 may contain more uncertainty than estimated. Additionally, there is a large gap in the data for the 1940s and 1950s, which limits the understanding into how the shoreline has changed over time. The NGI did not have any aerial photographs for these decades but other organisations may have. For example, the South African Air Force and Military may have conducted reconnaissance flights during and after World War 2 as the study site is situated very near to the Saldanha Military Base and Langebaanweg Air Force.

6.4 Recommendations for further research

In terms of remote sensing, there are numerous options to better advance this study. For example, the study could include methodologies outlined by Warnasuriya *et al*. (2020), whereby shoreline positions could be extracted from Google Earth Pro historical imagery. These high-resolution data would contain less uncertainty than the Landsat and Sentinel-2 derived shorelines and could be used to test the accuracy of *CoastSat*. Secondly, *CoastSat* could be used to provide yearly shoreline changes, such as Luijendijk *et al*. (2018), instead of only focusing on shorelines from every five year period.

CoastSat has subsequently been updated from the version used in the study. The new version allows users to plot and adjust the MNDWI pixel threshold values, as well as add their own training data to the classification. Thus, if this study were to be reproduced, classifications could be more tailored with training data from the site. Additionally, the CoastSat.slope extension could be applied with the FES2014 global tide model to assess the differences in beach steepness along the study site (Vos *et al*., 2020).

A key investigation would be to study this region in a more integrated approach by using various shoreline proxies to calculate the rates of change to not only the shoreline, but also the dune and vegetation edge, as set out by Pollard *et al*. (2019). This could then be combined with calculating the aerial extent of the Yzerfontein-Geelbek dune over time through land-cover change analysis of the historical aerial photographs and satellite imagery. This would allow for a better interpretation of how the whole beach profile and dune system have changed. Additionally, one could investigate wider changes to the ocean currents, swell-patterns and ocean temperatures using SeaSat satellite imagery from the 1970s, SAR imagery,

and the recently launched Sentinel-6, which specifically focuses on sea-level rise (Gens, 2010; ESA, 2021). Drones could be flown over the beach and dunes to create accurate topographic models, and meteorological satellite data could also be integrated to study the impact of storms on shoreline change. This plethora of data could then be analysed using much more advanced machine learning algorithms, as described by Beuzen and Splinter (2020), compared to the simple linear statistics of DSAS.

Alternatively, future research could integrate socio-economic data from Yzerfontein. Colenbrander and Sowman (2015) argue that socio-economic data and community engagement needs to be considered in coastal research, especially in South Africa. They claim that municipal coastal set-back lines are usually generated by private consultancies who rely on empirical geo-spatial modelling and not enough social information to understand the true realities of these coastal settings; stating that "such an approach is parochial and socially detached and a more inclusive and integrated approach grounded in and spanning localized social, cultural, economic, political, and ecological intricacies of the coastal space is required" (Colenbrander and Sowman, 2015: 270).

A potential recommendation is to amalgamate remote sensing and community engagement using the Australian crowd-sourcing initiative of CoastSnap, in Yzerfontein. This is where stainless steel structures are installed at strategic locations around beaches where the public can place their smartphones, take photos of the beach and share them via social media to a database to track changes in the shoreline (Splinter *et al*., 2018; Harley *et al*., 2019). This alternative approach allows for highly temporal data to be collected, and for the community to become involved in understanding coastal changes. The Yzerfontein community already

shows an awareness of the impact of coastal erosion by publishing an article about the June 2017 storm surge event in the local newspaper (Renwick, 2018), and there are multiple signposts along the beach promoting dune protection and rehabilitation (Figure 6.3).



Figure 6.3: Signposts around Yzerfontein promoting dune protection and rehabilitation (Source: Author's photographs, November 2020).

6.5 Summary

Chapter 6 has interpreted the main findings of the study and discussed how they relate to other studies conducted in the region, such as Franceschini (2003), Franceschini and Compton (2006), Kandel and Conard (2013) and Henrico *et al*. (2020). The limitations of the research are also presented, and several recommendations are given to address these limitations in future research.

Chapter 7:

CONCLUSION

7.1 Overview of research

This research report aimed to investigate the spatiotemporal changes to the southwestern shoreline of South Africa between 1937 and 2020 and to project future shoreline changes. This was achieved through integrating different remote sensing data sources and techniques. Firstly, historical aerial photographs from 1937, 1960 and 1977 were georeferenced, and their shoreline positions were manually digitised. Secondly, shoreline positions were automatically delineated from Landsat 5, 7 and 8 and Sentinel-2 imagery between 1985 and 2020 using the *CoastSat* toolkit and Google Earth Engine. These two datasets were then combined to calculate the amounts and rates of shoreline erosion and accretion that has taken place over these eight decades using the Digital Shoreline Analysis System (DSAS). Additionally, the short-term shoreline variability, seasonality and storm surge impact were investigated by creating cross-shore change profiles at specific locations along the shoreline, using Sentinel-2 data. Finally, DSAS was used to model future shoreline positions for 2030 and 2040 based on the long-term rates of change.

The main findings of this study show that the shorelines around Sixteen-Mile Beach and Yzerfontein have been dynamic over the last eight decades and have experienced a net shoreline retreat. The greatest erosion was experienced along the southern section of Sixteen-Mile Beach, within the West Coast National Park, while less shoreline change was experienced around the town of Yzerfontein. This could possibly be attributed to wider changes to the whole coastal and inland dune system that have been occurring over the

decades (Franceschini, 2003; Franceschini and Compton, 2006; Kandel and Conard, 2013; Henrico *et al*., 2020), or changes to the regional ocean and climate systems.

The linear regression rates of shoreline change were found to be less than those of Luijendijk *et al*. (2018) who conducted a global-scale investigation of shoreline change using Landsat satellite imagery between 1984 and 2016. Furthermore, the weighted linear regression rates revealed that only 47% of the study site experienced statistically significant rates of erosion, while 3% experienced statistically significant rates of accretion, and the majority of the study site (50%) experienced non-significant rates of shoreline change.

The large storm surge of June 2017 was a significant event that impacted on the whole study site and has re-shaped portions of the coastal dunes and shoreline. This was illustrated by the short-term analysis of shorelines delineated from Sentinel-2 imagery, thereby demonstrating how *CoastSat* can be effectively used in monitoring storm surge scenarios. One of the significant features of *CoastSat* is that it is scalable to shorelines all over the world. Therefore, short-term variability studies can be conducted at different beaches along the rest of South Africa, and the world, to assess the damage of storm surge events.

By utilising a combination of data sources and techniques, the study has been able to offset some limitations of certain data sources with the advantages of the other methods. For example, digitising historical aerial photographs has been the standard methodology in shoreline change analysis studies for well over 40 years, but this method is negatively influenced by human error and the lack of availability of images. Whereas *CoastSat* offers a

more objective, automated, and advanced methodology, which draws on Google Earth Engine's wide database of satellite imagery and machine learning capabilities.

7.2 Limitations and recommendations of research

As described in the Discussion, there are limitations to the data and methodologies that have been used in this study. These limitations are mainly attributed to the high uncertainty of the shoreline positions related to both the satellite sensors' large pixel size and the historical aerial photographs' georeferencing. The lack of accurate, historical and timely tidal data, as well as ground-survey data, also negatively impacts the reliability of the results.

Furthermore, there are many avenues to expand this research and build on the methodologies. This could be implemented by integrating even more remote sensing and non-remote sensing data. For example, a combination of SAR, meteorological satellite data, drone surveys, and crowd-sourced photographs would provide a more holistic understanding of the region's coastal dynamics. By measuring and monitoring these dynamic processes and drivers of change along South Africa's longest uninterrupted sandy beach, we can better understand how this growing tourism destination of Yzerfontein, and the West Coast National Park might be influenced by climate change and its subsequent impacts of coastal erosion.

REFERENCES

Amrouni, O., Hzami, A. and Heggy, E., 2019. Photogrammetric assessment of shoreline retreat in North Africa: Anthropogenic and natural drivers. *ISPRS Journal of Photogrammetry and Remote Sensing*, 157, pp.73-92.

Avery, G., Halkett, D., Orton, J., Steele, T., Tusenius, M. and Klein, R., 2008. The Ysterfontein 1 Middle Stone Age rock shelter and the evolution of coastal foraging. *Goodwin Series*, 10, pp.66-89.

Barnes, M.A., Turner, K., Ndarana, T. and Landman, W.A., 2021. Cape storm: A dynamical study of a cut-off low and its impact on South Africa. *Atmospheric Research*, 249, p.105290.

Benkhattab, F.Z., Hakkou, M., Bagdanavičiūtė, I., El Mrini, A., Zagaoui, H., Rhinane, H. and Maanan, M., 2020. Spatial–temporal analysis of the shoreline change rate using automatic computation and geospatial tools along the Tetouan coast in Morocco. *Natural Hazards*, 104, pp.519-536.

Beuzen, T. and Splinter, K., 2020. Machine learning and coastal processes. In Jackson, D.W.T. and Short, A.D., eds. *Sandy Beach Morphodynamics*, Elsevier, pp.689-710.

Bheeroo, R.A., Chandrasekar, N., Kaliraj, S. and Magesh, N.S., 2016. Shoreline change rate and erosion risk assessment along the Trou Aux Biches–Mont Choisy beach on the northwest coast of Mauritius using GIS-DSAS technique. *Environmental Earth Sciences*, 75(5), p.444.

Boak, E.H. and Turner, I.L., 2005. Shoreline definition and detection: a review. *Journal of Coastal Research*, 21(4), pp.688-703.

Boucher, C., 1981. Dune plumes in the western Cape. *Veld and Flora*, 67(1), p.11-13.

Browning, C. and Roberts, D.L., 2015. Lithostratigraphy of the Witzand Formation (Sandveld Group), South Africa. *South African Journal of Geology*, 118(3), pp.317-322.

Bruun, P., 1988. The Bruun rule of erosion by sea-level rise: a discussion on large-scale two-and three-dimensional usages. *Journal of Coastal Research*, 4(4), pp.627-648.

Burningham, H. and Fernandez-Nunez, M., 2020. Shoreline change analysis. In Jackson, D.W.T. and Short, A.D., eds. *Sandy Beach Morphodynamics*. Elsevier, pp.439-460.

Burningham, H. and French, J., 2017. Understanding coastal change using shoreline trend analysis supported by cluster-based segmentation. *Geomorphology*, 282, pp.131-149.

Callaghan, K.L., 2014. *The use of remote sensing and GIS in the identification and vulnerability detection of coastal erosion as a hazard in False Bay, South Africa*. Masters dissertation, Stellenbosch University, Stellenbosch.

Callaghan, K., Engelbrecht, J. and Kemp, J., 2015. The use of Landsat and aerial photography for the assessment of coastal erosion and erosion susceptibility in False Bay, South Africa. *South African Journal of Geomatics*, 4(2), pp.65-79.

Climate-Data.org, 2021. Yzerfontein Climate (South Africa). [Online] URL: https://en.climate-data.org/africa/south-africa/western-cape/yzerfontein-23414/, accessed on 22 September 2020.

Colenbrander, D.R. and Sowman, M.R., 2015. Merging socioeconomic imperatives with geospatial data: A non-negotiable for coastal risk management in South Africa. *Coastal Management*, 43(3), pp.270-300.

Compton, J.S., 2001. Holocene sea-level fluctuations inferred from the evolution of depositional environments of the southern Langebaan Lagoon salt marsh, South Africa. *The Holocene*, *11*(4), pp.395-405.

Compton, J.S., 2016. *The rocks and mountains of Cape Town*. 3rd impression. Earthspun Books, Cape Town.

Compton, J.S. and Franceschini, G., 2005. Holocene geoarchaeology of the sixteen mile beach barrier dunes in the Western Cape, South Africa. *Quaternary Research*, *63*(1), pp.99-107.

Cooper, J.A.G. and Pilkey, O.H., 2004. Sea-level rise and shoreline retreat: time to abandon the Bruun Rule. *Global and Planetary Change*, 43, pp.157-171.

Cooper, J.A.G., Masselink, G., Coco, G., Short, A.D., Castelle, B., Rogers, K., Anthony, E., Green, A.N., Kelley, J.T., Pilkey, O.H. and Jackson, D.W.T., 2020. Sandy beaches can survive sea-level rise. *Nature Climate Change*, 10, pp.260-263.

Crowell, M., Leatherman, S.P. and Buckley, M.K., 1991. Historical shoreline change: error analysis and mapping accuracy. *Journal of Coastal Research*, 7(3), pp.839-852.

Crowell, M., Leatherman, S.P. and Douglas, B., 2005. Erosion: Historical analysis and forecasting. *Encyclopedia of Coastal Science, Encyclopedia of Earth Sciences Series*, pp.428-432.

CSIR, 2014. *Environmental screening study for a proposed LNG terminal at Saldanha and associated pipeline infrastructures to Atlantis and Cape Town, Western Cape, South Africa*, CSIR Report No. CSIR/CAS/EMS/ER/2014/0012/B. Prepared for Western Cape Government.

De Boer, G. and Carr, A.P., 1969. Early maps as historical evidence for coastal change. *The Geographical Journal*, 135(1), pp.17-39.

Defeo, O., McLachlan, A., Schoeman, D.S., Schlacher, T.A., Dugan, J., Jones, A., Lastra, M. and Scapini, F., 2009. Threats to sandy beach ecosystems: a review. *Estuarine, Coastal and Shelf Science*, 81(1), pp.1-12.

Del Río, L. and Gracia, F.J., 2013. Error determination in the photogrammetric assessment of shoreline changes. *Natural hazards*, *65*(3), pp.2385-2397.

Del Río, L., Gracia, F.J. and Benavente, J., 2013. Shoreline change patterns in sandy coasts. A case study in SW Spain. *Geomorphology*, 196, pp.252-266.

Dolan, R., Hayden, B. and Heywood, J., 1978. A new photogrammetric method for determining shoreline erosion. *Coastal Engineering*, 2, pp.21-39.

Dolan, R., Fenster, M.S. and Holme, S.J., 1991. Temporal analysis of shoreline recession and accretion. *Journal of Coastal Research*, 7(3), pp.723-744.

Dolan, R., Fenster, M.S. and Holme, S.J., 1992. Spatial analysis of shoreline recession and accretion. *Journal of Coastal Research*, 8(2), pp.263-285.

El-Gamal, A.A., Balbaa, S.H., Rashed, M.A. and Mansour, A.S., 2020. Three decades monitoring of shoreline change pattern of Damietta Promontory, Nile Delta, Egypt. *Aquatic Science and Technology*, 8(2), pp.1-14.

Ellis, M.Y., 1978. *Coastal Mapping Handbook*. US Departments of Interior and Commerce, US Government Printing Office, Washington, DC.

Environmental Systems Research Institute (Esri), 2021. *Fundamentals of georeferencing a raster dataset*. [Online] URL: www.desktop.arcgis.com/en/arcmap/10.3/manage-data/raster-and-images/fundamentals-for-georeferencing-a-raster-dataset.htm, accessed on 3 March 2020.

European Space Agency (ESA), 2021. *Sentinel-2*. [Online] URL: www.sentinel.esa.int/web/sentinel/missions/sentinel-2 , accessed on 1 June 2020.

Fenster, M.S., Dolan, R. and Morton, R.A., 2001. Coastal storms and shoreline change: signal or noise? *Journal of Coastal Research*, 17(3), pp.714-720.

Fisher, J.S. and Overton, M.F., 1995. Interpretation of shoreline position from aerial photographs. In *Coastal Engineering 1994.* 24th International Conference on Coastal Engineering, pp. 1998-2003.

Flemming, B.W., 1977. Distribution of recent sediments in Saldanha Bay and Langebaan Lagoon. *Transactions of the Royal Society of South Africa*, 42(3-4), pp.317-340.

Flemming, B.W., 2015. *Depositional processes in Saldanha Bay and Langebaan Lagoon (Western Cape, South Africa)*. National Research Institute for Oceanology (NRIO), Stellenbosch, CSIR Research Report 362 (revised Edition), pp.233.

Flemming, B., 2020. Beach sand and its origins. In Jackson, D.W.T. and Short, A.D. (eds). *Sandy Beach Morphodynamics.* Elsevier, pp.15-37.

Ford, M., 2013. Shoreline changes interpreted from multi-temporal aerial photographs and high resolution satellite images: Wotje Atoll, Marshall Islands. *Remote Sensing of Environment*, *135*, pp.130-140.

Fourie, J.P., Ansorge, I., Backeberg, B., Cawthra, H.C., MacHutchon, M.R. and van Zyl, F.W., 2015. The influence of wave action on coastal erosion along Monwabisi Beach, Cape Town. *South African Journal of Geomatics*, *4*(2), pp.96-109.

Franceschini, G., 2003. *Geology of aeolian and marine deposits in the Saldanha Bay region, Western Cape, South Africa*. Doctoral thesis, University of Cape Town, Cape Town.

Franceschini, G., Compton, J.S. and Wigley, R.A., 2003. Sand transport along the Western Cape coast: gone with the wind? *South African Journal of Science*, 99(7), pp.317-318.

Franceschini, G. and Compton, J.S., 2006. Holocene evolution of the Sixteen Mile Beach Complex, Western Cape, South Africa. *Journal of Coastal Research*, 22(5), pp.1158-1166.

Gens, R., 2010. Remote sensing of coastlines: detection, extraction and monitoring. *International Journal of Remote Sensing*, 31(7), pp.1819-1836.

Godwyn-Paulson, P., Jonathan, M.P., Hernandez, F.R., Muthusankar, G. and Lakshumanan, C., 2020. Coastline variability of several Latin American cities alongside Pacific Ocean due to the unusual "Sea Swell" events of 2015. *Environmental Monitoring and Assessment*, 192(8), pp.522.

Gorelick, N., Hancher, M., Dixon, M., Ilyushchenko, S., Thau, D. and Moore, R., 2017. Google Earth Engine: Planetary-scale geospatial analysis for everyone. *Remote sensing of Environment*, 202, pp.18-27.

Hanekom N., Randall R.M., Nel, P. and Kruger, N. 2009. *West Coast National Park – State of Knowledge*. South African National Parks.

Hanson, H., 1989. GENESIS — A generalized shoreline change numerical model. *Journal of Coastal Research*, 5(1), pp.1-27.

Hapke, C.J., Himmelstoss, E.A., Kratzmann, M.G., List, J.H., and Thieler, E.R., 2011. *National assessment of shoreline change: Historical shoreline change along the New England and Mid-Atlantic coasts*. U.S. Geological Survey Open-File Report 2010-1118, 57p.

Harley, M.D., Kinsela, M.A., Sanchez-Garcia, E. and Vos, K., 2019. Shoreline change mapping using crowd-sourced smartphone images. *Coastal Engineering*, 150, pp.175-189.

Harris, L., Nel, R. and Schoeman, D., 2011. Mapping beach morphodynamics remotely: a novel application tested on South African sandy shores. *Estuarine, Coastal and Shelf Science*, *92*(1), pp.78-89.

Henrico, I., Ledwaba, T. and van Zyl, G., 2020. Measuring the effect of wind-driven processes on coastal dunes: a study of the Atlantis and Geelbek dune fields along the West Coast of South Africa. *Spatial Information Research*, 28, pp.569-577.

Himmelstoss, E.A., Henderson, R.E., Kratzmann, M.G., and Farris, A.S., 2018, *Digital Shoreline Analysis System (DSAS) version 5.0 user guide*. U.S. Geological Survey Open-File Report 2018–1179, 110 p.

Hinkel, J., Nicholls, R.J., Tol, R.S., Wang, Z.B., Hamilton, J.M., Boot, G., Vafeidis, A.T., McFadden, L., Ganopolski, A. and Klein, R.J., 2013. A global analysis of erosion of sandy beaches and sea-level rise: An application of DIVA. *Global and Planetary change*, 111, pp.150-158.

Honeycutt, M.G., Crowell, M. and Douglas, B.C., 2001. Shoreline-position forecasting: impact of storms, rate-calculation methodologies, and temporal scales. J*ournal of Coastal Research*, 17(3), pp.721-730.

Irrgang, A.M., Lantuit, H., Manson, G.K., Günther, F., Grosse, G. and Overduin, P.P., 2018. Variability in rates of coastal change along the Yukon coast, 1951 to 2015. *Journal of Geophysical Research: Earth Surface*, 123(4), pp.779-800.

Jackson Jr, C.W., Alexander, C.R. and Bush, D.M., 2012. Application of the AMBUR R package for spatio-temporal analysis of shoreline change: Jekyll Island, Georgia, USA. *Computers & Geosciences*, 41, pp.199-207.

Jackson, D.W.T. and Short, A. (eds.), 2020. *Sandy Beach Morphodynamics*. Elsevier. pp.1-13.

Kandel, A.W. and Conard, N.J., 2013. Stone Age economics and land use in the Geelbek Dunes. In Jerardino, A.M.S., Malan, A. and Braun, D.R. eds., *The Archaeology of the West Coast of South Africa*. Oxford: Archaeopress. pp.24-49.

Klemas, V., 2011. Remote sensing techniques for studying coastal ecosystems: An overview. *Journal of Coastal Research*, 27(1), pp.2-17.

Lemmen, A.C., 2011. *Second home development in South Africa*. Master's dissertation, Utrecht University, Netherlands.

Luijendijk, A., Hagenaars, G., Ranasinghe, R., Baart, F., Donchyts, G. and Aarninkhof, S., 2018. The state of the world's beaches. *Scientific Reports*, *8*(1), pp.6641.

Luijendijk, A. and de Vries, S., 2020. Global beach database. In Jackson, D.W.T. and Short, A.D. (eds). *Sandy Beach Morphodynamics.* Elsevier. pp.641-658.

Masselink, G., Hughes, M. and Knight, J., 2011. *Introduction to coastal processes and geomorphology*. 2nd edition. New York, Routledge.

Mauger, C.L. and Compton, J.S., 2011. Formation of modern dolomite in hypersaline pans of the Western Cape, South Africa. *Sedimentology*, 58(7), pp.1678-1692.

McBeth, F.H., 1956. A method of shoreline delineation. *Photogrammetric Engineering*, 22(2), pp.21-25.

McCurdy, P.G., 1947. *Manual of coastal delineation from aerial photographs* (No. 592). US Navy Hydrographic Office, Washington.

Mentaschi, L., Vousdoukas, M.I., Pekel, J.F., Voukouvalas, E. and Feyen, L., 2018. Global long-term observations of coastal erosion and accretion. *Scientific reports*, *8*(1), pp.12876.

Moore, L.J., 2000. Shoreline mapping techniques. *Journal of Coastal Research*, 16(1), pp.111-124.

Moore, L.J., Ruggiero, P., and List, J.H., 2006. Comparing mean high water and high water line shorelines: should proxy-datum offsets be incorporated into shoreline change analysis? *Journal of Coastal Research*, 22(4), pp.894-905.

Musekiwa, C., Cawthra, H.C., Unterner, M. and van Zyl, F.W., 2015. An assessment of coastal vulnerability for the South African coast. *South African Journal of Geomatics*, 4(2), pp.123-137.

National Geo-spatial Information (NGI), 2021. About NGI. [Online] URL: www.ngi.gov.za, accessed on 17 February 2020.

Nassar, K., Mahmod, W.E., Fath, H., Masria, A., Nadaoka, K. and Negm, A., 2019. Shoreline change detection using DSAS technique: Case of North Sinai coast, Egypt. *Marine Georesources & Geotechnology*, 37(1), pp.81-95.

Nazeer, M., Waqas, M., Shahzad, M.I., Zia, I. and Wu, W., 2020. Coastline Vulnerability Assessment Through Landsat and Cubesats in A Coastal Mega City. *Remote Sensing*, *12*(5), p.749.

Nebel, S.H., Trembanis, A.C. and Barber, D.C., 2012. Shoreline analysis and barrier island dynamics: decadal scale patterns from Cedar Island, Virginia. *Journal of Coastal Research*, *28*(2), pp.332-341.

Niang, A.J., 2020. Monitoring long-term shoreline changes along Yanbu, Kingdom of Saudi Arabia using remote sensing and GIS techniques. *Journal of Taibah University for Science*, 14(1), pp.762-776.

NOAA Office for Coastal Management, 2016. *Shoreline Mapping History.* [Online] URL: www.shoreline.noaa.gov/intro/index.html, accessed on 29 April 2020.

Novak, K., 1992. Rectification of digital imagery. *Photogrammetric engineering and remote sensing*, 58, pp.339-339.

Oppenheimer, M., B.C. Glavovic, J. Hinkel, R. van de Wal, A.K. Magnan, A. Abd-Elgawad, R. Cai, M. Cifuentes-Jara, R.M. DeConto, T. Ghosh, J. Hay, F. Isla, B. Marzeion, B. Meyssignac, and Z. Sebesvari, 2019: Sea Level Rise and Implications for Low-Lying Islands, Coasts and Communities. In: *IPCC Special Report on the Ocean and Cryosphere in a Changing Climate* [H.-O. Pörtner, D.C. Roberts, V. Masson-Delmotte, P. Zhai, M. Tignor, E. Poloczanska, K. Mintenbeck, A. Alegría, M. Nicolai, A. Okem, J. Petzold, B. Rama, N.M. Weyer (eds.)]. In press.

Orton, J., Avery, G., Halkett, D., Hart, T. and Kaplan, J., 2020. Precolonial coastal archaeology between Table Bay and Yzerfontein, Western Cape, South Africa: a review of historical and recent observations. *Southern African Humanities*, 33, pp.133-167.

Oyedotun, T.D., 2014. Shoreline geometry: DSAS as a tool for historical trend analysis. *Geomorphological Techniques*, *3*(2.2), pp.1-12.

Özpolat, E. and Demir, T., 2019. The spatiotemporal shoreline dynamics of a delta under natural and anthropogenic conditions from 1950 to 2018: A dramatic case from the Eastern Mediterranean. *Ocean & Coastal Management*, *180*, pp.104910.

Pajak, M.J. and Leatherman, S., 2002. The high water line as shoreline indicator. *Journal of Coastal Research*, 18(2) pp.329-337.

Pollard, J.A., Brooks, S.M. and Spencer, T., 2019. Harmonising topographic & remotely sensed datasets, a reference dataset for shoreline and beach change analysis. *Scientific data*, 6(42), pp.1-14.

Pollard, J.A., Spencer, T., Brooks, S.M., Christie, E.K. and Möller, I., 2020. Understanding spatio-temporal barrier dynamics through the use of multiple shoreline proxies. *Geomorphology,* 354, p.107058.

R Core Team, 2021. *R: A language and environment for statistical computing*. R Foundation for Statistical Computing, Vienna, Austria. URL: www.R-project.org/.

Rautenbach, C., Daniels, T., de Vos, M. and Barnes, M.A., 2020. A coupled wave, tide and storm surge operational forecasting system for South Africa: validation and physical description. *Natural Hazards*, 103, pp.1407-1439.

Renwick, 2018. *Coastal Erosion, Is Yzerfontein also being washed away?* I LOVE YZER DARLING Newspaper, The Summer Issue 2018, pp.41.

Roberts, D.L. and Berger, L., 1997. Last interglacial (c. 117 kyr) human footprints from South Africa. *South African Journal of Science*, 93(8), pp.349-350.

Roberts, D.L., Bateman, M.D., Murray-Wallace, C.V., Carr, A.S. and Holmes, P.J., 2009. West coast dune plumes: climate driven contrasts in dunefield morphogenesis along the western and southern South African coasts. *Palaeogeography, Palaeoclimatology, Palaeoecology*, *271*, pp.24-38.

Roberts, D.L., Matthews, T., Herries, A.I., Boulter, C., Scott, L., Dondo, C., Mtembi, P., Browning, C., Smith, R.M., Haarhoff, P. and Bateman, M.D., 2011. Regional and global context of the Late Cenozoic Langebaanweg (LBW) palaeontological site: West Coast of South Africa. *Earth-Science Reviews*, 106, pp.191-214.

Roberts, D.L., Cawthra, H. and Musekiwa, C., 2014. Dynamics of late Cenozoic aeolian deposition along the South African coast: a record of evolving climate and ecosystems. *Geological Society*, London, Special Publications, 388(1), pp.353-387.

Ruggiero, P. and List, J.H., 2009. Improving accuracy and statistical reliability of shoreline position and change rate estimates. *Journal of Coastal Research*, 25(5), pp.1069-1081.

Sarkar, D., Andrews, F., Wright, K., Klepeis, N. and Murrell, P., 2020. R Package 'Lattice' Version 0.20-41. URL: www.cran.r-project.org/web/packages/lattice/index.html.

Schoonees, J.S., Kluger, J.W.J. and Zwamborn, J.A., 1990. Causes of damage to Saldanha sand breakwater. *Coastal Engineering 1990*, pp.2416-2429.

Shalowitz, A.L., 1940. Our Changing Coastline. *Journal of Geography*, 39(1), pp.1-10.

South African History Online, 2020. *Tsaarsbank Beach, West Coast*. [Online] URL: www.sahistory.org.za/place/tsaarsbank-beach-west-coast, accessed on 12 May 2020.

Splinter, K.D., Harley, M.D. and Turner, I.L., 2018. Remote sensing is changing our view of the coast: Insights from 40 years of monitoring at Narrabeen-Collaroy, Australia. *Remote Sensing*, 10(11), p.1744.

Stafford, D.B. and Langfelder, J., 1971. Air photo survey of coastal erosion. *Photogrammetric Engineering*, 37(6), pp.565-575.

Stewart, W., Masson, S., Law, M. and Melly, B., 2013. *West Coast District Municipality Integrated Coastal Management Programme: Final Report*. Compiled by SRK Consulting (South Africa) (Pty) Ltd for the West Coast District Municipality. SRK Project Number 433368.

Teodoro, A.C., 2016. Optical satellite remote sensing of the coastal zone environment — An overview, in: Marghany, M. (Ed.), *Environmental Applications of Remote Sensing*. InTechOpen, pp.165-196.

Terres de Lima, L., Fernández-Fernández, S., Marcel de Almeida Espinoza, J., Albuquerque, M.D.G. and Bernardes, C., 2021. End Point Rate Tool for QGIS (EPR4Q): Validation Using DSAS and AMBUR. *ISPRS International Journal of Geo-Information*, 10(3), pp.162.

Theron, A.K. and Rossouw, M., 2008. *Analysis of potential coastal zone climate change impacts and possible response options in the southern African region*. Science Real and Relevant: 2nd CSIR Biennial Conference, CSIR International Convention Centre Pretoria, 17-18 November 2008, pp.10.

Thieler, E.R. and Danforth, W.W., 1994a. Historical shoreline mapping (I): Improving techniques and reducing positioning errors. Journal of Coastal Research, 10(3), pp.549-563.

Thieler, E.R. and Danforth, W.W., 1994b. Historical shoreline mapping (II): application of the digital shoreline mapping and analysis systems (DSMS/DSAS) to shoreline change mapping in Puerto Rico. *Journal of Coastal Research*, 10(3), pp.600-620.

Troch, C., Terblanche, L. and Henning, H., 2021. Modelling and measurement of low-frequency surge motion associated with extreme storm conditions in the Port of Cape Town. *Applied Ocean Research*, 106, pp.102452.

Umvoto Africa., 2011. *Sea Level Rise and Flood Risk Assessment for a Select Disaster Prone Area Along the Western Cape Coast. Phase 1 Report: West Coast District Municipality Sea Level Rise and Flood Risk Literature Review*. Prepared by Umvoto Africa (Pty) Ltd for the Provincial Government of the Western Cape Department of Environmental Affairs and Development Planning: Strategic Environmental Management.

United States Geological Survey (USGS), 2021a. *Digital Shoreline Analysis System (DSAS)*. [Online] URL: www.usgs.gov/centers/whcmsc/science/digital-shoreline-analysis-system-

dsas?qtscience_center_objects=0&qt-science_center_objects=0#qt-science_center_objects, accessed on 1 March 2020.

United States Geological Survey (USGS), 2021b. *Landsat Missions*. [Online] URL: www.usgs. gov/land-resources/nli/landsat/landsat-satellite-missions, accessed on 4 May 2020.

Van Weele, G., Breetzke, T. and Kamish R., 2014. Coastal Management/Set-back Lines for the West Coast District Final Project Report. Prepared by Royal Haskoning DHV for the Western Cape Department of Environmental Affairs and Development Planning.

Vos, K., Harley, M.D., Splinter, K.D., Simmons, J.A. and Turner, I.L., 2019a. Sub-annual to multi-decadal shoreline variability from publicly available satellite imagery. *Coastal Engineering*, 150, pp.160-174.

Vos, K., Splinter, K.D., Harley, M.D., Simmons, J.A. and Turner, I.L., 2019b. *CoastSat*: A Google Earth Engine-enabled Python toolkit to extract shorelines from publicly available satellite imagery. *Environmental Modelling & Software*, 122, p.104528.

Vos, K., Harley, M.D., Splinter, K.D., Walker, A. and Turner, I.L., 2020. Beach slopes from satellite-derived shorelines. *Geophysical Research Letters*, 47(14), e2020GL088365.

Vousdoukas, M.I., Ranasinghe, R., Mentaschi, L., Plomaritis, T.A., Athanasiou, P., Luijendijk, A. and Feyen, L., 2020. Sandy coastlines under threat of erosion. *Nature Climate Change*, 10(3), pp.260-263.

Warnasuriya, T.W.S., Kumara, M.P., Gunasekara, S.S., Gunaalan, K. and Jayathilaka, R.M.R.M., 2020. An Improved Method to Detect Shoreline Changes in Small-Scale Beaches Using Google Earth Pro. *Marine Geodesy*, 43:6, pp.541-572.

West Coast National Park, 2013. West Coast National Park Management Plan For the period 2013 -2023. [Online] URL: www.sanparks.org/assets/docs/conservation/parkman/westcoastapproved_plan.pdf, accessed on 10 March 2020.

Wigley, R., 2011. Geohazards in coastal areas. *Council for Geoscience*, Report number: 2011-0066.

Wurz, S., 2012. The significance of MIS 5 shell middens on the Cape coast: A lithic perspective from Klasies River and Ysterfontein 1. *Quaternary International*, 270, pp.61-69.

Yasir, M., Sheng, H., Fan, H., Nazir, S., Niang, A.J., Salauddin, M. and Khan, S., 2020. Automatic coastline extraction and changes analysis using remote sensing and GIS technology. *IEEE Access*, 8, pp.180156-180170.

Yzerfontein.net., 2021. *16 Mile Beach Yzerfontein*. [Online] URL: www.yzerfontein.net/16-mile-beach/, accessed on 7 March 2020.

Yzerfontein Tourism, 2021. *About*. [Online] URL: https://yzerfonteintourism.co.za/about, accessed on 2 February 2021.

Zagorski, P., Jarosz, K. and Superson, J., 2020. Integrated assessment of shoreline change along the Calypsostranda (Svalbard) from remote sensing, field survey and GIS. *Marine Geodesy*, 43:5, pp.433-471.

Zwemmer, I.D. and van't Hoff, I.J., 1982. Spending beach breakwater at Saldanha Bay. In *Coastal Engineering 1982*, pp.1248-1267.

APPENDICES

Table A1: List of data sources for maps.

Data type	Source	Figure
Medium-resolution satellite imagery	Sentinel-2 (USGS Earth Explorer)	2.1, 2.2, 2.3, 4.3, 4.5, 5.1, 5.2, 5.3
High-resolution satellite imagery	QGIS Bing high-resolution imagery, Esri High-resolution basemap (Maxar Technologies)	4.6 4.1, 5.6
Provincial Boundaries	Municipal Demarcation Board	2.1, 2.7
National Roads	National Geo-spatial Information (NGI)	2.1
West Coast National Park	The South African National Biodiversity Institute (SANBI)	2.1
Secondary and Residential roads	OpenStreetMap	2.2, 2.3
Geological Formations	Council for Geoscience (CGS)	2.7
Bathymetry	The General Bathymetric Chart of the Oceans (GEBCO)	2.7
Elevation	Shuttle Radar Topography Mission (SRTM)	2.7
Longshore-drift and swell barriers	Based on Compton (2016: pp.75)	2.7
Historical aerial photographs	National Geo-spatial Information (NGI)	4.1, 6.1

Table A1: List of Sentinel-2 A and B image acquisition dates for shoreline extraction

2015:	**2016:**	**2017:**	**2018:**
10-Aug-2015	7-Jan-2016	1-Jan-2017	4-Jan-2018
22-Oct-2015	10-Jan-2016	4-Jan-2017	9-Jan-2018
21-Nov-2015	20-Jan-2016	11-Jan-2017	11-Jan-2018
8-Dec-2015	30-Jan-2016	14-Jan-2017	16-Jan-2018
18-Dec-2015	9-Feb-2016	31-Jan-2017	19-Jan-2018
21-Dec-2015	16-Feb-2016	3-Feb-2017	24-Jan-2018
28-Dec-2015	7-Mar-2016	10-Feb-2017	26-Jan-2018
	10-Mar-2016	13-Feb-2017	29-Jan-2018
	27-Mar-2016	20-Feb-2017	31-Jan-2018
	6-Apr-2016	23-Feb-2017	3-Feb-2018
	6-May-2016	12-Mar-2017	13-Feb-2018
	16-May-2016	25-Mar-2017	15-Feb-2018
	19-May-2016	21-Apr-2017	20-Feb-2018
	26-May-2016	24-Apr-2017	25-Feb-2018
	5-Jun-2016	4-May-2017	28-Feb-2018
	8-Jun-2016	14-May-2017	17-Mar-2018
	25-Jul-2016	21-May-2017	20-Mar-2018
	4-Aug-2016	23-Jun-2017	22-Mar-2018
	17-Aug-2016	10-Jul-2017	27-Mar-2018
	24-Aug-2016	23-Jul-2017	1-Apr-2018
	27-Aug-2016	28-Jul-2017	11-Apr-2018
	3-Sep-2016	30-Jul-2017	14-Apr-2018
	23-Sep-2016	7-Aug-2017	16-Apr-2018
	3-Oct-2016	17-Aug-2017	21-Apr-2018
	13-Oct-2016	27-Aug-2017	29-Apr-2018
	23-Oct-2016	1-Sep-2017	4-May-2018
	26-Oct-2016	8-Sep-2017	6-May-2018
	5-Nov-2016	16-Sep-2017	14-May-2018
	12-Nov-2016	18-Sep-2017	16-May-2018
	15-Nov-2016	23-Sep-2017	26-May-2018
	2-Dec-2016	1-Oct-2017	3-Jun-2018
	5-Dec-2016	6-Oct-2017	5-Jun-2018
	22-Dec-2016	8-Oct-2017	10-Jun-2018
	25-Dec-2016	11-Oct-2017	13-Jun-2018
		13-Oct-2017	3-Jul-2018
		21-Oct-2017	5-Jul-2018
		26-Oct-2017	10-Jul-2018
		28-Oct-2017	15-Jul-2018
		31-Oct-2017	18-Jul-2018
		5-Nov-2017	23-Jul-2018
		7-Nov-2017	28-Jul-2018
		10-Nov-2017	30-Jul-2018
		17-Nov-2017	2-Aug-2018
		27-Nov-2017	9-Aug-2018
		30-Nov-2017	24-Aug-2018
		5-Dec-2017	29-Aug-2018
		7-Dec-2017	11-Sep-2018
		10-Dec-2017	28-Sep-2018
		12-Dec-2017	8-Oct-2018
		15-Dec-2017	13-Oct-2018
		20-Dec-2017	21-Oct-2018
		25-Dec-2017	26-Oct-2018
		27-Dec-2017	31-Oct-2018
		30-Dec-2017	7-Nov-2018
			10-Nov-2018
			17-Nov-2018
			22-Nov-2018
			25-Nov-2018
			30-Nov-2018
			7-Dec-2018
			10-Dec-2018
			15-Dec-2018
			17-Dec-2018
			20-Dec-2018
			25-Dec-2018
			27-Dec-2018
			30-Dec-2018

… continued on next page

Table A1: List of Sentinel-2 image acquisition dates for shoreline extraction … continued.

2019:			**2020:**				
1-Jan-2019	24-Aug-2019		1-Jan-2020	1-Mar-2020	30-Sep-2020		
4-Jan-2019	3-Sep-2019		9-Jan-2020	9-Mar-2020	10-Oct-2020		
6-Jan-2019	6-Sep-2019		14-Jan-2020	14-Mar-2020	12-Oct-2020		
9-Jan-2019	8-Sep-2019		16-Jan-2020	16-Mar-2020	15-Oct-2020		
14-Jan-2019	23-Sep-2019		24-Jan-2020	19-Mar-2020	22-Oct-2020		
16-Jan-2019	26-Sep-2019		26-Jan-2020	21-Mar-2020	30-Oct-2020		
19-Jan-2019	28-Sep-2019		3-Feb-2020	29-Mar-2020	1-Nov-2020		
21-Jan-2019	3-Oct-2019		5-Feb-2020	31-Mar-2020	4-Nov-2020		
24-Jan-2019	13-Oct-2019		8-Feb-2020	3-Apr-2020	11-Nov-2020		
26-Jan-2019	16-Oct-2019		10-Feb-2020	8-Apr-2020	19-Nov-2020		
31-Jan-2019	18-Oct-2019		15-Feb-2020	18-Apr-2020	26-Nov-2020		
5-Feb-2019	26-Oct-2019		18-Feb-2020	25-Apr-2020	29-Nov-2020		
10-Feb-2019	31-Oct-2019		23-Feb-2020	28-Apr-2020	4-Dec-2020		
13-Feb-2019	2-Nov-2019		25-Feb-2020	30-Apr-2020	6-Dec-2020		
15-Feb-2019	5-Nov-2019		28-Feb-2020	8-May-2020	16-Dec-2020		
18-Feb-2019	17-Nov-2019			15-May-2020	19-Dec-2020		
23-Feb-2019	22-Nov-2019			20-May-2020	26-Dec-2020		
25-Feb-2019	27-Nov-2019			30-May-2020			
5-Mar-2019	5-Dec-2019			4-Jun-2020			
15-Mar-2019	7-Dec-2019			7-Jun-2020			
25-Mar-2019	10-Dec-2019			17-Jun-2020			
27-Mar-2019	15-Dec-2019			19-Jun-2020			
11-Apr-2019	17-Dec-2019			22-Jun-2020			
16-Apr-2019	22-Dec-2019			24-Jun-2020			
21-Apr-2019	27-Dec-2019			7-Jul-2020			
24-Apr-2019	30-Dec-2019			12-Jul-2020			
26-Apr-2019				17-Jul-2020			
24-May-2019				19-Jul-2020			
13-Jun-2019				22-Jul-2020			
15-Jun-2019				24-Jul-2020			
18-Jun-2019				27-Jul-2020			
25-Jun-2019				1-Aug-2020			
30-Jun-2019				21-Aug-2020			
10-Jul-2019				23-Aug-2020			
13-Jul-2019				26-Aug-2020			
15-Jul-2019				7-Sep-2020			
20-Jul-2019				10-Sep-2020			
25-Jul-2019				12-Sep-2020			
9-Aug-2019				15-Sep-2020			
12-Aug-2019				17-Sep-2020			
17-Aug-2019				22-Sep-2020			

Table A2: List of software programmes used in research report.

Programme name	**Link to programme**
ArcGIS ArcMap (v 10.6)*	www.arcgis.com
CoastSat (v 1.0.5)	www.github.com/kvos/CoastSat
- Anaconda	- www.anaconda.com
- Jupyter Notebook	- www.jupyter.org
Datawrapper	www.datawrapper.de/
Digital Shoreline Analysis System	www.usgs.gov/centers/whcmsc/science/digital-
- (DSAS) (v 5.0)	shoreline-analysis-system-dsas
Draw.io (v 14.4.3)	www.github.com/jgraph/drawio-desktop/releases
Google Earth Engine	www.earthengine.google.com
Google Earth Pro	www.google.com/earth/versions/#earth-pro
iNZight for Data Analysis	www.inzight.nz/
QGIS (v 3.10)	www.qgis.org
R (v 4.0.2)	www.r-project.org
- Lattice Package (v 0.20-41)	- www.CRAN.R-project.org/package=lattice

*Requires a license. All other software programmes are opensource.